Lysine-Functionalized Nanodiamonds: Synthesis, Characterization and Potential as Gene Delivery Agents

A Thesis Submitted to the College of

Graduate Studies and Research

in Partial Fulfillment of the Requirements

for the Degree of Master of Science

in the College of Pharmacy and Nutrition

University of Saskatchewan

Saskatoon

By

Randeep Kaur

PERMISSION TO USE

In presenting this thesis in partial fulfillment of the requirements for a Postgraduate degree from the University of Saskatchewan, I agree that the Libraries of this University may make it freely available for inspection. I further agree that permission for copying of this thesis in any manner, in whole or in part, for scholarly purposes may be granted by the professor or professors who supervised my thesis work or, in their absence, by the Head of the Department or the Dean of the College in which my thesis work was done. It is understood that any copying or publication or use of this thesis or parts thereof for financial gain shall not be allowed without my written permission. It is also understood that due recognition shall be given to me and to the University of Saskatchewan in any scholarly use which may be made of any material in my thesis.

Requests for permission to copy or to make other uses of materials in this thesis in whole or part should be addressed to:

Dean of the College of Pharmacy & Nutrition
University of Saskatchewan
Saskatoon, Saskatchewan S7N 5C9
Canada

OR

Dean
College of Graduate Studies and Research
University of Saskatchewan
107 Administration Place
Saskatoon, Saskatchewan S7N 5A2
Canada

ABSTRACT

Detonation nanodiamonds (NDs), due to their 4-5 nm primary particle size, stable inert core, reactive surface, ability to form hydrogel, are emerging as intracellular delivery vehicle for small and large molecules. Despite several favorable characteristics, the use of NDs in biological systems is impeded by their high aggregation propensity in polar liquid medium. To develop NDs as potential gene delivery vectors, pristine carboxylated NDs (pNDs) were functionalized with lysine through covalent conjugation. Raman and FTIR spectroscopic determinations confirmed the functionalization of NDs with lysine molecules, while thermogravimetric analysis estimated a surface loading of 1.7 mmol/g. Through lysine-functionalization, the dispersion stability of NDs in water increased considerably, showing a zeta potential of +49 mV. The average particle size of pNDs as measured by dynamic light scattering was substantially reduced from 1281 to 21 nm after lysine functionalization. Atomic force microscopy further substantiated the disaggregation of pNDs achieved through lysine functionalization. The lysine-functionalized NDs (fNDs) were able to electrostatically bind and block the migration of the nucleic acids at a weight ratio of 5:1 and 20:1 of fNDs:pDNA and fNDs:siRNA, respectively, with a shift in zeta potential from negative to positive value. The particle size of the complexes stabilized around 110 nm for fNDs-pDNA and less than 280 nm for fNDs-siRNA at the weight ratios of 50:1 fNDs:nucleic acid. While the Raman-fluorescence maps were equivocal with regards to the cellular association of NDs, backscattering maps clearly indicated the interaction of the fNDs with the cells. Cellular internalization of a few fNDs was suggested by laser confocal scanning microscopy. MTT assay demonstrated no significant *in vitro* cytotoxicity of pNDs and fNDs in the concentration range from 4 to 250 μg/mL. Flow cytometeric assessment of the gene expression (GFP intensity measurements) suggested that a strong binding of siRNA with fNDs might have prevented the release of nucleic acid into the cytoplasm of the cells.

Overall, in this study, stable aqueous dispersion of NDs was generated using a mechanochemical approach feasible at a small laboratory scale, and early evidence was presented that the fNDs can be optimized for safe delivery of nucleic acids into mammalian cells.

ACKNOWLEDGEMENTS

First and foremost I would like to thank God for everything.

I would like to extend my heartfelt gratitude to my supervisor, Dr. Ildiko Badea, who provided me the opportunity to join her research group at University of Saskatchewan, and for her professional guidance and motivation throughout my project. Special thanks to the members of the advisory committee, Dr. Adil Nazarali and Dr. Ramaswami Sammynaiken for providing me with their professional support, knowledge and valued advices. I sincerely appreciate Dr. Ronald E Verrall and Dr. Jackson M Chitanda for providing advises in chemical synthesis. I also thank Jason Maley for his untiring technical assistance. I also greatly appreciate the technical assistance offered by Dr. Lee Wilson, Dr. Ferenc Borondics, Dr. Chitra Karunakaran and Ken Thoms. Very warm thanks to Deborah Michael for providing me technical assistance, friendly help and motivation throughout my project. I would like to extend my thanks to my colleagues and friends Jagbir Singh, Waleed Mohammed-Saeid, Masoomeh Poorghorban, Joshua Buse, McDonald Donkuru, Hanan Elsayed, and Andreea Badea for their friendly help.

I duly recognize Natural Sciences and Engineering Research Council of Canada for funding this research project and Apotex Inc. for providing me with the award to support my studies. I thank Tosoh Corporation, USA, for the kind donation of the YTZ® grinding media used in these studies.

I would like to show my gratitude and deep love to my parents (*Bhinderjit and Iqbal Singh*), sister (*Kawalpreet Kaur*) and brother (*Jasbir Singh*), whose constant love, financial support and encouragement cannot be expressed by words.

DEDICATION

I would like to dedicate my thesis to

- *To my loving mother, Bhinderjit, and father, Iqbal Singh, whose valuable advises, love, care and trust were of great support to me*
- *To my best friend, Inderjot Singh, who always motivated and supported me in studies*

TABLE OF CONTENTS

LIST OF TABLES

LIST OF FIGURES

LIST OF ABBREVIATIONS

AFM	Atomic force microscopy
ANOVA	Analysis of variance
Boc	(tert-Butoxy)carbonyl
$CHCl_3$	Choloroform
CLS	Canadian Light Source
cND	Carboxylated nanodiamonds
COCl	Acyl chloride
Compound 1	N'-(N^{α},N^{ε}-Bis-Boc-Lysyl),N''-(Fmoc)-diaminopropane
DCM	Dichloromethane
DIPEA	N,N-Diisopropylethyamine
DMEM	Dublecco's modified eagle medium
DMF	Dimethylformamide
DMSO	Dimethylsulfoxide
DNA	Deoxyribonucleic acid
DOX	Doxorubicin hydrochloride
E. coli	*Escherichia coli*
EDTA	Ethylene diamine tetra acetic acid,
EMEM	Eagle's minimum essential medium
FACS	Fluorescence activated cell sorting
FBS	Fetal bovine serum
FL	Filter
Fmoc	9-Fluorenylmethoxycarbonyl
fNDs	Lysine-functionalized nanodiamonds
GFP	Green fluorescent protein
HATU	N,N,N',N'-tetramethyl-O-(7-azabenzotriazol-1-yl)uranium hexafluorophosphate
HCPT	Hydroxycamptothecin
IR	Infrared

MeOH	Methanol
MTT	(Dimethylthiazol-2-yl)-2,5-Diphenyltetrazolium Bromide
NDs	Nanodiamonds
$(N\text{-}V)^-$	Negatively charged nitrogen vacancy
$(N\text{-}V)^0$	Neutral nitrogen vacancy
N-V-N	Nitrogen vacancy nitrogen
PBS	Phosphate buffer saline
PDI	Polydispersity index
pDNA	Plasmid deoxyribonucleic acid
PEI	Polyethyleneimine
pNDs	Pristine carboxylated nanodiamonds
RISC	RNA induced silencing complex
RNA	Ribonucleic acid
rNDs	Reoxidized nanodiamonds
siRNA	Small interfering ribonucleic acid
$SOCl_2$	Thionyl chloride
STXM	Scanning transmission X-ray spectromicroscopy

INTRODUCTION

Applications of detonation nanodiamonds (NDs) are gaining rapid significance in the biological sciences due to their favorable structural, chemical, optical and biological properties. NDs can improve the physiochemical characteristics and intracellular delivery of small molecules, large molecules and biotechnological products [1-4]. The intrinsic and induced fluorescence of NDs is a key feature for their use as cellular biomarkers [5,6]. However, NDs possess a strong tendency to aggregate to form micron-sized particles, when dispersed in a polar liquid media. These aggregated particles can induce toxic effects in the biological systems by blocking the vasculature and triggering immune responses [7]. Aggregation is also an impediment in cellular internalization [8].

Although ND dispersions of less than 10 nm particles were attained by high energy bead-assisted probe sonication in literature, the potential of contamination of the samples with sonotrode material and beads [9,10], and the risk of altering the intrinsic diamond structure is high. These deficiencies warrant research exploring an alternative, non-contaminating disaggregation approach that is feasible in laboratory settings. Functionalization of the NDs accompanied by the simple mechanical treatment could lead to the disaggregation of ND aggregates as well as produce a surface enriched in functional groups that could subsequently facilitate a higher loading of cargo, ultimately improving drug delivery efficiency.

Gene therapy is emerging as a promising alternative to conventional drug therapy for various inherited and acquired disorders [11]. However, there is a challenge to effectively deliver the transgene into the targeted cellular compartment due to its anionic nature and high molecular weight. For an effective cellular internalization and subsequent gene expression, the particles size of the carrier-genetic material should be less than 300 nm [12]. An overall positive charge on the complex is required for their effective cellular internalization [13,14] and endosomal release of the genetic material [14]. In addition, an optimal surface charge prevents aggregation of the nanoparticles and contributes to the overall colloidal stability of the dispersion.

Among various investigated non-viral vectors of the genetic materials, positively charged detonation NDs could emerge as the promising delivery candidates due to their biocompatibility,

nano-size and favorable surface chemistry for conjugating biomolecules [15]. In addition, the solid core of NDs could provide an additional advantage over soft nanoparticles (polymers and lipids) of protecting the attached genetic material from extracellular environmental changes and nuclease attack.

Therefore, my aim was to develop a methodology to generate a disaggregated population of NDs that could serve as vectors to deliver genetic materials across the cellular membranes.

Chapter 1
NANOTECHNOLOGY IN RELATION TO THE GENE THERAPY

1.1 Overview of Nanotechnology

Nanotechnology is a rapidly expanding field, dealing with the development of nano-sized materials, along with the techniques and equipment functioning at the nano-scale. According to Health Canada, at least one dimension of nanomaterials should be from 1 through 100 nm, or the nanomaterial should show novel nano-scale characteristic(s) when all the dimensions fall out of this range [16]. Since aggregation and functionalization can have a substantial effect on the size of some of the particles to exclude them from the nano category, the dimensions of the internal structure of particle were suggested to be included in the definition [17]. For biological applications, the size of nanomaterials usually ranges from 5 to 250 nm [18]. Some researchers and organizations such as FDA classify particles under 1000 nm as nanomaterials in pharmaceutical sciences [19-21].

The word nano is derived from a greek word "nanos" meaning dwarf and represents 10^{-9} of the accompanying suffix unit. The concept of nanotechnology was coined in 1959 by Nobel laureate Richard P. Feymann in his talk entitled "There is plenty of room at the bottom" [22]. Nanotechnology is emerging as a promising field in biological sciences as numerous vital components of the cellular machinery such as DNA, RNA, antibodies, enzymes, biochemical motors and molecule selective pumps fall within the nano-scale range as shown in Table 1.1. To probe these subcellular components and understand the processes occurring at this scale, probing machineries and tools should have comparable size ranges.

Particles acquire unique characteristics at the nano-level. Nanomaterials possess a large surface area to volume ratio, leading to an increase in their reactivity compared to micro and macro particles. There is a dominance of quantum effects at the nano-size, which affects their optical, electrical, thermal and magnetic behavior [23]. For example, gold particles differ considerably in their color, melting point and catalytic effects depending upon their size [24]. Other materials showing different characteristics at macro- and nano-scale level are listed in Table 1.2 [24].

Table 1.1: Various cellular machineries along with their typical sizes

Cellular component	Size (nm)	Reference
DNA (diameter)	2.5	[25]
Ribosome	20	[26]
tRNA length	10	[26]
ATP biochemical motor	10	[25]
Actin	10	[26]
Chymotrypsin	4.0	[26]
Hemoglobin	6.4	[27]
Width of cell membrane	6-10	[28]

Table 1.2: Size-dependent differences in physical properties of materials

Material	Macro-scale level	Nano-scale level
Copper	Opaque	Transparent
Platinum	Inert	Catalyst
Aluminum	Stable	Combustible
Silicon	Insulator	Conductor

1.2 Overview of Gene Therapy and its Barriers

Gene therapy deals with the treatment of inherited and acquired human diseases by inserting or replacing the missing or defective genes into the cell. Candidate diseases for gene therapy include hemophilia, liver hypercholesterolemia, cystic fibrosis, thalassemia, sickle-cell anemia, cancer, neurological, cardiovascular and infectious disorders [11]. Two main approaches for achieving gene therapy include induction of desired gene expression and modulation of the undesired gene expression. While the gene expression can be induced in cells by using therapeutic DNA encoding for the missing or defective genes, the silencing is achieved by using double stranded RNAs, small interfering RNAs (siRNA) and antisense oligodeoxyribonucleotides complementary to the targeted mRNA. DNA and siRNA differ in their site of action: generally, the DNA needs to be delivered into the nucleus of the cells to produce the desired gene expression, whereas the siRNA has to travel only to the cytoplasm to induce gene silencing [29] by degrading the mRNA possessing complementarity to its antisense strand [30].

The major obstacle to the use of naked nucleic acids as therapeutics is their inefficient cellular delivery. Physiochemical characteristics such as highly negative surface charge and large molecular weight are barriers in the efficient cellular internalization of the DNA [29,31] and siRNA [32,33]. In addition, the naked siRNA also triggers the immunogenic response when administered systemically [34,35]. While the DNA is extremely large for the efficient cellular uptake, the small size of siRNA also pose an additional challenge to its effective cellular delivery [36] as the particles having molecular weight less than 50 kDa are susceptible to excretion through glomerular filtration [32]. Intravenously administered naked siRNA having 21-23 base pairs (~13 kDa) accumulate in kidneys and experience rapid renal clearance [37,38]. Therefore, it is of paramount importance to increase the size of siRNA by complexing it with suitable nanocarriers to avoid its rapid excretion [36]. The scenario is different for plasmid DNA which contains several kilo basepairs; in this case, nanocarriers are required to condense the plasmid to a size range that can be internalized by the mammalian cells [29].

1.3 Use of Nanocarriers in Gene Delivery

The success in gene therapy relies on complexing the genetic material with suitable nanocarriers. These carriers can be broadly classified under two categories: viral vectors and non-viral vectors.

Viruses are natural machineries that have evolved to infect their hosts with high efficiency and exploit the cellular machinery of the infected cells for their own replication. The idea behind harnessing the viruses as gene delivery vectors capitalized on their highly infectious nature. Before using these biological machines to deliver the nucleic acids, their virulent genes are either deleted or inactivated [39], while preserving other useful regulatory sequences required for packaging and integration [13]. Moreover, the other viral coding sequences such as those involved in replication and producing capsid protein are also deleted from viral genome and are incorporated in a separate packaging construct [40]. This segregation of replication genes and non-coding viral sequences is essential to prevent the reversion of viral vector back to its pathogenic form [40]. The therapeutic genes are then introduced into the viral backbone to replace the deleted viral genes [13]. Some of the viral vectors utilized for delivering genetic material include retroviruses, adenoviruses, adeno-associated viruses and herpes simplex viruses [40].

Although viruses have high potential to invade the host cells, their application as gene delivery vectors is associated with many adverse effects. One of the most fatal consequences is the activation of the host's cellular immune system that recognizes viral vectors as the pathogenic forms of virus [13]. The intravenous administration of the viral vectors suffers from cellular non-specificity and distribution, which can result in fatal consequences due to the massive immunogenic response [13]. In a clinical trial held in September 1999, systemic administration of a modified adenoviral vector led to disseminated vascular coagulation and consequently, multiorgan failure, leading to the death of a patient after four days of treatment [41]. In addition, the random integration of the viral vector genome into the chromosome of host cells can lead to insertional malignancies that have been evidenced by the development of leukemia in animal models [42,43] and humans (1 out of 4) [44]. In addition to packaging restrictions in the size of gene, it is difficult to produce clinical grade vectors at low cost

[13,45,46]. Therefore, the use of non-viral vectors is preferred over the viral systems as these have low immunogenicity, can accommodate any size nucleic acid, are lower in cost and are relatively safe [46,47].

Among various non-viral vectors, detonation nanodiamonds (NDs) are emerging as a promising candidates for delivering genetic material into the mammalian cells due to their advantages such as narrow size distribution (4-5 nm), inert core, surface reactivity, low cytotoxicity, fluorescence, and potential to be characterized by Raman spectroscopy [15].

1.4 Important Parameters of Nanoparticles

1.4.1 Cellular Delivery of Nanoparticles

Macromolecules greater than 1 kDa cannot diffuse themselves through the cellular membrane [19], therefore their uptake is governed mainly by endocytosis. The endocytotic pathways can be classified into macropinocytosis (<1μm), clathrin-mediated endocytosis (~120 nm), caveolae-mediated endocytosis (~60 nm), and clathrin- and caveolae- independent endocytosis (~90 nm) [48]. These pathways are responsible for the uptake of nanoparticles depending upon the size and other surface characteristics of the particles.[19] In the clathrin-mediated endocytosis, the clathrin-coated pits invaginate and pinch off from the cellular membrane to form endocytic vesicles of 100-150 nm [49]. These vesicles, after uncoating [49], fuse with the sorting endosome (a type of primary endosome, with pH of 5.9 to 6.0), mature into late endosomes (pH 5.0 to 6.0), and then transform into lysosomes (pH 5.0–5.5) [48]. In order to evade degradation due to the acidic pH in the lysosomes, the genetic material needs to be released from the primary endosomes. The nanoparticles are not transported to the lysosomal compartment when internalized by the caveolae-mediated endocytosis [50]. Therefore, the ultimate fate of particles is highly dependent upon their mode of internalization.

Cationic nanoparticles such as polylysine, polyamidoamines, polyethyleneimine are suggested to be released from the endosomes by the “proton sponge” effect [31,51,52] and/or by endosomal membrane disruption [14]. The endosomal membrane is equipped with an ATPase proton pump that is responsible for an influx of protons into the endosomal lumen against the concentration gradient, creating the acidic environment [53,54]. Once trapped in the endosomes,

the cationic vectors with ionizable amine groups trigger the influx of H^+ due to their buffering capacity, which is accompanied by the inflow of chloride ions (to maintain charge neutrality), and water [51,55]. As a consequence, the endosome undergoes osmotic lysis leading to release of nanoparticles into the cytoplasm. Although these cationic molecules have a potential of disrupting the endosomal membranes, the integrity of the cellular membrane might not compromised due to the pH differences [56,57].

1.4.2 Characteristics of the Nucleic Acid Delivery Nanoparticles

The physiochemical properties of nanoparticles such as size, zeta potential and aggregation have a substantial effect on the behavior of the nano-formulation in physiological systems. Therefore these parameters should be controlled and characterized critically.

1.4.2.1 Size

One of the strategies for effective cellular uptake and transfection is to control the particle size of the carrier and the carrier-nucleic acid complex. Systemic administration of the foreign particles causes activation of the human complement system that consequently leads to their rapid clearance from the circulation, predominantly when the particles are larger than 200 nm [58]. Alternatively, if the particles are too small, less than 5 nm, they will be cleared prematurely from the circulation via extravasation or renal route [19]. The size range between 100 to 300 nm for the nanocarrier-nucleic acid complex is suggested to have the highest potential for the efficient cellular interaction, uptake and endosomal release [12]. Although the size of caveolae pits range from 50 to 100 nm size [59], the internalization of latex beads of 500 nm was suggested to occur by this pathway [60]. Beads of less than 200 nm diameter were taken up by clathrin-mediated endocytosis in non-phagocytic cells [60]. Another study demonstrated a significantly higher gene expression by using larger polyplexes compared to the smaller sized in neuroblastoma and erythromyeloid cells [61]. Based upon the distribution profile of the particles *in vivo*, it has been suggested that the size range of rigid nanoparticle should be between 100 to 200 nm [19].

1.4.2.2 Surface Charge

Genetic materials with highly anionic phosphate backbone when administered without delivery vehicle experience poor interaction with the negatively charged cell surface, resulting in poor cellular uptake and consequently poor gene expression [12,31]. Therefore, it is crucial to design carriers with the positive charges that can neutralize the negative charges of nucleic acids and facilitate their interaction with the cellular surfaces [31,62]. The positively charged carrier-DNA complexes promote cellular endocytosis of the particles by altering the structural properties and ion permeability of the cell membrane [63]. The overall positive charge is an essential prerequisite for the effective cellular association of particles and their subsequent internalization [59].

In addition, the surface charge of the particle also determine the colloidal stability of the dispersion and can be predicted by measuring the zeta potential of the system [64]. According to the conventional Derjaguin-Landau-Verwey-Overbeek (DLVO) theory, the interaction between two particles is the sum of the electrostatic repulsion and the van der Waals attraction [65]. Since the behavior of nano-scale particles in the liquid medium is strongly dominated by the inter-particle forces [66], in order to achieve stable dispersion, one should consider generating like-charged surfaces that could provide sufficient electrostatic repulsion between the particles to maintain their dispersion stability [66]. Dispersions with zeta potential below a critical value of 20-30 mV are considered to be relatively unstable and tend to coagulate easily [67].

However, caution should be taken while designing the formulation since an excess of positive charge can induce toxic effects by disrupting the cellular membrane [18,68]. Nanotechnology Characterization Laboratory, Frederick, MD indicated a positive relationship between the zeta potential and the cytotoxic effects [69]. A study compared anionic and cationic charges on the gold nanoparticles and found that the cationic particles possess a relatively higher cytotoxicity [70]. Similar results were observed by using cationic polystyrene nanospheres *in vitro* and *in vivo* [71]. Therefore, an optimal positive charge on the particle is desired that should favor colloidal stability and interaction with cellular membrane without inducing cytotoxicity.

1.4.2.3 Aggregation

As the surface area to volume ratio of the particles increases with the decrease in the size, the Van der Waals forces along with electrostatic interactions and chemical bonding dominate [7], leading to a significant aggregation of nanoparticles [72]. Systemic administration of aggregating nanoparticles can result in the occlusion of the blood flow in the blood vessels, causing severe embolism [7,27]. Aggregated particles could also accumulate in various organs of the body, leading to severe consequences such as pulmonary embolism, myocardial infarction, stroke and microinfarction [27]. Furthermore, agglomeration can also initiate an immune response [7]. Aggregated carbon nanotubes have shown higher *in vitro* toxic effects compared to their dispersed state [73]. Aggregation of nanoparticles may adversely affect their interactions with the cellular membranes to ultimately influence the cellular uptake [8,74], although the effect is not yet clear [75].

Maintaining nano-scale particle size necessitates the use of mechanochemical treatment that not only leads to disaggregation but also prevents the re-aggregation of particles. Mechanical treatment such as sonication can break the aggregates without affecting the surface properties of particles, and then chemical functionalization can sterically and/or electrostatically stabilize the dispersion [72]. Therefore, mechanochemical treatment has a potential to reduce the size of aggregated particles and maintain their dispersion stability.

1.5 References

1. Chow EK, Zhang XQ, Chen M, Lam R, Robinson E, Huang H, Schaffer D, Osawa E, Goga A, Ho D: Nanodiamond therapeutic delivery agents mediate enhanced chemoresistant tumor treatment. *Science Translational Medicine* 2011, 3:73ra21.

2. Li J, Zhu Y, Li W, Zhang X, Peng Y, Huang Q: Nanodiamonds as intracellular transporters of chemotherapeutic drug. *Biomaterials* 2010, 31:8410-8418.

3. Shimkunas RA, Robinson E, Lam R, Lu S, Xu X, Zhang XQ, Huang H, Osawa E, Ho D: Nanodiamond-insulin complexes as pH-dependent protein delivery vehicles. *Biomaterials* 2009, 30:5720-5728.

4. Zhang XQ, Chen M, Lam R, Xu X, Osawa E, Ho D: Polymer-functionalized nanodiamond platforms as vehicles for gene delivery. *ACS Nano* 2009, 3:2609-2616.

5. Vlasov II, Shenderova O, Turner S, Lebedev OI, Basov AA, Sildos I, Rähn M, Shiryaev AA, Van Tendeloo G: Nitrogen and luminescent nitrogen-vacancy defects in detonation nanodiamond. *Small* 2010, 6:687-694.

6. Mohan N, Chen CS, Hsieh HH, Wu YC, Chang HC: In vivo imaging and toxicity assessments of fluorescent nanodiamonds in caenorhabditis elegans. *Nano Letters* 2010, 10:3692-3699.

7. Sharma A, Madhunapantula SV, Robertson GP: Toxicological considerations when creating nanoparticle-based drugs and drug delivery systems. *Expert Opinion on Drug Metabolism and Toxicology* 2012, 8:47-69.

8. Dhawan A, Sharma V: Toxicity assessment of nanomaterials: Methods and challenges. *Analytical and Bioanalytical Chemistry* 2010, 398:589-605.

9. Ozawa M, Inaguma M, Takahashi M, Kataoka F, Krüger A, Osawa E: Preparation and behavior of brownish, clear nanodiamond colloids. *Advanced Materials* 2007, 19:1201-1206.

10. Barnard AS: Self-assembly in nanodiamond agglutinates. *Journal of Materials Chemistry* 2008, 18:4038-4041.

11. Verma IM, Somia N: Gene therapy - Promises, problems and prospects. *Nature* 1997, 389:239-242.

12. Donkuru M, Badea I, Wettig S, Verrall R, Elsabahy M, Foldvari M: Advancing nonviral gene delivery: lipid- and surfactant-based nanoparticle design strategies. *Nanomedicine (London,England)* 2010, 5:1103-1127.

13. Thomas CE, Ehrhardt A, Kay MA: Progress and problems with the use of viral vectors for gene therapy. *Nature Reviews Genetics* 2003, 4:346-358.

14. Zhang ZY, Smith BD: High-generation polycationic dendrimers are unusually effective at disrupting anionic vesicles: Membrane bending model. *Bioconjugate Chemistry* 2000, 11:805-814.

15. Schrand AM, Hens SAC, Shenderova OA: Nanodiamond particles: Properties and perspectives for bioapplications. *Critical Reviews in Solid State and Materials Sciences* 2009, 34:18-74.

16. Health Canada. Interim policy statement on Health Canada's working definition for nanomaterials; 2010. Available from: URL: http://www.hc-sc.gc.ca/sr-sr/pubs/nano/pol-eng.php or http://www.hc-sc.gc.ca/sr-sr/consult/_2010/nanomater/draft-ebauche-eng.php (accessed 27 March 2012)

17. European Commission, Scientific Committee on Emerging and Newly Identified Health Risks (SCENIHR). Opinion on the scientific aspects of the existing and proposed definitions relating to products of nanoscience and nanotechnologies 29 November 2007.

18. Garnett MC, Kallinteri P: Nanomedicines and nanotoxicology: Some physiological principles. *Occupational Medicine (Oxford, England)* 2006, 56:307-311.

19. Petros RA, Desimone JM: Strategies in the design of nanoparticles for therapeutic applications. *Nature Reviews Drug Discovery* 2010, 9:615-627.

20. FDA: Manual of Policies and Procedures: MAPP 5015.9, Reporting format for nanotechnology-related information in CMC review. *Center for Drug Evaluation and Research (CDER), Office of Pharmaceutical Science (OPS)* June 2010.

21. Yezhelyev MV, Gao X, Xing Y, Al-Hajj A, Nie S, O'Regan RM: Emerging use of nanoparticles in diagnosis and treatment of breast cancer. *The Lancet Oncology* 2006, 7:657-667.

22. Feynman RP: There's plenty of room at the bottom. *Engineering and Science* February 1960, 23:22-36.

23. Rathod KB, Patel MB, Parmar PK, Kharadi SR, Patel PV, Patel KS: Glimpses of current advances of nanotechnology in therapeutics. *International Journal of Pharmacy and Pharmaceutical Sciences* 2011, 3:8-12.

24. Ochekpe NA, Olorunfemi PO, Ngwuluka NC: Nanotechnology and drug delivery part 1: Background and applications. *Tropical Journal of Pharmaceutical Research* 2009, 8:265-274.

25. Roco MC: Towards a US National Nanotechnology Initiative. *Journal of Nanoparticle Research* 1999, 1:435-438.

26. Vo-Dinh T: Nanotechnology in Biology and medicine: The new frontier. In *Nanotechnology in Biology and Medicine: Methods, Devices, and Applications*. Edited by Vo-Dinh T: CRC Press; 2007:1-9.

27. Faraji AH, Wipf P: Nanoparticles in cellular drug delivery. *Bioorganic and Medicinal Chemistry* 2009, 17:2950-2962.

28. Walker Jr B, Mouton CP: Nanotechnology and nanomedicine: A primer. *Journal of the National Medical Association* 2006, 98:1985-1988.

29. Gary DJ, Puri N, Won YY: Polymer-based siRNA delivery: Perspectives on the fundamental and phenomenological distinctions from polymer-based DNA delivery. *Journal of Controlled Release* 2007, 121:64-73.

30. Ameres SL, Martinez J, Schroeder R: Molecular Basis for Target RNA Recognition and Cleavage by Human RISC. *Cell* 2007, 130:101-112.

31. Wiethoff CM, Middaugh CR: Barriers to nonviral gene delivery. *Journal of Pharmaceutical Sciences* 2003, 92:203-217.

32. Whitehead KA, Langer R, Anderson DG: Knocking down barriers: Advances in siRNA delivery. *Nature Reviews Drug Discovery* 2009, 8:129-138.

33. Takahashi Y, Nishikawa M, Takakura Y: Nonviral vector-mediated RNA interference: Its gene silencing characteristics and important factors to achieve RNAi-based gene therapy. *Advanced Drug Delivery Reviews* 2009, 61:760-766.

34. Judge A, MacLachlan I: Overcoming the innate immune response to small interfering RNA. *Human Gene Therapy* 2008, 19:111-124.

35. Kabilova TO, Meschaninova MI, Venyaminova AG, Nikolin VP, Zenkova MA, Vlassov VV, Chernolovskaya EL: Short double-stranded RNA with immunostimulatory activity: Sequence dependence. *Nucleic Acid Therapeutics* 2012, 22:196-204.

36. Huang L, Liu Y: In vivo delivery of RNAi with lipid-based nanoparticles. *Annual Review of Biomedical Engineering* 2011, 13:507-530.

37. Santel A, Aleku M, Keil O, Endruschat J, Esche V, Fisch G, Dames S, Löffler K, Fechtner M, Arnold W, et al.: A novel siRNA-lipoplex technology for RNA interference in the mouse vascular endothelium. *Gene Therapy* 2006, 13:1222-1234.

38. Van De Water FM, Boerman OC, Wouterse AC, Peters JGP, Russel FGM, Masereeuw R: Intravenously administered short interfering RNA accumulates in the kidney and

selectively suppresses gene function in renal proximal tubules. *Drug Metabolism and Disposition* 2006, 34:1393-1397.

39. Bicknell KA, Brooks G: Methods for delivering DNA to target tissues and cells. In *Gene Therapy: The Use of DNA as a Drug*. Edited by Brooks G: Pharmaceutical Press; 2002:23-49.

40. Kay MA, Glorioso JC, Naldini L: Viral vectors for gene therapy: The art of turning infectious agents into vehicles of therapeutics. *Nature Medicine* 2001, 7:33-40.

41. Marshall E: Gene therapy death prompts review of adenovirus vector. *Science* 1999, 286:2244-2245.

42. Heckl D, Schwarzer A, Haemmerle R, Steinemann D, Rudolph C, Skawran B, Knoess S, Krause J, Li Z, Schlegelberger B, et al.: Lentiviral Vector Induced Insertional Haploinsufficiency of Ebf1 Causes Murine Leukemia. *Molecular Therapy* 2012, 20:1187-95

43. Li Z, Düllmann J, Schiedlmeier B, Schmidt M, Von Kalle C, Meyer J, Forster M, Stocking C, Wahlers A, Frank O, et al.: Murine leukemia induced by retroviral gene marking. *Science* 2002, 296:497.

44. Hacein-Bey-Abina S, Von Kalle C, Schmidt M, Le Deist F, Wulffraat N, McIntyre E, Radford I, Villeval JL, Fraser CC, Cavazzana-Calvo M, et al.: A serious adverse event after successful gene therapy for X-linked severe combined immunodeficiency. *New England Journal of Medicine* 2003, 348:255-256.

45. Crystal RG: Transfer of genes to humans: Early lessons and obstacles to success. *Science* 1995, 270:404-410.

46. Templeton NS, Lasic DD: New directions in liposome gene delivery. *Molecular Biotechnology* 1999, 11:175-180.

47. Templeton NS: Myths concerning the use of cationic liposomes in vivo. *Expert Opinion on Biological Therapy* 2003, 3:57-69.

48. Conner SD, Schmid SL: Regulated portals of entry into the cell. *Nature* 2003, 422:37-44.

49. Takei K, Haucke V: Clathrin-mediated endocytosis: Membrane factors pull the trigger. *Trends in Cell Biology* 2001, 11:385-391.

50. Bareford LM, Swaan PW: Endocytic mechanisms for targeted drug delivery. *Advanced Drug Delivery Reviews* 2007, 59:748-758.

51. Akinc A, Thomas M, Klibanov AM, Langer R: Exploring polyethylenimine-mediated DNA transfection and the proton sponge hypothesis. *Journal of Gene Medicine* 2005, 7:657-663.

52. Dinçer S, Türk M, Pişkin E: Intelligent polymers as nonviral vectors. *Gene Therapy* 2005, 12:S139-S145.

53. Yamashiro DJ, Fluss SR, Maxfield FR: Acidification of endocytic vesicles by an ATP-dependent proton pump. *Journal of Cell Biology* 1983, 97:929-934.

54. Grabe M, Oster G: Regulation of organelle acidity. *Journal of General Physiology* 2001, 117:329-343.

55. Tang MX, Redemann CT, Szoka Jr FC: In vitro gene delivery by degraded polyamidoamine dendrimers. *Bioconjugate Chemistry* 1996, 7:703-714.

56. Wolff JA, Rozema DB: Breaking the bonds: Non-viral vectors become chemically dynamic. *Molecular Therapy* 2008, 16:8-15.

57. Asokan A, Cho MJ: Exploitation of intracellular pH gradients in the cellular delivery of macromolecules. *Journal of Pharmaceutical Sciences* 2002, 91:903-913.

58. Moghimi SM, Hunter AC, Murray JC: Nanomedicine: Current status and future prospects. *FASEB Journal* 2005, 19:311-330.

59. Hillaireau H, Couvreur P: Nanocarriers' entry into the cell: Relevance to drug delivery. *Cellular and Molecular Life Sciences* 2009, 66:2873-2896.

60. Rejman J, Oberle V, Zuhorn IS, Hoekstra D: Size-dependent internalization of particles via the pathways of clathrin-and caveolae-mediated endocytosis. *Biochemical Journal* 2004, 377:159-169.

61. Ogris M, Steinlein P, Kursa M, Mechtler K, Kircheis R, Wagner E: The size of DNA/transferrin-PEI complexes is an important factor for gene expression in cultured cells. *Gene Therapy* 1998, 5:1425-1433.

62. Akinc A, Lynn DM, Anderson DG, Langer R: Parallel synthesis and biophysical characterization of a degradable polymer library for gene delivery. *Journal of the American Chemical Society* 2003, 125:5316-5323.

63. Kabanov AV, Kabanov VA: DNA complexes with polycations for the delivery of genetic material into cells. *Bioconjugate Chemistry* 1995, 6:7-20.

64. Zhang Y, Yang M, Portney NG, Cui D, Budak G, Ozbay E, Ozkan M, Ozkan CS: Zeta potential: A surface electrical characteristic to probe the interaction of nanoparticles with

normal and cancer human breast epithelial cells. *Biomedical Microdevices* 2008, 10:321-328.

65. Kim T, Lee K, Gong MS, Joo SW: Control of gold nanoparticle aggregates by manipulation of interparticle interaction. *Langmuir* 2005, 21:9524-9528.

66. Singh BP, Menchavez R, Takai C, Fuji M, Takahashi M: Stability of dispersions of colloidal alumina particles in aqueous suspensions. *Journal of Colloid and Interface Science* 2005, 291:181-186.

67. George Zografi HS, James Swarbrick: Disperse systems. In *Remington's Pharmaceutical Sciences*, edn 18. Edited by Gennaro AR: Mack Publishing Company; 1990:257-309.

68. Nel AE, Mädler L, Velegol D, Xia T, Hoek EMV, Somasundaran P, Klaessig F, Castranova V, Thompson M: Understanding biophysicochemical interactions at the nano-bio interface. *Nature Materials* 2009, 8:543-557.

69. McNeil SE: Nanoparticle therapeutics: a personal perspective. *Wiley interdisciplinary reviews. Nanomedicine and nanobiotechnology* 2009, 1:264-271.

70. Goodman CM, McCusker CD, Yilmaz T, Rotello VM: Toxicity of gold nanoparticles functionalized with cationic and anionic side chains. *Bioconjugate Chemistry* 2004, 15:897-900.

71. Xia T, Kovochich M, Liong M, Zink JI, Nel AE: Cationic polystyrene nanosphere toxicity depends on cell-specific endocytic and mitochondrial injury pathways. *ACS Nano* 2008, 2:85-96.

72. Powers KW, Palazuelos M, Moudgil BM, Roberts SM: Characterization of the size, shape, and state of dispersion of nanoparticles for toxicological studies. *Nanotoxicology* 2007, 1:42-51.

73. Wick P, Manser P, Limbach LK, Dettlaff-Weglikowska U, Krumeich F, Roth S, Stark WJ, Bruinink A: The degree and kind of agglomeration affect carbon nanotube cytotoxicity. *Toxicology Letters* 2007, 168:121-131.

74. Alkilany AM, Murphy CJ: Toxicity and cellular uptake of gold nanoparticles: What we have learned so far? *Journal of Nanoparticle Research* 2010, 12:2313-2333.

75. Albanese A, Chan WCW: Effect of gold nanoparticle aggregation on cell uptake and toxicity. *ACS Nano* 2011, 5:5478-5489.

Chapter 2

NANODIAMONDS AS NOVEL NANOMATERIALS FOR BIOMEDICAL APPLICATIONS- DRUG DELIVERY AND IMAGING SYSTEMS

Kaur R, Badea I. International Journal of Nanomedicine.2012;1(7): In Press

Abstract

Detonation nanodiamonds (NDs) are emerging as delivery vehicles for small chemical drugs and macromolecular biotechnology products due to their 4 to 5 nm primary particle size, stable inert core, reactive surface and ability to form hydrogels. Nanoprobe technology capitalizes on the intrinsic fluorescence, high refractive index and a unique Raman signal of the NDs, rendering them attractive for *in vitro* and *in vivo* imaging applications. This review provides a brief introduction of the various types of NDs and describes the development of procedures that have led to stable single-digit-sized ND dispersions, a crucial feature for drug delivery systems and nanoprobes. Various approaches used for functionalizing the surface of NDs are highlighted along with a discussion on their biocompatibility status. The utilization of NDs to provide sustained release and improve dispersion of hydrophobic molecules, of which chemotherapeutic drugs are the most investigated, is described. The prospects of improving the intracellular delivery of nucleic acids by using NDs as a platform are exemplified. Photoluminescent and optical scattering properties of NDs together with their applications in cellular labeling are reviewed. Considering the progress that has been made in understanding the properties of NDs, they can be envisioned as highly efficient drug delivery and imaging biomaterials for animals and humans.

2.1 Introduction

Elemental carbon has six electrons with an electronic configuration of $1s^2$ $2s^2$ $2p^2$ in its ground state. The two electrons of the 1s orbital are core electrons, while the other four are valence electrons. The sp^2 hybridization of carbon atoms leads to the formation of the two-dimensional planar hexagonal structure of graphite. In this type of arrangement, the central carbon is linked to three other carbon atoms by σ-bonds with the remaining electron of the p_z-orbital forming a delocalized cloud of π electrons over the graphitic structure. The sp^3 hybridization of carbon atoms forms a rigid diamond structure with tetrahedral symmetry, where all the four valence electrons of the carbon atom each form an σ bond with the neighboring carbon atoms. The general lack of free electrons in the bulk structure of diamond accounts for their inertness. However, the surface structure of the material is different from the bulk, due to the relaxation at the surface and the need to terminate the bonds. Thus, the terminating structure on diamond surfaces involves univalent species such as H or OH or any deliberate terminating groups for both nano- and larger gem diamonds (synthetic and natural).

Nanodiamonds (NDs) have attracted a great deal of scientific and technological interest due to their unique structural, chemical, biological, mechanical and optical properties. Based upon their primary particle sizes, Shenderova and McGuire classified NDs into nanocrystalline particles (1 to ≥150 nm), ultrananocrystalline particles (2 to 10 nm) and diamondoids (1 to 2 nm) [1]. The ultrananocrystalline diamond particles are of particular interest for biomedical applications and focus has been largely placed on detonation NDs with primary particle size of 4 to 5 nm [2].

Figure 2.1 shows the classification of diamonds based on synthetic production methods. These include chemical vapor deposition diamonds, high-pressure high-temperature diamonds and detonation NDs.

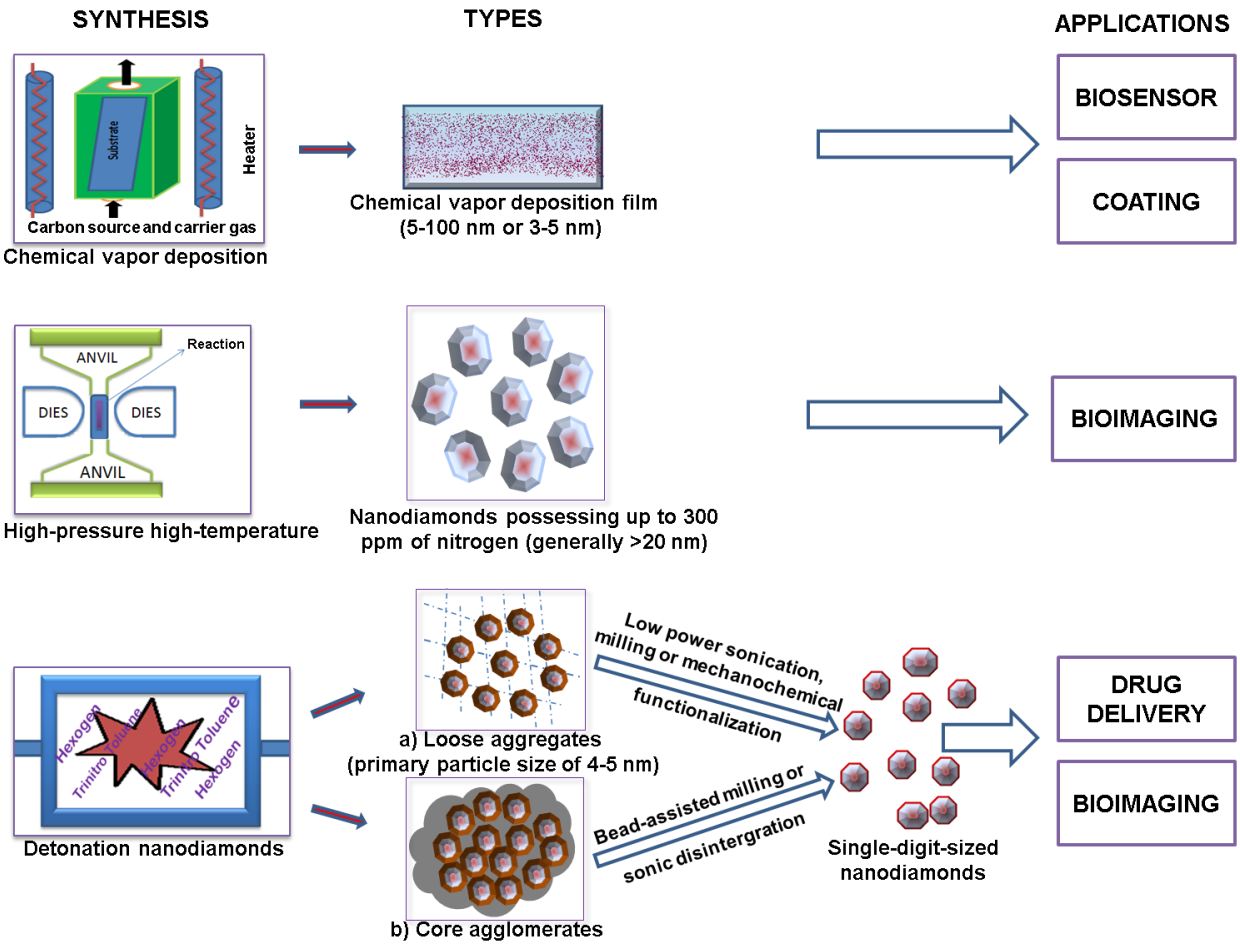

Figure 2.1: A schematic representation of types of nanodiamonds based upon their synthesis procedures and applications.

Deposition of carbon vapors on a diamond or non-diamond substrate leads to the formation of diamond films [3], of which nanocrystalline and ultrananocrystalline types are of major interest, due to their superior mechanical and wear resistant properties. Depending on the growth precursors (hydrogen-rich and carbon-poor precursors) and other deposition parameters such as biasing voltage, surface temperature and film pressure, the grain size of nanocrystalline diamond films can vary from 5 to 100 nm [4,5]. The ultrananocrystalline diamond films, with a much smaller grain size of 3 to 5 nm are usually synthesized under hydrogen-poor and argon-rich conditions [6-8]. In addition to the difference in grain size, these two types of diamond films also differ in the sp^2 carbon content. The nanocrystalline diamond films grown in a methane-rich environment possess up to 50% sp^2- bonded carbon structure, which decreases drastically to less than 0.1% with the decrease in the amount of methane [9]. For the ultrananocrystalline diamond films, the sp^2- bonded carbon fraction ranges from 2 to 5% [9]. Scanning transmission electron microscopic images of nanocrystalline [4] and ultrananocrystalline [10] diamond films are shown in Figure 2.2.

The ultrananocrystalline diamond films are emerging as superior substrates to that of silicon, platinum and quartz for coating biomedical implants [11,12]. This advantage is due to their low cytotoxicity, dense structure, high surface roughness, sp^2 structural boundaries and surface dangling bonds [11,12]. These films also exhibit desired characteristics for producing micro-electro-mechanical devices due to their robustness, high Young's modulus, high acoustic velocity, high resistance to fracture and low coefficient of friction (~0.01–0.1) [13-16]. Similarly, high stability, superior electrochemical properties, selectivity in binding biological materials and biocompatibility of the nanocrystalline diamond films have opened up their potential in the development of biosensors [17,18].

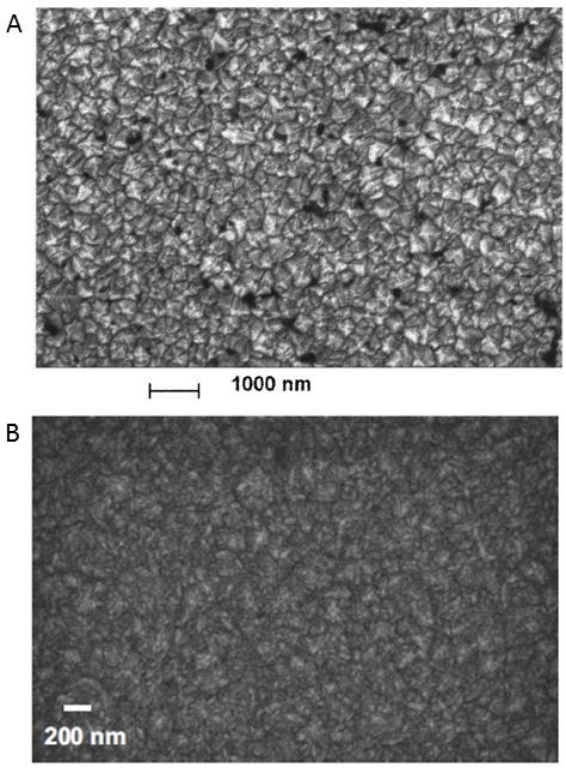

Figure 2.2: Scanning electron microscopic image of nanocrystalline and ultrananocrystalline diamond film.

Scanning electron microscopic image of (A) nanocrystalline [4] and (B) ultrananocrystalline [10] diamond film grown on silicon substrate. "Reprinted (A) with permission from [4]. Copyright (2003), American Institute of Physics." "Reprinted (B) with permission from [10]. Copyright (2007) by the American Physical Society."

Synthetic diamonds produced by a high-pressure high-temperature technique could contain 100 to 300 ppm of nitrogen [19-22]. High energy irradiation of these diamond particles causes damage by knocking a diamond carbon atom out of the structure, creating vacancies (V) [23]. Upon thermal annealing, these vacancies move closer to the nitrogen (N) centers to form nitrogen-vacancy (N-V) color defect centers [23]. These centers are responsible for the emission of fluorescence [24]. Hence, high-pressure high-temperature synthetic diamonds have been widely explored as imaging agents in cellular models [19,22,25]. However, the high production cost and the general inability to produce diamond particles smaller than 20 nm are significant barriers to their use in biomedical sciences.

The third category of diamonds, detonation NDs, also known as ultradispersed diamonds, are synthesized relatively inexpensively on a large scale by detonation of carbon explosives with a $C_mH_nN_oO_p$ composition [26]. An overall negative oxygen balance of the explosive mixtures is required in the detonation chamber [26] to prevent the complete combustion of the carbon into its gaseous products. Generally, a mixture of trinitrotoluene and hexogen in a mass ratio ranging from 40:60 to 70:30 is utilized [27]. A shock wave produced by the detonator compresses and heats the composition mixture, leading to its explosion [26]. A large amount of energy is released during this exothermic process, which consequently raises the temperature in the detonation chamber to 3000-4000ºC and the pressure to 20-30 GPa, to favor the synthesis of the diamond particles (Figure 2.3) [28,29]. After the detonation is complete, a rapid cooling is achieved either by using an inert cooling gas (dry synthesis) or water (wet synthesis) [29]. The cooling of the detonation products is crucial to minimize transformation of the diamond phase into the graphitic forms, in accordance with the phase diagram (Figure 2.3) [28,29]. The average primary particle size of NDs generated by this technique is 4 to 5 nm (Figure 2.4) [28,30].

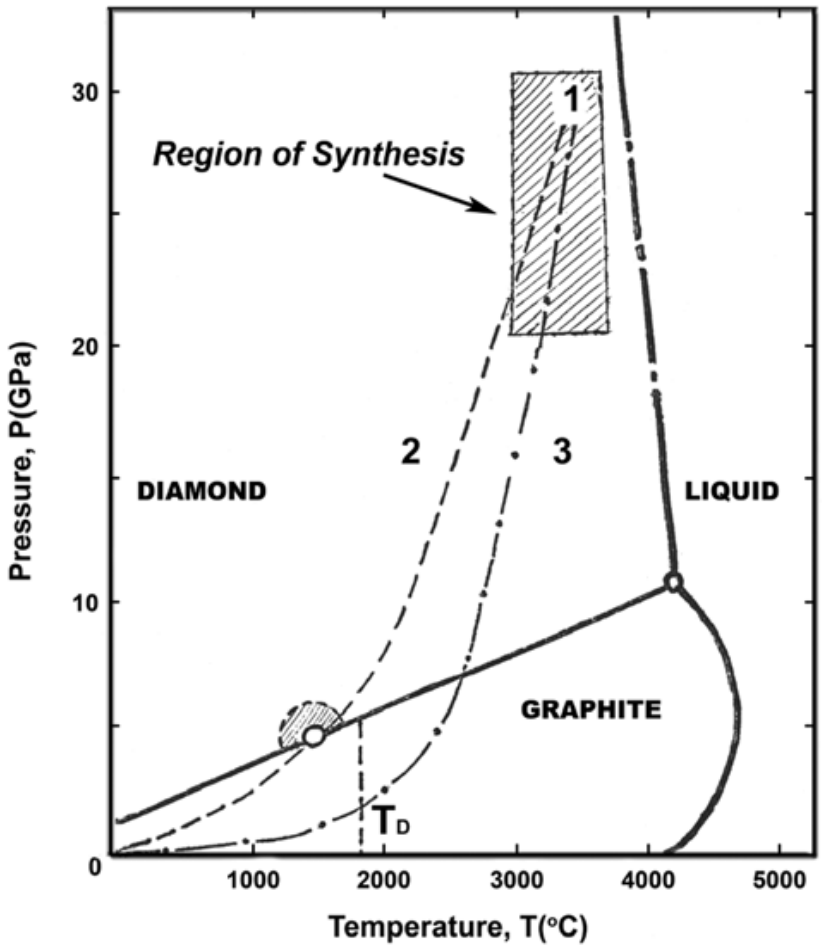

Figure 2.3: Pressure-Temperature phase diagram for carbon.

Phase diagram for carbon depicting the (1) pressure and temperature requirements for synthesis of detonation nanodiamonds, and cooling profile of products produced by (2) wet detonation synthesis and (3) dry detonation synthesis [29]. "Reproduced courtesy of IOP Publishing Ltd".
Note: T_D represents Debye temperature.

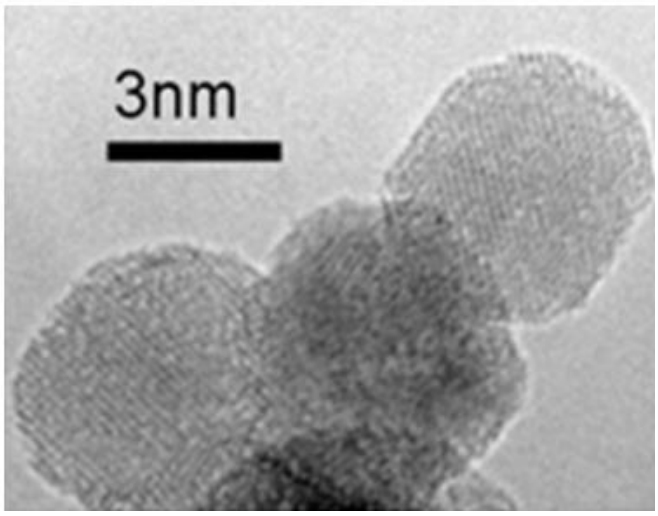

Figure 2.4: High resolution transmission electron microscopic image of detonation nanodiamonds.

Image is courtesy of Bogdan Palosz, IHPP, Warsaw, Poland

Although the primary particle size of NDs obtained by the detonation technique is well suited for biomedical studies, the detonation products need to be extensively purified. Depending on the materials and matrices present during their production, detonation NDs can contain oxides and carbides, including those of iron, chromium, silicon, calcium, copper, potassium, titanium and sulfur, in addition to carbon soot [26]. To remove surface metallic impurities, NDs are treated with classic acidic treatments consisting of sulfuric acid, and its mixtures with nitric acid or potassium dichromate [31]. A hydrofluoric acid and nitric acid combination has also been used to eliminate metallic contaminants from the particles [32]. The oxidization and subsequent removal of sp^2- bonded carbon structures, present either in amorphous or graphitic forms, is achieved by the use of liquid oxidizers such as sodium peroxide, a chromium trioxide and sulfuric acid mixture, or a nitric acid and hydrogen peroxide mixture [31]. Thermal oxidation process, uses temperatures of 400 to 430ºC to allow the oxidation of sp^2- bonded carbon species in the air, with negligible alteration in sp^3- bonded carbon structures [33]. These temperature requirements for the selective oxidation of sp^2- bonded carbon species were confirmed by Pichot et al [32]. The oxidation of NDs at a high temperature using air, containing ozone, is another approach that results in the removal of the majority of sp^2- hybridized carbon structures [34]. The ozone-air treatment, also known as the gas phase treatment, is ecological and efficient as the purification of NDs is achieved without using the corrosive liquid oxidizers [34].

Although the size, shape and surface properties of NDs are determined by the nature of explosion and purification conditions, their basic structure follows a core and shell model [2]. The diamond carbon forms the inert core and the surface shell is partially comprised of graphitic structures [30,35,36]. In addition, a wide variety of functional groups such as carboxyl, hydroxyl, lactone, anhydride, ketone and ether can be present on the surface of these ND particles [36,37]. The acid purification treatment increases the density of carboxylic and hydroxylic groups on the surface of NDs, resulting in their hydrophilicity.

The economical large-scale production of detonation NDs provided considerable impetus to technological applications. For example, the antifriction properties of NDs and their soot make them ideal candidates as wear-protective additives [38]. The stability of these particles at extreme temperatures may lead to their storage in liquid nitrogen and use in composite manufacturing [39]. The large surface area of NDs is suitable for adsorbing biomolecules,

presenting them as an attractive material for isolating proteins [40,41] and pathogenic microorganisms [42]. However, it was not until the identification and characterization of single-digit-sized NDs in the dispersion medium that NDs were applied in biomedical sciences.

2.2 NDs in the Biomedical Field

The application of NDs in biological sciences requires the stable dispersion in a formulation medium, the ability to conjugate with biomolecules, an inherent biocompatibility and the ability to penetrate target tissues and cells.

2.2.1 Dispersion of NDs

Detonation NDs possess a strong propensity to aggregation when dispersed in a liquid formulation medium, hindering their biomedical applications. Several attempts to explain the aggregation phenomenon have focused on surface forces. The harsh conditions in the detonation chamber could create dangling bonds on the ND surfaces [43]. These free electron surfaces are sufficiently reactive to form functional groups, which then interact via various intermolecular surface forces such as van der Walls and dipole-dipole interactions, and hydrogen bonding [43]. In addition, these surface groups can also react to create covalent bonds between the primary particles, producing core aggregates [44]. Another study suggests that electrostatic forces induced by the oppositely charged facets of polyhedral shaped NDs are the primary cause for creating core aggregates [45]. This finding was supported later with the aid of electron microscopy and computer simulations [46]. Other than the surface forces, the "graphitic soot like structures" around the particles can also bind individual ND particles together into core aggregates (Figure 2.1) [35,36].

Conventional techniques of disintegration such as milling, emulsification and low power sonication have been ineffective in breaking down the tightly bound core aggregates of NDs to less than 10 nm [35]. Therefore, in an attempt to achieve primary-sized NDs, milling was carried out using an excessive amount of 100-µm silica beads [35]. Single-digit-sized NDs were obtained after an hour of sonication of the diluted milled suspension and the stability of the resulting aqueous colloid was maintained for a year [35]. However, reconstitution with water after drying the nanodispersion resulted in reaggregation with 2.3 µm size aggregates [35]. Bead-

assisted sonic disintegration using zirconia beads has also gained interest for breaking the ND aggregates in aqueous medium to single-digit-sized particles [47]. This mechanical technique involves the combination of shear forces induced by beads with their acceleration during cavitation created by intense ultrasonic waves. These primary sized NDs exhibited very good colloidal stability in polar solvents such as water and DMSO [47]. However, contamination from the beads [35] and sonotrode material itself can be a barrier for these technologies [45,48] in addition to the structural alterations [49].

Bead-assisted milling [47,50] or sonication [48] yielded clear, but dark brown nanodispersions of diamond particles. It should be noted that sonication creates microbubbles in liquid media, which implode violently, generating a local temperature of ~1900 K at the bubble-liquid interface [51]. The shock waves produced during high power sonication cause high-speed collision of the beads with ND particles, which can lead to the conversion of the diamond carbon into its graphitic form, according to the diamond-graphitic phase transition phenomenon occurring at temperatures greater than 1200 K [52]. Similarly, a temperature of 1800 K can be attained during milling collisions when the speed of the blades is between 0.1 to 10 cm/s [49,50]. This could explain the black coloration of the colloids observed after high speed milling or high-power bead-assisted probe sonication.

Mechanochemical treatment, which involves the breaking of ND aggregates by mechanical energy and the concurrent loading of electrolytes or surfactants on a newly created surface, was also explored to achieve stable dispersions with a noticeable size reduction [53]. However, a primary dispersed particle size of less than 10 nm was not achieved [53]. Ultracentrifugation, a contamination-free procedure, resulted in 4 nm size NDs that formed a stable colloidal dispersion in water [54]. The yield of single-digit-sized particles was only 1% after centrifugation of the ND suspension at an acceleration of 2.80×10^5 g for 40 minutes [54]. Increasing the centrifugation time to 240 hours at an acceleration of 2.0×10^4 g did not improve the yield significantly, generating 6% of NDs with an average size of 8 nm [54]. Hence there is still a need for development of easy, feasible, contamination-free techniques that can result in disaggregation of NDs at the laboratory scale.

2.2.2 Surface Modification of NDs

All together, the nano-size, the larger surface area, and potential for purification with oxidizing agents, make NDs a viable candidate for surface functionalization. Figure 2.5 summarizes approaches used in the past to introduce various functionalities on the surface of NDs [44,55-61]. One of the earliest modifications of the ND surface involved the generation of surface radicals, which then acted as substrates for synthesizing carboxylic [55] and dicarboxylic acid [56] functionalized NDs. For a high surface loading, it is essential to achieve surface uniformity. Reactions with hydrogen [55,56], chlorine [57], and fluorine [58] have been explored to attain surface homogeneity as well as reactivity enhancement. The surfaces of chlorinated NDs were further modified with hydroxyl, amine and carbon fluoride groups [57]. Finally, reactions of NDs with alkyllithium, ethylenediamine and glycine ethyl ester hydrochloride generated alkyl, amino and glycine substituted NDs, respectively [58].

Surface functionalization has also emerged as a novel treatment for reducing aggregate sizes of NDs. Functionalization with long alkyl chains reduced the particle size from 15 μm to 150-450 nm [59]. The long alkyl chain-modified NDs showed an enhanced dispersibility in organic solvents compared to their pristine form [59]. Similarly, surface modification with fluorine contributed to size reduction from 1930 to 160 nm [58]. A noticeable size reduction of the micrometer-sized pristine NDs to ~ 50 nm was also achieved upon reduction of the ND surface groups with borane, which, after being grafted with alkyl silane, were used to synthesize biotinylated NDs with a surface loading of 1.45 mmol/g [61].

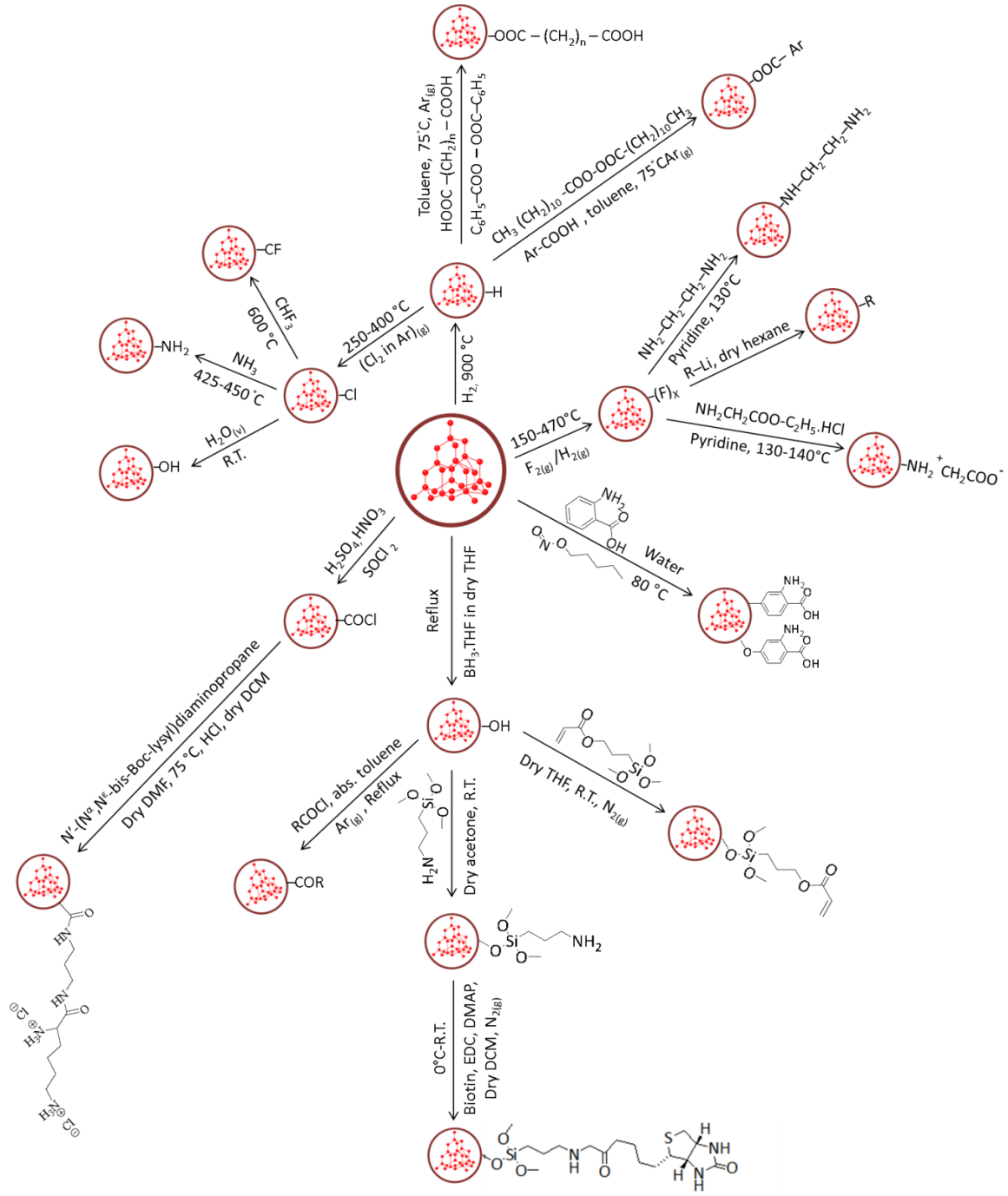

Figure 2.5: A schematic representation of approaches used for modification of nanodiamond surfaces.

Abbreviations: Abs, Absolute; R.T., Room temperature; R, alkyl group; Ar, aromatic group; THF, tetrahydrofuran; DMAP, (dimethylamino)pyridine; EDC, (1-ethyl-3-[(3-dimethyl amino)propyl] carbodiimidehydrochloride)

2.2.3 Biocompatibility Studies of NDs

The intrinsic biocompatibility of detonation NDs has been supported by the results of a number of studies [62-67], however, some studies have refuted this claim by arguing that NDs can induce toxic responses under certain conditions [68,69].

Biocompatibility of 2 to10 nm sized acid- or base-purified NDs was first demonstrated in neuroblastoma, macrophages, keratinocytes and PC-12 cells [62]. By considering the mitochondrial activity as a key determinant of cellular viability, NDs up to a concentration of 100 µg/mL were reported not to be cytotoxic over a 24 hour incubation period [62]. In addition, NDs showed higher biocompatibility than carbon black, and single and multi-walled carbon nanotubes [62,63]. When incubated for 24 hours with NDs at the concentration range of 25 to 100 µg/mL, no significant cell death occurred in neuroblastoma cells [63]. Similarly, alveolar macrophages maintained the cellular viability upon exposure to 25 µg/mL concentration of NDs for 24 hours [63]. In addition to mitochondrial function, the inflammatory activity of cells has also been a key determinant of the toxic effects of nanomaterials [67]. There was no significant increase in the gene expression of inflammation biomarkers, such as interleukin-6, tumor necrosis factor-alpha and nitric oxide synthase, in murine macrophages after incubation with a 100 µg/mL concentration of NDs [67]. In addition, no attenuation in the gene expression level of Bcl-x, which generally diminishes with an increased risk of apoptosis, endorsed the intrinsic biocompatibility of these diamond nanoparticles [67].

Various studies have demonstrated that the toxicity of NDs can vary depending upon their surface chemistry [69,70], type of cell line [69] and the treatment medium [68] composition. The amine terminated NDs exhibited a higher toxicity (~22% cell death) than hydroxyl (~11%) and carboxyl group (~7%) terminated NDs in human embryonic kidney cells at a concentration of up to 200 µg/mL [70]. The carboxylated NDs did not show any significant genotoxic effects in mouse embryonic fibroblasts [71], but induced DNA damage in mouse embryonic stem cells [69], although to a lesser extent than that occurred with multi-walled carbon nanotubes [72]. In another instance, a 100% viability of human cervical cancer (Hela) cells was observed after incubating them with 0.1-100 µg/mL NDs in a medium containing serum for 24 hours [68]. In the absence of serum, this viability dropped dramatically to almost

0% within 6 hours of dosage with 50 μg/mL NDs [68]. A similar behavior has been also observed with other nanoparticles such as carbon black [73] and silica [74]. Although there is no clear explanation of serum-dependent cytotoxicity of nanoparticles so far, several hypotheses have been put forth. It is believed that serum can have a protective effect on the cells by coating the surface of nanoparticles that are thought to have inherent cytotoxic effects [68,73,75]. While on the one hand, serum is found to enhance the dispersion stability of the nanoparticles [68,73,76], on the other hand, serum promotes aggregation [74]. The cellular internalization of nanoparticles was observed to be higher in the absence of serum than in its presence [73,74], which might be one of the reasons for the lower cellular toxicity of nanoparticles when incubated with serum. Another study found that nanoparticles could adsorb the essential micronutrients from the medium and hence indirectly produce cytotoxic effects by depleting the cellular structures of essential nutrients [77]. Finally, the serum proteins themselves are essential for the growth of the cell, thus their absence can have a negative effect on overall cell proliferation. However, it is important to note that in some studies, NDs did not show significant toxicity, even when incubated with cells in medium lacking serum [62,63].

In addition to the cellular studies, some *in vivo* studies have also been conducted to evaluate the toxicity of NDs. Intravenous administration of 125 mg of modified NDs did not cause any death in rabbits [78]. Neither the red blood cell count nor the hemoglobin level of rabbits decreased after 15 minutes of administering 50 mg of modified NDs, intravenously [78]. However, after 48 hours of injection, the levels of biochemical molecules such as total bilirubin, triglyceride, low density lipoproteins, aspartate aminotransferase and γ-glutamyltranspeptidase altered significantly [78]. In another study, an oral administration of 0.002 to 0.05 wt.% of ND hydrosols to mice, in place of water, for 6 months showed no significant abnormalities in growth or organs weight [39]. The NDs exhibited low pulmonary toxicity and were cleared from the lungs after 90 days of intratracheal instillation in ICR strain mice [79]. Furthermore, the clearance of XenoFluor 750 labeled NDs from all the body organs of wild type FVB/N mice occurred in 3 to 10 days after tail vein injection at a dose of 120 μg [80].

In summary, NDs have shown biocompatibility in various cell lines and some animal models with minimal or no cytotoxicity, demonstrating their potential for biomedical applications. However the purity, surface chemistry and dimensions of particles should be

considered carefully. More comprehensive and long term animal studies need to be conducted to verify the safety of NDs before proceeding to human clinical trials.

2.2.4 Cellular Uptake of NDs

A number of studies have demonstrated the ability of NDs to internalize into cells [19,25,62,64-66,81-83]. Faklaris et al demonstrated that NDs having an average size of 46 nm internalize into Hela cells predominantly by clathrin-mediated endocytosis after 2 hours of incubation [83]. In addition to the clathrin-mediated endocytic pathways, 100 nm sized NDs were also found to be internalized via macropinocytosis by cancer and stem cells after 4 hours of incubation [71]. The intracellular localization of the NDs suggests that these nanoparticles have a potential to be employed for the intracellular delivery of therapeutic molecules. While the NDs used in these studies showed only perinuclear localization with no translocation to the nucleus [71,83], fenton-treated NDs were detected in the nucleus of Hela cells [84]. The internalization of NDs into cells could be dependent upon their surface characteristics [84], incubation time period, and other physiochemical parameters such as size, shape, aggregation etc. Nuclear internalization of NDs opens up perspectives for their use as delivery agents for nucleic acids. Figure 2.6 summarizes the prominent applications of NDs in the biomedical field.

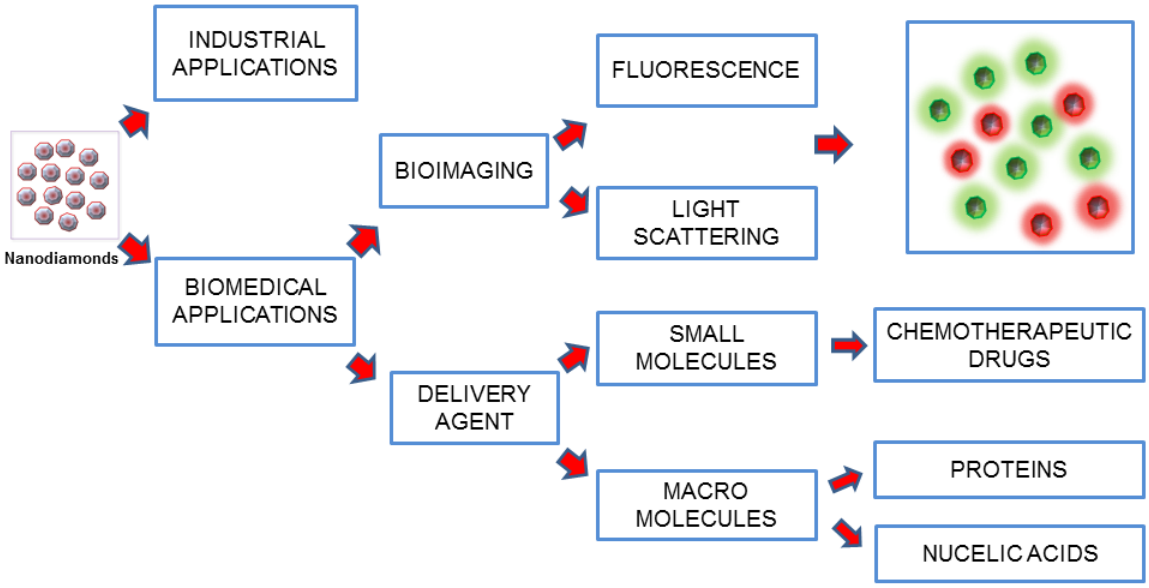

Figure 2.6: A schematic representation of the applications of nanodiamonds.

2.3 Applications of NDs as Drug Delivery Agents

The large surface area of biocompatible NDs having several surface functionalities is ideal for conjugating various biochemical entities. The suitability of the carrier can be projected from its loading capacity as well as from its ability to protect and retain the inherent therapeutic effects of the attached entities. A high loading capacity allows a high concentration of payload to be delivered while using a lesser amount of delivery agent itself. In parallel to the loading capacity, the release of payload from the carrier is also important. The feasibility to tune the release of cargo from the carrier is advantageous in developing novel applications of these delivery agents, such as controlled and sustained release delivery. Diamond nanoparticles are being investigated globally for improving the intracellular delivery of small molecules and biotechnological products, with a major focus on chemotherapeutic agents. Although some studies have made use of the ND surfaces to bind drugs via chemical bonding,[85,86] the majority have focused on physical adsorption procedures [67,68,80,87]. This simple process of loading cargo onto the carrier via physical interactions avoids the use of complex chemical reactions, which in addition to high cost, can also affect the therapeutic activity of the attached entity by causing structural alterations [88].

The use of NDs as a small molecule delivery agent, using chemotherapeutic drugs as model drugs, has been exemplified by various studies.

2.3.1 Delivery of Small Molecules

In 2007, the suitability of NDs to act as a delivery agent of doxorubicin hydrochloride (DOX) was evaluated [67]. The investigation was based on the rationale that the surface carboxylic and hydroxylic groups of detonation NDs can interact efficiently with the amine groups of DOX via ionic forces when dispersed in aqueous medium [67]. The surface loading of DOX on NDs increased from 0.5 to 10 wt.% upon addition of 1% sodium chloride solution to their aqueous dispersion, and the removal of salt favored the release of DOX [67]. NDs loaded with DOX were suggested to assemble in the form of loose clusters, such that a certain amount of DOX adsorbed on the NDs surface resides within the cavity of the cluster (Figure 2.7A) [67]. This strategy of drug entrapment in loose aggregates of NDs could provide an advantage by

minimizing the systemic adverse effects of the naked DOX [67]. Thus, ND-based delivery systems could overcome the limitation to the use of high concentrations of chemotherapeutic drugs [89] in cancer treatments. In addition, the lower cytotoxicity of the ND-DOX composite in mouse macrophages and human colorectal cancer cells compared to bare DOX in a 48 hour period could be beneficial in sustained drug release [67].

Another study, published in 2010, proposed NDs as efficient multifunctional delivery agents for the chemotherapeutic drug, 10-hydroxycamptothecin (HCPT) [68]. Similar to the previous study by Huang et al [67], NDs were able to adsorb the drug onto their surfaces via simple physical forces [68]. However in this case, the surface loading of HCPT was considerably enhanced to 50 wt.% from 0.4 wt.% with an increase in pH of the HCPT solution from 7 to 8.2, rather than by means of salination [68]. NDs released HCPT slowly into the PBS medium over a period of 5 days, with only 38% release observed in the first 24 hours [68]. In addition, the ND-HCPT complex showed almost 2.5 times higher cytotoxicity in Hela cells compared to the chemotherapeutic activity of HCPT alone, credited to the ND triggered intracellular delivery of HCPT [68]. Bovine serum albumin adsorbed on the surface of NDs rapidly (< 1 hour) while HCPT showed a gradual adsorption (> 120 hours) [68]. Based on this differential adsorption, a model suggesting porous clusters of NDs was developed in which small molecules diffuse inside the clusters (Figure 2.7A) and the large molecules adsorb only on the outer surface of NDs (Figure 2.7B) [68]. Hence, NDs can facilitate the intracellular delivery of both small molecule drugs and large therapeutic biomolecules.

Detonation NDs have also been utilized to increase the aqueous dispersibility of hydrophobic drugs. Poorly-water soluble chemotherapeutic drugs such as, Purvalanol A with therapeutic activity against liver cancer [90], and 4-hydroxytamoxifen with a high potential to treat breast cancer [91,92], are soluble in the polar, organic solvents DMSO and ethanol, respectively [87]. The use of non-aqueous solvents limits the parenteral administration of these formulations in clinically relevant settings. However, when formulated with NDs, the aqueous dispersibility of Purvalanol A and 4-hydroxytamoxifen enhanced markedly [87]. By adsorbing the drug on their surfaces, NDs considerably reduced particle size and increased the zeta potential of these drugs in water, promoting their dispersibility and, potentially, cellular uptake [87]. Similar to the previous studies, NDs preserved the therapeutic activity of the drugs as

demonstrated by DNA fragmentation and MTT assay for ND-4-hydroxytamoxifen and ND-Purvalanol A composites, respectively [87]. These findings suggest that NDs could play an important role in designing injectable formulations of water insoluble drugs.

The efficacy of NDs to deliver chemotherapeutic drugs was examined recently in animal models for the first time [80]. In addition to generalized toxicity, large particle size and poor water solubility, chemotherapeutic drugs also suffer from acquired and intrinsic chemoresistance of tumor cells [93]. Among various other factors, overexpression of P-glycoprotein on the cellular membranes, causing premature efflux of the drug from cells, is the leading cause in developing chemoresistance in mammalian tumor cells [94,95]. This challenge could be addressed by using a delivery system that not only enhances the uptake of the chemotherapeutic drugs but also retains them in the cancer cells for a longer period of time. The study revealed that DOX bound to the ND surface was significantly more toxic towards DOX resistant mouse LT2-Myc liver and 4T1 mammary tumor models compared to bare DOX [80]. The high chemotherapeutic efficacy of the ND-DOX composite was attributed to ND mediated DOX retention in tumors cells as determined by fluorescence microscopy and quantitative analysis [80]. Moreover, long term treatment showed superiority of the DOX bound to ND over the bare DOX in preventing tumor growth [80]. NDs not only circumvented the premature efflux of DOX from tumor cells, but also improved the adverse effects of naked DOX, by significantly reducing myelosuppression and early mortality [80]. In addition, NDs increased the circulation half time of DOX from 0.83 to 8.43 hours [80], which further validated their sequestering behavior, which was proposed in earlier studies [67,68].

In summary, formulation of chemotherapeutic drugs with NDs improves the pharmaceutical properties of the agents by high surface loading, improved aqueous dispersibility, sustained release, and enhanced retention in chemo-resistant cells. These properties are due to the hydrophilic functional group-enriched surface, large surface to volume ratio, ability to form loose clusters, improved cellular delivery, and biocompatibility of the NDs. Hence, NDs are suitable platforms to build nanoparticles for overcoming some of the major deficiencies of the chemotherapeutic drugs.

In addition to small molecules, NDs have also shown potential as delivery agents for protein, DNA and RNA.

2.3.2 Delivery of Biotechnology Products

The potential of NDs as a targeted protein delivery vehicle was evaluated in a pH-dependent system [96]. By means of physical adsorption, NDs achieved a considerably high surface loading of bovine insulin (~80%) in pH-neutral water at a weight ratio of 1:4 of insulin:ND [96]. Similar to a previous study [87], the physiochemical properties of the insulin, including size, zeta potential and polydispersity index, improved after interacting with NDs [96]. It suggests that NDs have the ability to facilitate uniform sized complex formation [96]. Further, the release of insulin from the surface of NDs was almost 20 times higher at a pH of 10.5 as compared to that obtained in neutral pH medium [96]. The applicability of ND-bound-insulin was verified by MTT assay in serum-starved murine macrophages [96]. A higher cellular viability was observed with sodium hydroxide treated ND-insulin in comparison to neutral pH treated ND-insulin [96]. Similar results were obtained by measuring the gene expression of Insulin 1 and granulocyte colony stimulating factor in serum starved mouse adipocytes [96]. Hence, formulations of insulin can be designed with NDs to target the recovery of injured tissues [97] that have a basic pH due to bacterial growth [96,98].

Although there is compelling evidence to support the utilization of NDs as drug delivery agents for small molecules, their potential as gene delivery vectors has been less widely explored. The major obstacle to the use of naked nucleic acids as therapeutics is their inefficient cellular delivery. Physicochemical characteristics such as high negative surface charge and large molecular weight are barriers in the efficient cellular internalization of the DNA [99,100] and siRNA [101,102]. While DNA is too large for cellular uptake, the relatively small size of siRNA also poses an additional challenge to its cellular delivery, as particles having a molecular weight less than 50 kDa are susceptible to excretion through glomerular filtration [101,103]. Zhang et al, investigated NDs as a platform to build enhanced plasmid DNA delivery systems (Figure 2.7C) [104]. At first, they coated NDs with polyethyleneimine 800 (PEI800), and then allowed them to interact with luciferase plasmid DNA via electrostatic forces [104]. NDs were found to enhance the transfection efficiency of the polymer by 70 fold at a 15:1 weight ratio of ND-PEI800:pDNA in Hela cells, which might be due to ND mediated cellular and nuclear uptake of the plasmid DNA [104]. Similar to DNA delivery, the ND-based complex (ND-PEI800) was

used to deliver anti-green fluorescent protein-small interfering RNA (siRNA) to breast cancer cells expressing green fluorescent protein (Figure 2.7D) [105]. Compared to the PEI:siRNA, the ND-PEI800:siRNA complex at a weight ratio of 3:1 showed almost two fold higher knockdown in cellular green fluorescent protein expression [105]. In the presence of serum in the treatment medium, ND PEI800:siRNA complex showed better knockdown in green fluorescent protein expression as well as lower cytotoxicity than Lipofectamine that is a gold standard for *in vitro* delivery of nucleic acids [105]. Therefore, NDs have potential to enhance the transfection ability of polymers while remaining biocompatible to the cell lines.

However, there are limited studies of the applications of NDs as drug delivery agents so far. More studies are needed to verify their potential and to translate their use as a delivery agent into clinical applications.

Figure 2.7: A schematic representation of the binding behavior of nanodiamonds with different biomolecules.

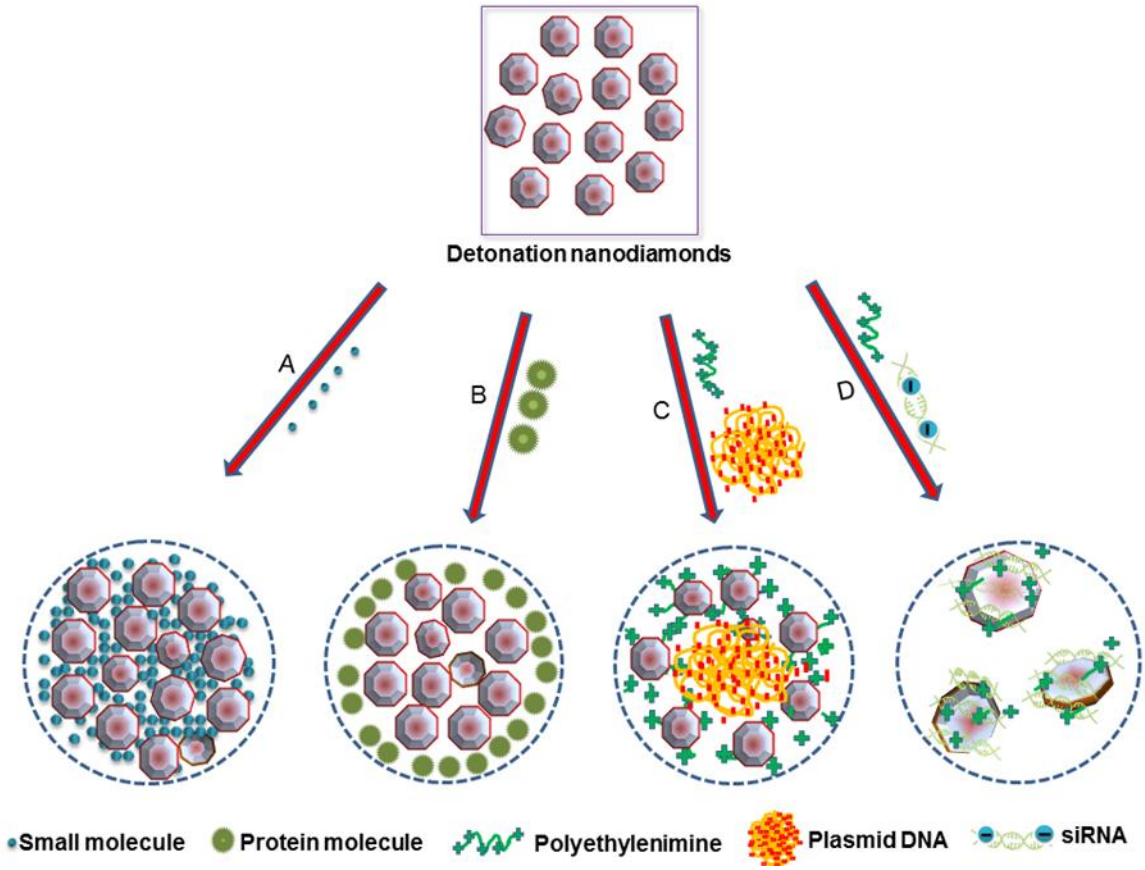

A schematic diagram to represent the binding of detonation nanodiamonds with (a) small molecules [67,68], (b) proteins [68], (c) plasmid DNA [104] and (d) siRNA [105].

2.4 NDs as Bioimaging Agents

2.4.1 Fluorescence of the NDs

Based upon the presence or lack of nitrogen impurities in the crystal lattice structure, the natural diamonds are classified as type I or type II, respectively [106]. The arrangement of nitrogen impurities is used to sub-classify type I diamonds into type Ia and type Ib [107]. While type Ib contains atomically dispersed single substitutional nitrogen impurities (C-centers), type Ia diamonds comprise an aggregated form of nitrogen [107]. The latter are categorized further into type IaA, having two aggregated nitrogen atoms (A-center), type IaB, having platelets and four aggregated nitrogen atoms surrounding the nearest lattice vacancy (B-center), and type IaA/B, possessing the characteristics of both type IaA and type IaB [107].

Besides natural diamonds, synthetic diamonds manufactured under high-pressure high-temperature conditions are also known to contain a high amount of nitrogen in the form of impurities [108]. The natural diamonds have mainly aggregated nitrogen defects (type Ia), while synthetic high-pressure high-temperature diamonds are predominantly embellished with single substitutional nitrogen centers (type Ib) [109]. Irradiation damage of type Ib diamond crystals creates intrinsic defects such as vacancies, which upon thermal annealing move towards nitrogen centers (N), and get trapped within to form nitrogen vacancy (N-V) color defect centers [23]. Generally, irradiation of these diamond particles is carried out by high energy electron (~2-MeV) [110-112] or proton (~3-MeV) [64,113] beam using Van de Graaff or tandem particle accelerators, respectively. These sources generate vacancies but are difficult to install in usual pharmaceutical or biomedical laboratory settings due to their high cost, complicated setup and safety issues [19]. Hence, to increase the feasibility of the production of fluorescent NDs on a wider scale, a moderate scale energy helium ion (40-keV) beam emanating from a radio frequency positive ion source was proposed [19]. Even though a much lower energy source was used in this irradiation process, none of the essential fluorescence spectral features were lost apart from a decrease in fluorescence intensity, when compared to the fluorescence spectra generated by 3-MeV energy proton beam irradiated particles [19]. This method not only benefited the laboratories having ordinary infrastructure in producing fluorescent NDs, but also

increased the yield of fluorescent NDs by creating a higher number of vacancies compared to electron and proton beam irradiated NDs [19,113,114].

Irradiated synthetic type Ib NDs, after 2 hours of annealing at 800°C, generated mainly two types of N-V defect centers, neutral nitrogen vacancy $(N\text{-}V)^0$ with zero phonon line at 575 nm and negatively charged nitrogen vacancy $(N\text{-}V)^-$ with zero phonon line at 638 nm [19,83,111]. Among all the color centers, $(N\text{-}V)^-$ dominate the fluorescence spectra of type Ib diamonds [23,112]. This defect center absorbs light photons at ~560 nm and fluoresces brightly at ~700 nm with a quantum efficiency close to 1 [115]. Therefore, these centers offer characteristically bright red fluorescence to diamond particles upon excitation with green-yellow light [22] and hence have found applications for high-pressure high-temperature NDs in imaging studies [19,25].

Extreme photostability of $(N\text{-}V)^-$ defect centers [116,117] provides a greater advantage to NDs to emerge as an excellent candidate for long-term cellular imaging over commonly used fluorophores. The red fluorescent NDs (100 nm) remained stable with no observed photobleaching, upon continuous exposure to a 100 W lamp power for 480 minutes, whereas similarly sized red fluorescent polystyrene nanospheres photobleached within 30 minutes of photoexcitation [64]. In another instance, no photobleaching occurred in both 100 and 35 nm sized red fluorescent NDs when photoexcited with 8 kW/cm^2 power density of light for 5 minutes [25]. On the other hand, under the same photoexcitation conditions, the fluorescence of Alexa Fluor 546 conjugated to DNA faded completely in 12 seconds [25]. Additionally, the fluorescence of red NDs was found to be significantly brighter than that emitted by Alexa Fluor 546 dye [25]. The evidence of photostability has also been determined for a 7 nm sized red fluorescent diamond nanocrystal that did not show any sign of photobleaching over a time period of 30 seconds [118]. In addition to resistance to photobleaching, the fluorescence of NDs (35 and 100 nm in size) was also found to be immune to photoblinking on a time scale of 1 ms [25]. Moreover, due to the deep location of $(N\text{-}V)^-$ centers in the lattice structure of NDs [119,120], the fluorescence remains unaffected by surface alterations, as evidenced by NDs functionalized with carboxylic acid [64], polylysine [25] and transferrin [121] groups. Therefore, the intrinsic photostablity of NDs opens avenues for carrying out chemical modification of their surface for specific imaging applications.

Furthermore, the red fluorescent NDs could also be more advantageous compared to organic fluorophores in obtaining bright contrast images in the cells. The absorption and emission wavelength of cellular endogenous components such as flavins, collagens, lipofuscins and coenzymes, ranging from 280 to 630 nm [122,123], coincides with most of the organic fluorophores used for cellular imaging [124]. Thus, it provides an undesirable, strong background to the fluorescence signal. However, the fluorescent NDs can act as an ideal candidate in this case as emission of the dominant color center of NDs, $(N\text{-}V)^-$, occurs above 690 nm [25,64], well separated from the cellular autofluorescence region. In addition, the average fluorescence lifetime of NDs is 17 ns [25,118], which is considerably longer than the lifetime of fluorescent organic dyes (<5 ns) and most of the cellular endogenous fluorophores (<6 ns) [122]. Hence, by applying time-gating [125] it is possible to collect the fluorescence of the NDs alone with minimal background cellular autofluorescence, thereby providing a high contrast imaging of NDs in the cells, which could not feasible with most of the commonly used organic fluorophores [25]. Table 2.1 lists the advantages of using red fluorescent NDs as a fluorescent tag for *in vitro* or *in vivo* tracking applications.

Table 2.1: Highlights of the unique fluorescence properties of nanodiamonds

Properties	Advantages
High quantum efficiency	Bright fluorescence
Photostability over longer time periods	Long term tracking of nanodiamonds in cells
Emission wavelength >690 nm	High contrast imaging of nanodiamonds
Longer fluorescence lifetime	High contrast imaging of nanodiamonds
Deeper location of nitrogen vacancy centers	No alteration in fluorescence due to surface modification

Similar to the N-V defect centers of type Ib synthetic diamonds, the nitrogen-vacancy-nitrogen (N-V-N) or H3 defects centers [24,126] in natural type Ia diamond nanocrystals can be created by irradiating them with a high energy (3-MeV) proton or a medium energy (40-keV) helium ion beam followed by annealing at 800°C [82]. H3 defect centers have a zero phonon line at 503 nm, with absorption and fluorescence emission at 470 and 530 nm, respectively [22]. Therefore, type Ia NDs with H3 centers are known as green fluorescent NDs.

Other than the natural and high-pressure high-temperature NDs containing nitrogen impurities, researchers are also trying to understand the fluorescence characteristics of detonation NDs. However, considering the actual composition of the explosive mixture (~20 mass% of nitrogen) used to synthesize these particles, they might contain a high concentration of nitrogen [127] either in their core structure or in the form of surface defects. At first, these nanoparticles were suggested to be devoid of C-centers and were believed to be unsuitable for imaging applications [21]. The absence of zero phonon lines corresponding to the nitrogen vacancy centers in irradiated and annealed detonation NDs suggested structural defects to be the origin of their fluorescence [128]. Z-contrast scanning transmission microscopy, high-resolution transmission electron microscopy and electron energy loss spectroscopy identified nitrogen in the core structure of detonation NDs [129]. Recently, Vlasov et al detected stable (N-V) color centers in detonation NDs having a size greater 30 nm after their irradiation and thermal annealing treatment [127]. While the occurrence of (N-V) color centers in the bulk structure of detonation NDs of less than 10 nm size has been questioned in various studies [130,131], Smith et al showed the presence of these centers in single-digit-sized irradiation damaged and annealed NDs [132]. Moreover, (N-V) color centers have also been discovered in non-irradiated, 5 nm sized detonation NDs [133]. The NDs synthesized by detonation technique are shown to possess up to 3 at.% of nitrogen impurities [127,134].

NDs, due to their bright fluorescence, high photostability with sufficiently long lifetime and excellent biocompatibility, are emerging as efficient and safe candidates for cellular imaging.

In 2007, Fu et al explored the fluorescent properties of a single 100 nm red fluorescent ND to examine the binding pattern of negatively charged DNA with a positively charged ND [25]. Firstly, the molecules of T4 DNA labeled with TOTO-1 fluorophore were allowed to interact electrostatically with polyL-lysine coated carboxylated fluorescent NDs in a buffer [25]. The diluted solution containing a single fluorescent ND and DNA was then added into a microchannel of a coverglass plate terminated with amino groups, followed by DNA stretching using microchannel combing methodology [25]. After laser excitation of the sample at 514 nm, fluorescence was detected using a wide-field epifluorescence microscope equipped with 545 to 605 nm and 675 to 685 nm wavelength channels [25]. By overlapping the fluorescence emitted from TOTO-1 dye and the ND, detected by the shorter wavelength channel, with that of ND alone, detected by the longer wavelength channel, it was discovered that the DNA interacts with the positively charged single ND through a wrapping arrangement (Figure 2.8) [25]. By using the fluorescence intensity of the ND as a control, it was observed that over a time period of 13.9 s, a 35 nm ND travels within $1\times1\ \mu m^2$ area close to the nucleus of Hela cells [25]. To compare the photostability of TOTO-1 dye with fluorescent ND, samples were excited for 40 seconds at 514 nm [25]. No sign of photobleaching was observed in the ND whereas the dye started fading within the first 5 seconds [25]. This study shows that a single fluorescent ND can function as tracking agent and probe to investigate the interaction between biomolecules.

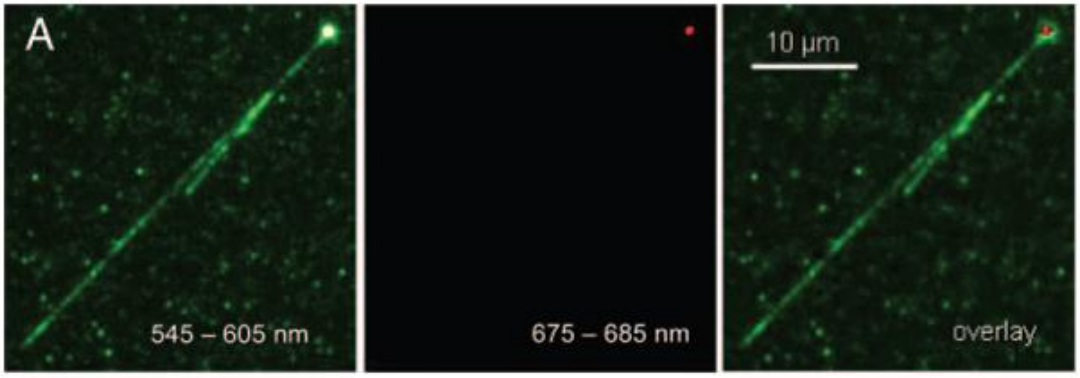

Figure 2.8: Use of fluorescence of nanodiamonds in predicting DNA interaction with a positively charged nanodiamond.

Overlay image (right) demonstrating the wrapping of TOTO-1 dye labeled T4DNA (green color, V-shape) around the surface of a single polyL-lysine coated fluorescent nanodiamond (red color). Reprinted with permission from [25]. "Copyright (2007) National Academy of Sciences, U.S.A."

In 2009, Weng et al investigated the uptake mechanism of transferrin in Hela cells using fluorescent properties of NDs as a biomolecule label [121]. They oxidized 100 nm red fluorescent NDs and conjugated transferrin to their surfaces through an amide linkage to form ND-transferrin conjugates [121]. These bioconjugates were then incubated for an hour at a concentration of 10 μg/mL with Hela cells over-expressing transferrin receptors [121]. To further verify the findings, ND-transferrin complexes were also added to Hela cells in which their transferrin receptors were presaturated by adding an excess of transferrin [121]. Upon excitation of the treated Hela cell samples using a 514.5 nm laser source, confocal fluorescence images were obtained by collecting fluorescence from 663 to 738 nm, thereby excluding most of the cellular autofluorescence background and providing high contrast images of NDs in cells (Figure 2.9) [121]. While the successful internalization of transferrin was observed in Hela cells over-expressing transferrin receptors, no noticeable uptake occurred in transferrin receptor presaturated Hela cells as evidenced by the absence of ND fluorescence emission in the latter [121]. Hence, by using the fluorescence of NDs as a marker, it was confirmed that uptake of transferrin in Hela cells occurs through receptor mediated endocytosis [121]. Moreover, 100 nm size NDs did not interfere in the binding of transferrin to its receptor and subsequent cellular uptake [121]. As well, it was verified that the fluorescence of NDs originates from the lattice color defect center rather than surface defects, as the surface conjugation of NDs with transferrin, and transferrin-ND—transferrin receptor interactions had no adverse effects on their fluorescence properties [121]. Hence this result shows that NDs can act as an efficient label to examine the cellular uptake mechanism of various biomolecules.

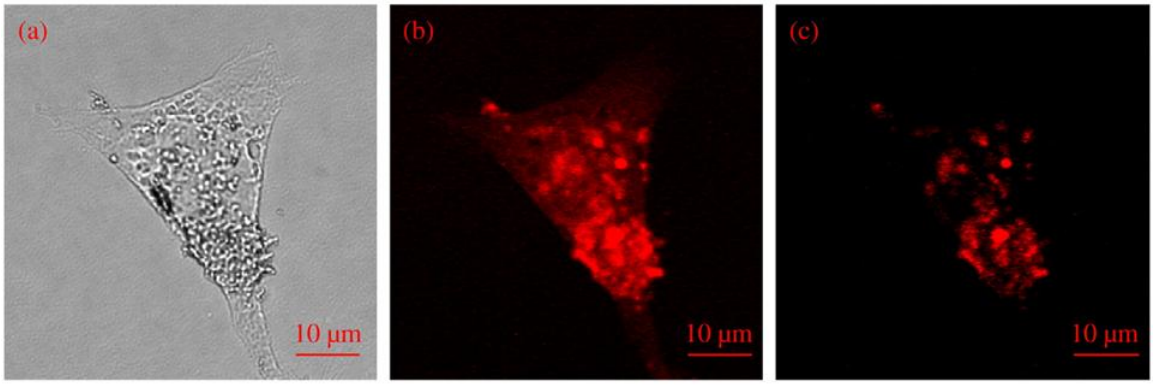

Figure 2.9: Use of long wavelength emission of nanodiamonds in obtaining high contrast cellular images.

Images of single Hela cell treated with ND-transferrin complex: (a) bright-field image, (b) confocal scanning image obtained by collecting all the fluorescence emission above 550 nm and (c) confocal scanning image obtained by collecting the fluorescence emission only from 663–738 nm. 514.5 nm laser was used as excitation source. "Reprinted from [121] Copyright (2008), with permission from Elsevier."

In addition to exploring the red fluorescence of type Ib irradiated/annealed synthetic NDs as cellular biomarker by various researchers [25,110,121], Mkandawire et al in 2009, proposed the use of untreated detonation NDs, emitting green fluorescence, for labeling live cells [135]. Immunoconjugated ND complexes were prepared by covalently coupling actin and mitochondrial targeted antibodies to the surface of oxidized NDs [135]. The actin antibody-ND and mitochondria antibody-ND immunoconjugates were then allowed internalization by Hela cells using maltotriose shelled 4^{th} generation dendrimers [135]. Using the green fluorescence of the NDs as a marker, live-cell fluorescence microscopic images of the treated cells, collected at 535/40 nm wavelength, revealed selective targeting of actin and mitochondria by actin antibody-ND and mitochondria antibody-ND immunoconjugates, respectively [135]. Moreover, with the rational selection of an antibody, NDs could also be designed to image the specific structures of the cells [135].

Further to the *in vitro* studies, Mohan et al in 2010, traced the movement of bare and bioconjugated red fluorescent NDs in *Caenorhabditis elegans* (Figure 2.10), a hermaphrodite having an optically transparent body [136]. The worms were deprived of *Escherichia coli* (*E. coli*), and then fed bare and dextran-/bovine serum albumin-conjugated carboxylated NDs [136]. The location of NDs in the worms was determined by differential interference and wide-field epifluorescence microscopic images, obtained by collecting the emission from the sample above 600 nm wavelength upon excitation with green yellow light (510-560 nm) [136]. The bare NDs were found to be localized in the lumen of the worm 12 hours past administration with no signs of intestinal absorption [136]. However, the excretion of these NDs took place within an hour when the worms were fed on *E. coli* [136]. In contrast to the bare NDs, a major fraction of the bioconjugated NDs was taken up by the intestinal cells of the worm and remained there for 24 hours despite *E. coli* feeding [136]. The high intestinal absorption of bioconjugated NDs compared to bare NDs was believed to be due to enhanced dispersibility of the NDs as a result of surface functionalization and/or triggering of certain cellular uptake pathways [136].

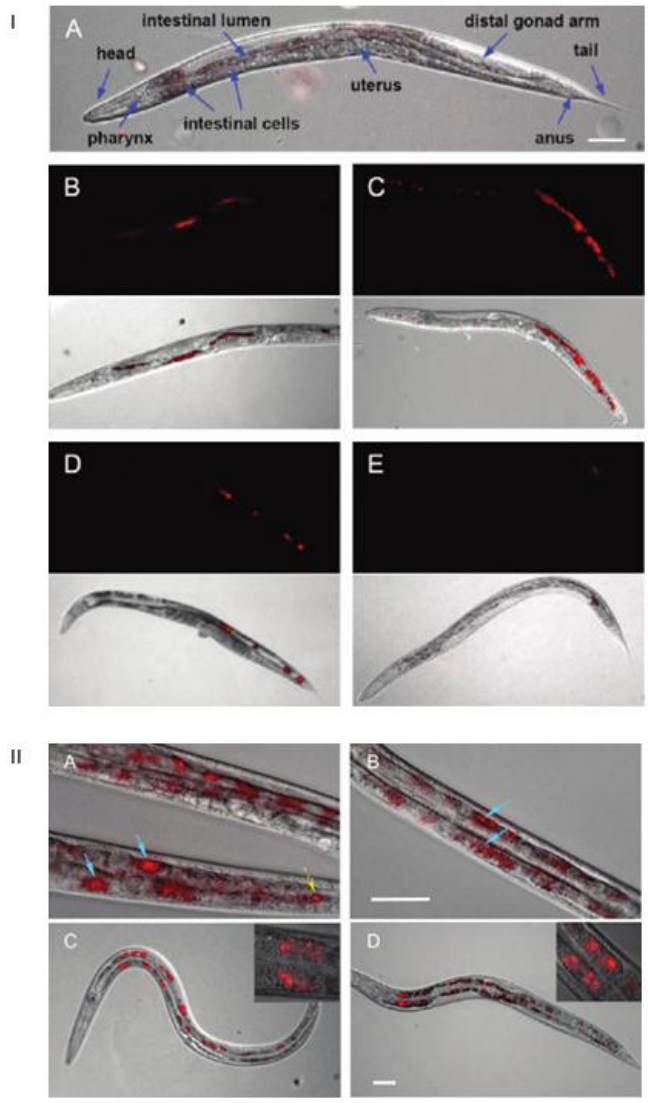

Figure 2.10: Internalization behavior of bare and surface functionalized nanodiamonds in *Caenorhabditis elegans*.

(I) Images of *Caenorhabditis elegans*: (A) an untreated worm with labeled organ morphology; worms after oral administration of bare NDs for (B) 2 hours and (C) 12 hours; worms fed with bare NDs for 2 hours with subsequent administration of *E. coli* for (D) 20 minutes (E) and 40 minutes. (B-E), Top, epifluorescence images; Bottom, epifluorescence and differential interference merged contrast images. (II) epifluorescence and differential interference contrast merged images of *Caenorhabditis elegans*: worms after 3 hours oral administration of (A) dextran conjugated NDs (B) bovine serum albumin conjugated NDs; worms fed *Escherichia coli* for 1 hour after treatment with (**C**) dextran-conjugated NDs and (**D**) bovine serum albumin-conjugated NDs for 3 hours . Blue arrows indicate internalization of NDs in intestinal cells, yellow arrow indicate localization of NDs in lumen of worm. "Reprinted with permission from [136]. Copyright (2010) American Chemical Society."

No photobleaching or photoblinking of NDs was observed even after 48 hours of continuous excitation with light [136]. Furthermore, observation of the lifespan, brood size, reactive oxygen species as well as stress response level demonstrated high biocompatibility of the NDs [136]. This study shows the potential for the use of the fluorescent properties of NDs in long term tracking of biomolecules in organisms, and as tools for marking human organelles [136].

To date, there are a number of publications showing the utilization of ND fluorescence for imaging, mostly in the cells and less commonly in translucent organisms. However, further studies need to be carried out to demonstrate the usefulness of NDs as imaging agents in animals and humans. Imaging organisms that do not possess translucent membranes could pose a challenge.

2.4.2 Elastic and Inelastic Light Scattering Imaging

In addition to the fluorescence, NDs have a refractive index of 2.42, thus possess characteristic optical scattering properties [119]. This property was explored by Smith et al by obtaining differential interference contrast microscopic images of 55 nm sized NDs internalized into 3T3 mammalian epithelial cells [137]. Based upon the differences in refractive indices of cellular structures and diamond, the diamond nanocrystal causes 300 times higher Rayleigh light scattering than the cellular structures of comparable sizes [138]. This offers an advantage to using NDs for obtaining high contrast imaging in the cells. In addition to elastic scattering [137], NDs are also capable of scattering light inelastically and hence are Raman-active [139,140]. The phonon mode of the diamond carbon shows a sharp and distinguished Raman signal at 1332 cm^{-1} [141] providing an opportunity for spectroscopic characterization and mapping of NDs in the cells. Raman spectroscopy is a non-invasive, non-toxic technique, therefore possesses potential to be used for detection and imaging of NDs in biological samples. Also, Raman spectroscopic measurements do not require complicated sample preparation and conditions that are hard to maintain, such as vacuum. Therefore, in addition to the fluorescent tag, NDs can also be used as an optical scattering nanoprobe in cellular studies.

In 2007, Perevedentseva et al used NDs as nanobioprobes to observe biomolecule-bacterial interactions *in vivo*, using the unique Raman signal of NDs as a detection marker [139]. Physical adsorption of lysozymes was performed on carboxylated NDs and the resultant carboxylated ND-lysozyme complex was then allowed to interact with *E. coli* [139]. The optical microscope located the *E. coli*, while the confocal Raman spectrometer mapped the Raman signals from the NDs [139]. As the lysozyme was adsorbed onto the surface of the NDs, the overlay of optical and Raman images, revealed the interaction sites of the lysozyme with *E. coli* (Figure 2.11) [139]. This dual imaging provided a simple method to observe the interaction of molecules with living cells [139]. Furthermore, there was no reduction in the bactericidal activity of lysozymes upon adsorption onto the NDs surface, proving that NDs did not interfere with the therapeutic activity of the attached entity [139].

The same group in 2007 investigated the use of NDs to predict the location of growth hormone receptors in human lung cancer cells by identifying the sp^3 carbon Raman signals of NDs [140]. Growth hormone-ND complexes were created by carboxylating and covalently linking 100 nm sized NDs to the growth hormone [140]. When mapped by confocal Raman spectrophotometry, the NDs bound to growth hormone were located on the surface of a cell, while the unconjugated carboxylated NDs were internalized into the cells [140]. These observations verified the extracellular location of the growth hormone receptor using the Raman signal of the ND as a label [140]. This study provided a relatively easy and direct method of locating receptors at the cellular level. This method could be beneficial in investigating the receptor-mediated internalization of biomolecules and diagnosing diseases such as cancers involving the alteration in expression of certain receptors [140].

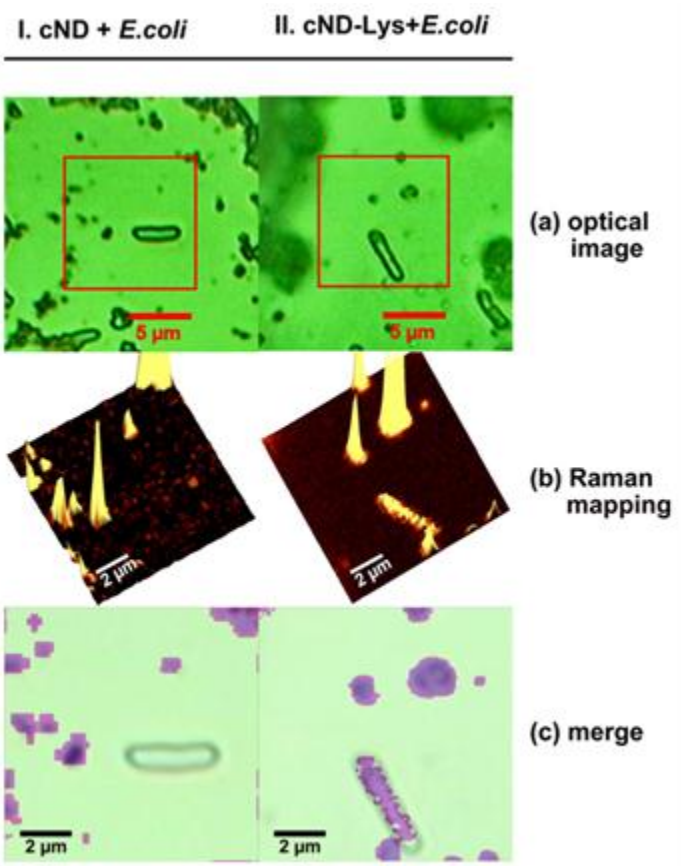

Figure 2.11: Use of nanodiamonds for predicting interaction between lysozymes and *Escherichia coli*.

Lysozymal interaction sites revealed with *E. coli*: I.carboxylated NDs and *E. coli*, II. carboxylated NDs-lysoszyme complex and *E. coli*. (a) Optical images identifying *E. coli*; (b) confocal Raman mapping identifying nanodiamonds present in the square area outlined in optical image; (c) merging of the optical image with Raman mapping demonstrating the interaction of lysozyme with *E. coli* [139].“Reproduced courtesy of IOP Publishing Ltd".

2.5 Conclusions

Continued investigation and understanding of disaggregation methods, surface properties, functionalization, biocompatibility, cellular fate, fluorescence as well as optical scattering characteristics of NDs have opened new horizons for their applications in the biomedical field. NDs have shown great potential to emerge as a platform for delivering drugs into biological systems due to their biocompatibility, high loading capacity and ability to cross cellular membranes. These particles have imparted sustained release and hydrophilic characteristics to water insoluble drugs, and have opened the possibilities for systemic administration of highly effective, hydrophobic chemotherapeutic molecules. While (N-V) defect centers are responsible for conferring fluorescence to NDs, the scattering properties originates from their high refractive index and Raman optical activity. These properties provide imaging capabilities to NDs for their detection in the cell. The multifunctional characteristics of NDs can be utilized to improve the delivery of drugs in conjunction with imaging their fate in biological systems, which can revolutionize studies in the area of life sciences. This unique biomaterial could be further explored as a gene delivery vehicle and a label to identify the biomolecular targets of drugs.

2.6 References

1. Shenderova OA, Mc.Guire G: Types of nanocrystalline diamond. In *Ultrananocrystalline Diamond: Synthesis, Properties, and Applications*. Edited by Shenderova OA, Gruen DM: William Andrew Publishing; 2006:79-114.

2. Mochalin VN, Shenderova O, Ho D, Gogotsi Y: The properties and applications of nanodiamonds. *Nature Nanotechnology* 2012, 7:11-23.

3. Gracio JJ, Fan QH, Madaleno JC: Diamond growth by chemical vapour deposition. *Journal of Physics D: Applied Physics* 2010, 43.

4. Philip J, Hess P, Feygelson T, Butler JE, Chattopadhyay S, Chen KH, Chen LC: Elastic, mechanical, and thermal properties of nanocrystalline diamond films. *Journal of Applied Physics* 2003, 93:2164-2171. DOI: http://dx.doi.org/10.1063/1.1537465.

5. Zhou D, Gruen DM, Qin LC, McCauley TG, Krauss AR: Control of diamond film microstructure by Ar additions to CH4/H2 microwave plasmas. *Journal of Applied Physics* 1998, 84:1981-1989.

6. Qin LC, Zhou D, Krauss AR, Gruen DM: TEM characterization of nanodiamond thin films. *Nanostructured Materials* 1998, 10:649-660.

7. Espinosa HD, Peng B, Prorok BC, Moldovan N, Auciello O, Carlisle JA, Gruen DM, Mancini DC: Fracture strength of ultrananocrystalline diamond thin films - Identification of Weibull parameters. *Journal of Applied Physics* 2003, 94:6076-6084.

8. Angadi MA, Watanabe T, Bodapati A, Xiao X, Auciello O, Carlisle JA, Eastman JA, Keblinski P, Schelling PK, Phillpot SR: Thermal transport and grain boundary conductance in ultrananocrystalline diamond thin films. *Journal of Applied Physics* 2006, 99:114301.

9. Butler JE, Sumant AV: The CVD of nanodiamond materials. *Chemical Vapor Deposition* 2008, 14:145-160.

10. Sumant AV, Grierson DS, Gerbi JE, Carlisle JA, Auciello O, Carpick RW: Surface chemistry and bonding configuration of ultrananocrystalline diamond surfaces and their effects on nanotribological properties. *Physical Review B - Condensed Matter and Materials Physics* 2007, 76:235429. Link: http://link.aps.org/doi/10.1103/PhysRevB.76.235429.

11. Bajaj P, Akin D, Gupta A, Sherman D, Shi B, Auciello O, Bashir R: Ultrananocrystalline diamond film as an optimal cell interface for biomedical applications. *Biomedical Microdevices* 2007, 9:787-794.

12. Shi B, Jin Q, Chen L, Auciello O: Fundamentals of ultrananocrystalline diamond (UNCD) thin films as biomaterials for developmental biology: Embryonic fibroblasts growth on the surface of (UNCD) films. *Diamond and Related Materials* 2009, 18:596-600.

13. Krauss AR, Auciello O, Gruen DM, Jayatissa A, Sumant A, TucekJ, Mancini DC, Moldovan N, Erdemir A, Ersoy D, et al.: Ultrananocrystalline diamond thin films for MEMS and moving mechanical assembly devices. *Diamond and Related Materials* 2001, 10:1952-1961.

14. Auciello O, Birrell J, Carlisle JA, Gerbi JE, Xiao X, Peng B, Espinosa HD: Materials science and fabrication processes for a new MEMS technology based on ultrananocrystalline diamond thin films. *Journal of Physics Condensed Matter* 2004, 16:R539-R552.

15. Auciello O, Sumant AV: Status review of the science and technology of ultrananocrystalline diamond (UNCD™) films and application to multifunctional devices. *Diamond and Related Materials* 2010, 19:699-718.

16. Sumant AV, Auciello O, Carpick RW, Srinivasan S, Butler JE: Ultrananocrystalline and nanocrystalline diamond thin films for MEMS/NEMS applications. *MRS Bulletin* 2010, 35:281-288.

17. Hupert M, Muck A, Wang J, Stotter J, Cvackova Z, Haymond S, Show Y, Swain GM: Conductive diamond thin-films in electrochemistry. *Diamond and Related Materials* 2003, 12:1940-1949.

18. Yang W, Auciello O, Butler JE, Cai W, Carlisle JA, Gerbi J, Gruen DM, Knickerbocker T, Lasseter TL, Russell Jr JN, et al.: DNA-modified nanocrystalline diamond thin-films as stable, biologically active substrates. *Nature Materials* 2002, 1:253-257.

19. Chang YR, Lee HY, Chen K, Chang CC, Tsai DS, Fu CC, Lim TS, Tzeng YK, Fang CY, Han CC, et al.: Mass production and dynamic imaging of fluorescent nanodiamonds. *Nature Nanotechnology* 2008, 3:284-288.

20. Sonnefraud Y, Cuche A, Faklaris O, Boudou JP, Sauvage T, Roch JF, Treussart F, Huant S: Diamond nanocrystals hosting single nitrogen-vacancy color centers sorted by photon-correlation near-field microscopy. *Optics Letters* 2008, 33:611-613.

21. Boudou JP, Curmi PA, Jelezko F, Wrachtrup J, Aubert P, Sennour M, Balasubramanian G, Reuter R, Thorel A, Gaffet E: High yield fabrication of fluorescent nanodiamonds. *Nanotechnology* 2009, 20:235602.

22. Chang HC: Development and Use of Fluorescent Nanodiamonds as Cellular Marker. In *Nanodiamonds: Applications in Biology and Nanoscale Medicine*. Edited by Ho D: Springer; 2009:127-150.

23. Davies G, Lawson SC, Collins AT, Mainwood A, Sharp SJ: Vacancy-related centers in diamond. *Physical Review B* 1992, 46:13157-13170.

24. Clark CD, Norris CA: Photoluminescence associated with the 1.673, 1.944 and 2.498 eV centres in diamond. *Journal of Physics C: Solid State Physics* 1971, 4:2223-2229.

25. Fu CC, Lee HY, Chen K, Lim TS, Wu HY, Lin PK, Wei PK, Tsao PH, Chang HC, Fann W: Characterization and application of single fluorescent nanodiamonds as cellular biomarkers. *Proceedings of the National Academy of Sciences of the United States of America* 2007, 104:727-732. DOI: 10.1073/pnas.0605409104

26. Dolmatov VY: Detonation synthesis ultradispersed diamonds: Properties and applications. *Russian Chemical Reviews* 2001, 70:607-626.

27. Dolmatov VY: Synthesis and post-synthesis treatment of detonation nanodiamonds. In *Ultrananocrystalline Diamond: Synthesis, Properties, and Applications*. Edited by Shenderova OA, Gruen DM: William Andrew Publishing; 2006:347-377.

28. Shenderova OA, Zhirnov VV, Brenner DW: Carbon nanostructures. *Critical Reviews in Solid State and Materials Sciences* 2002, 27:227-356.

29. Baidakova M, Vul A: New prospects and frontiers of nanodiamond clusters. *Journal of Physics D: Applied Physics* 2007, 40:6300-6311. DOI: 10.1088/0022-3727/40/20/S14

30. Aleksenskii AE, Baidakova MV, Vul AY, Siklitskii VI: The structure of diamond nanoclusters. *Physics of the Solid State* 1999, 41:668-671.

31. Shenderova OA, Hens SAC: Detonation nanodiamond particles processing, modification and bioapplications. In *Nanodiamonds: Applications in Biology and Nanoscale Medicine*. Edited by Ho D: Springer; 2010:79-116.

32. Pichot V, Comet M, Fousson E, Baras C, Senger A, Le Normand F, Spitzer D: An efficient purification method for detonation nanodiamonds. *Diamond and Related Materials* 2008, 17:13-22.

33. Osswald S, Yushin G, Mochalin V, Kucheyev SO, Gogotsi Y: Control of sp2/sp3 carbon ratio and surface chemistry of nanodiamond powders by selective oxidation in air. *Journal of the American Chemical Society* 2006, 128:11635-11642.

34. Petrov I, Shenderova O, Grishko V, Grichko V, Tyler T, Cunningham G, McGuire G: Detonation nanodiamonds simultaneously purified and modified by gas treatment. *Diamond and Related Materials* 2007, 16:2098-2103.

35. Krüger A, Kataoka F, Ozawa M, Fujino T, Suzuki Y, Aleksenskii AE, Vul AY, Osawa E: Unusually tight aggregation in detonation nanodiamond: Identification and disintegration. *Carbon* 2005, 43:1722-1730.

36. Krueger A: The structure and reactivity of nanoscale diamond. *Journal of Materials Chemistry* 2008, 18:1485-1492.

37. Jiang T, Xu K: FTIR study of ultradispersed diamond powder synthesized by explosive detonation. *Carbon* 1995, 33:1663-1671.

38. Dolmatov VY: Detonation nanodiamonds in oils and lubricants. *Journal of Superhard Materials* 2010, 32:14-20.

39. Schrand AM, Hens SAC, Shenderova OA: Nanodiamond Particles: Properties and Perspectives for Bioapplications. *Critical Reviews in Solid State and Materials Sciences* 2009, 34:18-74.

40. Bondar VS, Pozdnyakova IO, Puzyr AP: Applications of nanodiamonds for separation and purification of proteins. *Physics of the Solid State* 2004, 46:758-760.

41. Purtov KV, Puzyr AP, Bondar VS: Nanodiamond sorbents: New carriers for column chromatography of proteins. *Doklady Biochemistry and Biophysics* 2008, 419:72-74.

42. Dolmatov VY: Applications of detonation nanodiamond. In *Ultrananocrystalline Diamond: Synthesis, Properties, and Applications*. Edited by Shenderova OA, Gruen DM: William Andrew Publishing; 2006:477-527.

43. Pentecost A, Gour S, Mochalin V, Knoke I, Gogotsi Y: Deaggregation of nanodiamond powders using salt- and sugar-assisted milling. *ACS Applied Materials and Interfaces* 2010, 2:3289-3294.

44. Krüger A, Liang Y, Jarre G, Stegk J: Surface functionalisation of detonation diamond suitable for biological applications. *Journal of Materials Chemistry* 2006, 16:2322-2328.

45. Barnard AS: Self-assembly in nanodiamond agglutinates. *Journal of Materials Chemistry* 2008, 18:4038-4041.

46. Chang LY, Sawa E, Barnard AS: Confirmation of the electrostatic self-assembly of nanodiamonds. *Nanoscale* 2011, 3:958-962.

47. Ozawa M, Inaguma M, Takahashi M, Kataoka F, Krüger A, Osawa E: Preparation and behavior of brownish, clear nanodiamond colloids. *Advanced Materials* 2007, 19:1201-1206.

48. Liang Y, Ozawa M, Krueger A: A general procedure to functionalize agglomerating nanoparticles demonstrated on nanodiamond. *ACS Nano* 2009, 3:2288-2296.

49. Osawa E: Recent progress and perspectives in single-digit nanodiamond. *Diamond and Related Materials* 2007, 16:2018-2022.

50. Eidelman ED, Siklitsky VI, Sharonova LV, Yagovkina MA, Vul AY, Takahashi M, Inakuma M, Ozawa M, Osawa E: A stable suspension of single ultrananocrystalline diamond particles. *Diamond and Related Materials* 2005, 14:1765-1769.

51. Suslick KS, Hammerton DA, Cline RE: The sonochemical hot spot. *Journal of the American Chemical Society* 1986, 108:5641-5642.

52. Aleksenskii AE, Baidakova MV, Vul AY, Davydov VY, Pevtsova YA: Diamond-graphite phase transition in ultradisperse-diamond clusters. *Physics of the Solid State* 1997, 39:1007-1015.

53. Xu X, Yu Z, Zhu Y, Wang B: Effect of sodium oleate adsorption on the colloidal stability and zeta potential of detonation synthesized diamond particles in aqueous solutions. *Diamond and Related Materials* 2005, 14:206-212.

54. Morita Y, Takimoto T, Yamanaka H, Kumekawa K, Marino S, Aonuma S, Kimura T, Komatsu N: A facile and scalable process for size-controllable separation of nanodiamond particles as small as 4 nm. *Small* 2008, 4:2154-2157.

55. Tsubota T, Tanii S, Ida S, Nagata M, Matsumoto Y: Chemical modification of diamond surface with various carboxylic acids by radical reaction in liquid phase. *Diamond and Related Materials* 2004, 13:1093-1097.

56. Ida S, Tsubota T, Tanii S, Nagata M, Matsumoto Y: Chemical modification of the diamond surface using benzoyl peroxide and dicarboxylic acids. *Langmuir* 2003, 19:9693-9698.

57. Ando T, Nishitani-Gamo M, Rawles RE, Yamamoto K, Kamo M, Sato Y: Chemical modification of diamond surfaces using a chlorinated surface as an intermediate state. *Diamond and Related Materials* 1996, 5:1136-1142.

58. Liu Y, Gu Z, Margrave JL, Khabashesku VN: Functionalization of nanoscale diamond powder: Fluoro-, alkyl-, amino-, and amino acid-nanodiamond derivatives. *Chemistry of Materials* 2004, 16:3924-3930.

59. Krueger A, Boedeker T: Deagglomeration and functionalisation of detonation nanodiamond with long alkyl chains. *Diamond and Related Materials* 2008, 17:1367-1370.

60. Krueger A, Ozawa M, Jarre G, Liang Y, Stegk J, Lu L: Deagglomeration and functionalisation of detonation diamond. *Physica Status Solidi (A) Applications and Materials* 2007, 204:2881-2887.

61. Krueger A, Stegk J, Liang Y, Lu L, Jarre G: Biotinylated nanodiamond: Simple and efficient functionalization of detonation diamond. *Langmuir* 2008, 24:4200-4204.

62. Schrand AM, Huang H, Carlson C, Schlager JJ, Osawa E, Hussain SM, Dai L: Are diamond nanoparticles cytotoxic? *Journal of Physical Chemistry B* 2007, 111:2-7.

63. Schrand AM, Dai L, Schlager JJ, Hussain SM, Osawa E: Differential biocompatibility of carbon nanotubes and nanodiamonds. *Diamond and Related Materials* 2007, 16:2118-2123.

64. Yu SJ, Kang MW, Chang HC, Chen KM, Yu YC: Bright fluorescent nanodiamonds: No photobleaching and low cytotoxicity. *Journal of the American Chemical Society* 2005, 127:17604-17605.

65. Liu KK, Cheng CL, Chang CC, Chao JI: Biocompatible and detectable carboxylated nanodiamond on human cell. *Nanotechnology* 2007, 18:325102.

66. Chao JI, Perevedentseva E, Chung PH, Liu KK, Cheng CY, Chang CC, Cheng CL: Nanometer-sized diamond particle as a probe for biolabeling. *Biophysical Journal* 2007, 93:2199-2208.

67. Huang H, Pierstorff E, Osawa E, Ho D: Active nanodiamond hydrogels for chemotherapeutic delivery. *Nano Letters* 2007, 7:3305-3314.

68. Li J, Zhu Y, Li W, Zhang X, Peng Y, Huang Q: Nanodiamonds as intracellular transporters of chemotherapeutic drug. *Biomaterials* 2010, 31:8410-8418.

69. Xing Y, Xiong W, Zhu L, Osawa E, Hussin S, Dai L: DNA damage in embryonic stem cells caused by nanodiamonds. *ACS Nano* 2011, 5:2376-2384.

70. Marcon L, Riquet F, Vicogne D, Szunerits S, Bodart JF, Boukherroub R: Cellular and in vivo toxicity of functionalized nanodiamond in Xenopus embryos. *Journal of Materials Chemistry* 2010, 20:8064-8069.

71. Liu K-K, Wang C-C, Cheng C-L, Chao J-I: Endocytic carboxylated nanodiamond for the labeling and tracking of cell division and differentiation in cancer and stem cells. *Biomaterials* 2009, 30:4249-4259.

72. Zhu L, Chang DW, Dai L, Hong Y: DNA damage induced by multiwalled carbon nanotubes in mouse embryonic stem cells. *Nano Letters* 2007, 7:3592-3597.

73. Zhu Y, Li W, Li Q, Li Y, Zhang X, Huang Q: Effects of serum proteins on intracellular uptake and cytotoxicity of carbon nanoparticles. *Carbon* 2009, 47:1351-1358.

74. Drescher D, Orts-Gil G, Laube G, Natte K, Veh RW, Österle W, Kneipp J: Toxicity of amorphous silica nanoparticles on eukaryotic cell model is determined by particle agglomeration and serum protein adsorption effects. *Analytical and Bioanalytical Chemistry* 2011, 400:1367-1373.

75. Kittler S, Greulich C, Gebauer JS, Diendorf J, Treuel L, Ruiz L, Gonzalez-Calbet JM, Vallet-Regi M, Zellner R, Köller M, et al.: The influence of proteins on the dispersability and

cell-biological activity of silver nanoparticles. *Journal of Materials Chemistry* 2010, 20:512-518.

76. Casey A, Davoren M, Herzog E, Lyng FM, Byrne HJ, Chambers G: Probing the interaction of single walled carbon nanotubes within cell culture medium as a precursor to toxicity testing. *Carbon* 2007, 45:34-40.

77. Guo L, Von Dem Bussche A, Buechner M, Yan A, Kane AB, Hurt RH: Adsorption of essential micronutrients by carbon nanotubes and the implications for nanotoxicity testing. *Small* 2008, 4:721-727.

78. Puzyr AP, Baron AV, Purtov KV, Bortnikov EV, Skobelev NN, Mogilnaya OA, Bondar VS: Nanodiamonds with novel properties: A biological study. *Diamond and Related Materials* 2007, 16:2124-2128.

79. Yuan Y, Wang X, Jia G, Liu JH, Wang T, Gu Y, Yang ST, Zhen S, Wang H, Liu Y: Pulmonary toxicity and translocation of nanodiamonds in mice. *Diamond and Related Materials* 2010, 19:291-299.

80. Chow EK, Zhang XQ, Chen M, Lam R, Robinson E, Huang H, Schaffer D, Osawa E, Goga A, Ho D: Nanodiamond therapeutic delivery agents mediate enhanced chemoresistant tumor treatment. *Science Translational Medicine* 2011, 3:73ra21.

81. Faklaris O, Garrot D, Joshi W, Druon F, Boudou JP, Sauvage T, Georges P, Curmi PA, Treussart F: Detection of single photoluminescent diamond nanoparticles in cells and study of the internalization pathway. *Small* 2008, 4:2236-2239.

82. Wee TL, Mau YW, Fang CY, Hsu HL, Han CC, Chang HC: Preparation and characterization of green fluorescent nanodiamonds for biological applications. *Diamond and Related Materials* 2009, 18:567-573.

83. Faklaris O, Joshi V, Irinopoulou T, Tauc P, Sennour M, Girard H, Gesset C, Arnault JC, Thorel A, Boudou JP, et al.: Photoluminescent diamond nanoparticles for cell labeling: Study of the uptake mechanism in mammalian cells. *ACS Nano* 2009, 3:3955-3962.

84. Martín R, Álvaro M, Herance JR, García H: Fenton-treated functionalized diamond nanoparticles as gene delivery system. *ACS Nano* 2010, 4:65-74.

85. Li X, Shao J, Qin Y, Shao C, Zheng T, Ye L: TAT-conjugated nanodiamond for the enhanced delivery of doxorubicin. *Journal of Materials Chemistry* 2011, 21:7966-7973.

86. Liu KK, Zheng WW, Wang CC, Chiu YC, Cheng CL, Lo YS, Chen C, Chao JI: Covalent linkage of nanodiamond-paclitaxel for drug delivery and cancer therapy. *Nanotechnology* 2010, 21:315106.

87. Chen M, Pierstorff ED, Lam R, Li SY, Huang H, Osawa E, Ho D: Nanodiamond-mediated delivery of water-insoluble therapeutics. *ACS Nano* 2009, 3:2016-2022.

88. Mohanraj VJ, Chen Y: Nanoparticles -A Review. *Tropical Journal of Pharmaceutical Research* 2006, 5:561-573.

89. Sinha R, Kim GJ, Nie S, Shin DM: Nanotechnology in cancer therapeutics: Bioconjugated nanoparticles for drug delivery. *Molecular Cancer Therapeutics* 2006, 5:1909-1917.

90. Goga A, Yang D, Tward AD, Morgan DO, Bishop JM: Inhibition of CDK1 as a potential therapy for tumors over-expressing MYC. *Nature Medicine* 2007, 13:820-827.

91. Nayfield SG, Karp JE, Ford LG, Dorr FA, Kramer BS: Potential role of tamoxifen in prevention of breast cancer. *Journal of the National Cancer Institute* 1991, 83:1450-1459.

92. Fisher B, Costantino JP, Wickerham DL, Cecchini RS, Cronin WM, Robidoux A, Bevers TB, Kavanah MT, Atkins JN, Margolese RG, et al.: Tamoxifen for the prevention of breast cancer: Current status of the National Surgical Adjuvant Breast and Bowel Project P-1 study. *Journal of the National Cancer Institute* 2005, 97:1652-1662.

93. Liang XJ, Chen C, Zhao Y, Wang PC: Circumventing tumor resistance to chemotherapy by nanotechnology. *Methods in molecular biology (Clifton, N.J.)* 2010, 596:467-488.

94. Peer D, Karp JM, Hong S, Farokhzad OC, Margalit R, Langer R: Nanocarriers as an emerging platform for cancer therapy. *Nature Nanotechnology* 2007, 2:751-760.

95. Moorthi C, Manavalan R, Kathiresan K: Nanotherapeutics to overcome conventional cancer chemotherapy limitations. *Journal of Pharmacy and Pharmaceutical Sciences* 2011, 14:67-77.

96. Shimkunas RA, Robinson E, Lam R, Lu S, Xu X, Zhang XQ, Huang H, Osawa E, Ho D: Nanodiamond-insulin complexes as pH-dependent protein delivery vehicles. *Biomaterials* 2009, 30:5720-5728.

97. Liu Y, Petreaca M, Yao M, Martins-Green M: Cell and molecular mechanisms of keratinocyte function stimulated by insulin during wound healing. *BMC Cell Biology* 2009, 10:1.

98. Schneider LA, Korber A, Grabbe S, Dissemond J: Influence of pH on wound-healing: A new perspective for wound-therapy? *Archives of Dermatological Research* 2007, 298:413-420.

99. Wiethoff CM, Middaugh CR: Barriers to nonviral gene delivery. *Journal of Pharmaceutical Sciences* 2003, 92:203-217.

100. Gary DJ, Puri N, Won YY: Polymer-based siRNA delivery: Perspectives on the fundamental and phenomenological distinctions from polymer-based DNA delivery. *Journal of Controlled Release* 2007, 121:64-73.

101. Whitehead KA, Langer R, Anderson DG: Knocking down barriers: Advances in siRNA delivery. *Nature Reviews Drug Discovery* 2009, 8:129-138.

102. Takahashi Y, Nishikawa M, Takakura Y: Nonviral vector-mediated RNA interference: Its gene silencing characteristics and important factors to achieve RNAi-based gene therapy. *Advanced Drug Delivery Reviews* 2009, 61:760-766.

103. Van De Water FM, Boerman OC, Wouterse AC, Peters JGP, Russel FGM, Masereeuw R: Intravenously administered short interfering RNA accumulates in the kidney and selectively suppresses gene function in renal proximal tubules. *Drug Metabolism and Disposition* 2006, 34:1393-1397.

104. Zhang XQ, Chen M, Lam R, Xu X, Osawa E, Ho D: Polymer-functionalized nanodiamond platforms as vehicles for gene delivery. *ACS Nano* 2009, 3:2609-2616.

105. Chen M, Zhang XQ, Man HB, Lam R, Chow EK, Ho D: Nanodiamond vectors functionalized with polyethylenimine for siRNA delivery. *Journal of Physical Chemistry Letters* 2010, 1:3167-3171.

106. Ramdas AK: Electronic excitations in isotopically controlled diamonds:infrared and Raman spectroscopy of acceptor-bound holes. In *Properties, Growth and applications of Diamond*. Edited by Neves AJ, Nazaré MH: INSPEC; 2001:21-27.

107. Kiflawi I, Lawson SC: Aggregates of nitrogen in diamond. In *Properties, Growth and Applications of Diamond*. Edited by Neves AJ, Nazaré, Helana M: INSPEC; 2001:130-135.

108. Vaijayanthimala V, Chang HC: Functionalized fluorescent nanodiamonds for biomedical applications. *Nanomedicine* 2009, 4:47-55.

109. Mainwood A: Nitrogen and nitrogen-vacancy complexes and their formation in diamond. *Physical Review B* 1994, 49:7934-7940.

110. Neugart F, Zappe A, Jelezko F, Tietz C, Boudou JP, Krueger A, Wrachtrup J: Dynamics of diamond nanoparticles in solution and cells. *Nano Letters* 2007, 7:3588-3591.

111. Treussart F, Jacques V, Wu E, Gacoin T, Grangier P, Roch JF: Photoluminescence of single colour defects in 50 nm diamond nanocrystals. *Physica B: Condensed Matter* 2006, 376-377:926-929.

112. Davies G, Hamer MF: Optical Studies of the 1.945 eV Vibronic Band in Diamond. *Proceedings of the Royal Society of London.A.Mathematical and Physical Sciences* 1976, 348:285-298.

113. Wee TL, Tzeng YK, Han CC, Chang HC, Fann W, Hsu JH, Chen KM, Yu EC: Two-photon excited fluorescence of nitrogen-vacancy centers in proton-irradiated type Ib diamond. *Journal of Physical Chemistry A* 2007, 111:9379-9386.

114. Lawson SC, Fisher D, Hunt DC, Newton ME: On the existence of positively charged single-substitutional nitrogen in diamond. *Journal of Physics Condensed Matter* 1998, 10:6171-6180.

115. Hui YY, Chang YR, Mohan N, Lim TS, Chen YY, Chang HC: Polarization modulation spectroscopy of single fluorescent nanodiamonds with multiple nitrogen vacancy centers. *Journal of Physical Chemistry A* 2011, 115:1878-1884.

116. Gruber A, Dräbenstedt A, Tietz C, Fleury L, Wrachtrup J, Von Borczyskowski C: Scanning confocal optical microscopy and magnetic resonance on single defect centers. *Science* 1997, 276:2012-2014.

117. Collins AT, Thomaz MF, Jorge MIB: Luminescence decay time of the 1.945 eV centre in type Ib diamond. *Journal of Physics C: Solid State Physics* 1983, 16:2177-2181.

118. Tisler J, Balasubramanian G, Naydenov B, Kolesov R, Grotz B, Reuter R, Boudou JP, Curmi PA, Sennour M, Thorel A, et al.: Fluorescence and spin properties of defects in single digit nanodiamonds. *ACS Nano* 2009, 3:1959-1965.

119. Hui YY, Cheng CL, Chang HC: Nanodiamonds for optical bioimaging. *Journal of Physics D: Applied Physics* 2010, 43:374021.

120. Gali A, Fyta M, Kaxiras E: Ab initio supercell calculations on nitrogen-vacancy center in diamond: Electronic structure and hyperfine tensors. *Physical Review B - Condensed Matter and Materials Physics* 2008, 77:155206.

121. Weng MF, Chiang SY, Wang NS, Niu H: Fluorescent nanodiamonds for specifically targeted bioimaging: Application to the interaction of transferrin with transferrin receptor. *Diamond and Related Materials* 2009, 18:587-591. DOI: 10.1016/j.diamond.2008.07.012

122. Koenig K, Schneckenburger H: Laser-induced autofluorescence for medical diagnosis. *Journal of Fluorescence* 1994, 4:17-40.

123. Aubin JE: Autofluorescence of viable cultured mammalian cells. *Journal of Histochemistry and Cytochemistry* 1979, 27:36-43.

124. Lichtman JW, Conchello JA: Fluorescence microscopy. *Nature Methods* 2005, 2:910-919.

125. Dahan M, Laurence T, Pinaud F, Chemla DS, Alivisatos AP, Sauer M, Weiss S: Time-gated biological imaging by use of colloidal quantum dots. *Optics Letters* 2001, 26:825-827.

126. Davies G: The effect of nitrogen impurity on the annealing of radiation damage in diamond. *Journal of Physics C: Solid State Physics* 1972, 5:2534-2542.

127. Vlasov II, Shenderova O, Turner S, Lebedev OI, Basov AA, Sildos I, Rähn M, Shiryaev AA, Van Tendeloo G: Nitrogen and luminescent nitrogen-vacancy defects in detonation nanodiamond. *Small* 2010, 6:687-694.

128. Borjanovic V, Lawrence WG, Hens S, Jaksic M, Zamboni I, Edson C, Vlasov I, Shenderova O, McGuire GE: Effect of proton irradiation on photoluminescent properties of PDMS-nanodiamond composites. *Nanotechnology* 2008, 19:455701.

129. Kvit AV, Zhirnov VV, Tyler T, Hren JJ: Aging effect and nitrogen distribution in diamond nanoparticles. *Composites Part B: Engineering* 2004, 35:163-166.

130. Vlasov II, Barnard AS, Ralchenko VG, Lebedev OI, Kanzyuba MV, Saveliev AV, Konov VI, Goovaerts E: Nanodiamond photoemitters based on strong narrow-band luminescence from silicon-vacancy defects. *Advanced Materials* 2009, 21:808-812.

131. Barnard AS, Sternberg M: Can we predict the location of impurities in diamond nanoparticles? *Diamond and Related Materials* 2007, 16:2078-2082.

132. Smith BR, Inglis DW, Sandnes B, Rabeau JR, Zvyagin AV, Gruber D, Noble CJ, Vogel R, Ösawa E, Plakhotnik T: Five-nanometer diamond with luminescent nitrogen-vacancy defect centers. *Small* 2009, 5:1649-1653.

133. Bradac C, Gaebel T, Naidoo N, Sellars MJ, Twamley J, Brown LJ, Barnard AS, Plakhotnik T, Zvyagin AV, Rabeau JR: Observation and control of blinking nitrogen-vacancy centres in discrete nanodiamonds. *Nature Nanotechnology* 2010, 5:345-349.

134. Turner S, Lebedev OI, Shenderova O, Vlasov II, Verbeeck J, Van Tendeloo G: Determination of size, morphology, and nitrogen impurity location in treated detonation nanodiamond by transmission electron microscopy. *Advanced Functional Materials* 2009, 19:2116-2124.

135. Mkandawire M, Pohl A, Gubarevich T, Lapina V, Appelhans D, Rödel G, Pompe W, Schreiber J, Opitz J: Selective targeting of green fluorescent nanodiamond conjugates to mitochondria in HeLa cells. *Journal of Biophotonics* 2009, 2:596-606.

136. Mohan N, Chen CS, Hsieh HH, Wu YC, Chang HC: In vivo imaging and toxicity assessments of fluorescent nanodiamonds in caenorhabditis elegans. *Nano Letters* 2010, 10:3692-3699. DOI: 10.1021/nl1021909

137. Smith BR, Niebert M, Plakhotnik T, Zvyagin AV: Transfection and imaging of diamond nanocrystals as scattering optical labels. *Journal of Luminescence* 2007, 127:260-263.

138. Colpin Y, Swan A, Zvyagin AV, Plakhotnik T: Imaging and sizing of diamond nanoparticles. *Optics Letters* 2006, 31:625-627.

139. Perevedentseva E, Cheng CY, Chung PH, Tu JS, Hsieh YH, Cheng CL: The interaction of the protein lysozyme with bacteria E. coli observed using nanodiamond labelling. *Nanotechnology* 2007, 18:315102. DOI: 10.1088/0957-4484/18/31/315102.

140. Cheng CY, Perevedentseva E, Tu JS, Chung PH, Cheng CL, Liu KK, Chao JI, Chen PH, Chang CC: Direct and in vitro observation of growth hormone receptor molecules in A549 human lung epithelial cells by nanodiamond labeling. *Applied Physics Letters* 2007, 90:163903.

141. Knight DS, White WB: Characterization of diamond films by Raman spectroscopy. *Journal of Materials Research* 1989, 4:385-393.

Chapter 3
HYPOTHESIS, OBJECTIVES AND RESEARCH OVERVIEW

3.1 Hypothesis

Mechanochemical functionalization of detonation nanodiamonds with lysine will lead to their significant disaggregation.

The resulting lysine-functionalized nanodiamond particles will bind genetic materials by forming nano-sized complexes to deliver them into mammalian cells.

3.2 Objectives

3.2.1 Objective 1

- To carry out covalent functionalization of nanodiamonds with lysine, attached to a 3-carbon length spacer (1,3 diaminopropane), to obtain positively charged disaggregated nanoparticles.

3.2.2 Objective 2

- To characterize and evaluate the degree of functionalization of nanodiamonds with lysine-spacer.

3.2.3 Objective 3

- To determine the physiochemical properties of lysine-functionalized nanodiamonds and evaluate their binding properties with genetic materials to form “diamoplexes”.

3.2.4 Objective 4

- To evaluate *in vitro* toxicity of pristine carboxylated and lysine-functionalized nanodiamonds, cellular interaction of lysine-functionalized nanodiamonds, and investigate the gene delivery efficacy of the selected “diamoplexes” in Hela cell line.

3.3 Research Overview

Pristine carboxylated nanodiamonds (pNDs) when dispersed in an aqueous medium assemble to form micron-sized aggregates. Several attempts were made to disaggregate these NDs by using surfactants, bath sonication, probe sonication and sonication with grinding media (Appendix A). Moreover, the time-dependent effects of bath and probe sonication on the dispersion stability of NDs were also examined (Appendix A). None of these approaches were successful in achieving a considerable disaggregation; in some cases, there was no disaggregation observed, while in other instances, re-aggregation occurred immediately after removing the mechanical energy treatment. Therefore, my aim was to develop an approach that could lead to a considerable disaggregation of NDs such that the resulting disaggregated particles have the potential to act as carriers of nucleic acids.

To serve the purposes of disaggregation and generation of positive charge on NDs, functionalization of NDs with lysine, accompanied with the mechanical disaggregation, was carried out. Firstly, these two techniques together were expected to bring disaggregation of ND aggregate diamond particles, based upon the rationale that the moment the mechanical treatment will disaggregate the diamond particles, the lysine functionalization on the NDs surfaces will generate inter-particle steric hindrances, thereby circumventing their re-aggregation. Secondly, the lysine molecule attached to NDs, due to its basicity, was expected to provide an overall positive charge to the surfaces of each lysine-functionalized NDs (fNDs) at neutral pH, thereby making them the suitable candidates for binding nucleic acids. Moreover, the like-positive charges on the surfaces of fNDs were expected to contribute towards post-functionalization disaggregation by generating inter-particle repulsive behavior.

To verify the successful functionalization of NDs with lysine, Raman and Fourier Transform Infrared spectroscopy was performed. The Raman spectroscopy has the potential to identify the diamond carbon as well as the other functional groups that show a change in polarizability with the molecular vibrations, therefore was considered to be the most suitable technique to examine the functionalization of NDs with lysine. But the fluorescence induced swamping of Raman signals in fND spectra, required me to perform infrared spectroscopic

measurements as well, to verify the functionalization of NDs. Moreover, the Raman and infrared spectroscopy, due to their different selection rules, are complementary to each other and therefore generally used together for characterization purposes. Thermogravimetric analysis was performed to quantitate the surface loading on the ND surfaces.

To determine if the current approach of mechanochemical functionalization was effective in inducing disaggregation of the ND aggregates, dynamic light scattering and atomic force microscopic measurements were carried out. Dynamic light scattering measures the hydrodynamic diameter of the material, hence useful in determining the actual size of the particles in their formulation medium; whereas the atomic force microscopy assist in visualization of particles, hence suitable to provide a visual evidence of disaggregation. In addition, the zeta potential of fNDs dispersion in water was measured to find out if the dispersions were stable enough to advocate their use for *in vitro* studies.

To examine the binding behavior of the disaggregated fNDs with plasmid DNA (pDNA) and small interfering RNA (siRNA), gel-retardation assay, dynamic light scattering and zeta potential measurements were performed. The gel-retardation assay was expected not to show the migration of the nucleic acids towards anode if fNDs were binding nucleic acid effectively. The purpose of using pDNA and siRNA was to probe the differences in binding patterns of two, structurally different genetic materials with the same solid-core positively charged nanoparticles, if any. Furthermore, it is crucial to determine the size of carrier-nucleic acid complex as the particles with the size less than 300 nm are required for the efficient cellular internalization. Other than the size, the surface of carrier-nucleic acid complex should have positive charge for effective interaction with cell surface that would favor their cellular uptake. Moreover, the overall positive zeta potential of the fNDs-nucleic acid complex would also indicate the absence of any unbound nucleic acids.

To test the biocompatibility of NDs, MTT cytotoxicity assay performed. As majority of the transfection studies are performed in cell culture medium lacking serum, therefore it was important to determine if the lack of serum have a substantial effect on cellular viability. Therefore, both the treatment conditions, with serum and without serum, were tested. To further

substantiate its potential as an efficient delivery agent, the material itself should demonstrate cellular interaction and ultimately internalization, which in this study was examined by using Raman-fluorescence, backscattering and laser scanning confocal microscopy. The rationale of using Raman-fluorescence mapping was based upon the observed fluorescence of the NDs in Raman spectral measurements, thus were expected to generate a higher Raman intensity regions in the NDs treated cells compared to the untreated cells or the cellular regions devoid of NDs. Although the Raman-fluorescence mapping demonstrated the high intensity regions with NDs treated cells, but neither the diamond peak was successfully identified nor were the distinct areas, requiring me to use another technique to test the cellular association of NDs. As the diamond has a higher refractive index and density than the cell, therefore ND particles were expected to produce elastic scattering of the incident light at a relatively higher intensity, which could indicate their presence in the cells. The backscattering mapping provided a clear evidence of interaction of fNDs with cells, however as the imaging was conducted only in two dimensional frameworks, the cellular internalization cannot be proved from these. Three dimensional confocal microscopy was performed on fNDs treated cells based upon the rationale of detection of NDs in the cells using their intrinsic fluorescence.

Finally, to determine the efficacy of fNDs to deliver anti GFP-siRNA in GFP expressing cells, fluorescence activated cell sorting was performed. The siRNA bound to the fNDs were expected to knockdown the GFP considerably, decreasing the overall GFP fluorescence intensity in the fNDs-siRNA treated cell population in comparison to the naked siRNA treated cells.

Chapter 4

LYSINE-FUNCTIONALIZED NANODIAMONDS: SYNTHESIS, PHYSIOCHEMICAL CHARACTERIZATION AND NUCELIC ACID BINDING STUDIES

Kaur R, Chitanda JM, Michel D, Maley J, Borondics F, Yang P, Verrall RE, Badea I.
International Journal of Nanomedicine.2012;1(7):3851-3866.

Abstract

Purpose: Detonation nanodiamonds (NDs) are carbon-based nanomaterials that, because of their size (4–5 nm), stable inert core, alterable surface chemistry, fluorescence, and biocompatibility, are emerging as bioimaging agents and promising tools for the delivery of biochemical molecules into cellular systems. However, diamond particles possess a strong propensity to aggregate in liquid formulation media, restricting their applicability in biomedical sciences. Here, the authors describe the covalent functionalization of NDs with lysine in an attempt to develop nanoparticles able to act as suitable non-viral vectors for transferring genetic materials across cellular membranes.

Methods: NDs were oxidized and functionalized by binding lysine moieties attached to a three-carbon-length linker (1,3-diaminopropane) to their surfaces through amide bonds. Raman and Fourier transform infrared spectroscopy, zeta potential measurement, dynamic light scattering, atomic force microscopic imaging, and thermogravimetric analysis were used to characterize the lysine-functionalized NDs. Finally, the ability of the functionalized diamonds to bind plasmid DNA and small interfering RNA was investigated by gel electrophoresis assay and through size and zeta potential measurements.

Results: NDs were successfully functionalized with the lysine linker, producing surface loading of 1.7 mmol g^{-1} of ND. These modified NDs formed highly stable aqueous dispersions with a zeta potential of 49 mV and particle size of approximately 20 nm. The functionalized NDs were found to be able to bind plasmid DNA and small interfering RNA by forming nano-sized "diamoplexes".

Conclusion: The lysine-substituted ND particles generated in this study exhibit stable aqueous formulation and show potential for use as carriers for genetic materials.

4.1 Introduction

In recent years, the scientific community has become increasingly interested in detonation nanodiamonds (NDs) because of their unique structural, chemical, optical, and biological characteristics [1]. NDs were first produced in Russia in the 1960s through the incomplete combustion of carbon-containing explosives [2]. While these diamond nanoparticles initially attracted the attention of the industrial world and have been utilized to improve the physical properties of polymers, the shelf life of mechanical tools, and in the electrochemical coating of metals [3], investigations into their nano-scale properties have recently placed significance on their biological applications [4-6].

The most attractive feature of NDs is their uniform nano-scale size distribution. The primary particle size of a ND ranges from 4 to 5 nm [1,7,8], with a chemically inert diamond core and a shell comprising sp^2-hydridized carbon structures [9]. Various oxygen-containing functional groups are found on the surface of NDs [8,10,11], opening the potential for their conjugation with biochemical moieties. Surface modifications of NDs can be achieved through either a physical or a covalent (amide or ester bonding) interaction. Physical adsorption of NDs has been widely accomplished using toxins [12], proteins [13,14], chemotherapeutic drugs [5,6,15], and nucleic acids [16,17]. Carboxylic [18,19] and nitrogen-containing [20] functional groups have been successfully grafted onto NDs using a radical generation mechanism, while alkyl-, amino-, and amino acid-functionalized diamonds have been created through the chemical modification of fluorinated NDs with alkyl lithium, ethylenediamine, or glycine ethyl ester hydrochloride, respectively [21]. Moreover, NDs have also been functionalized with amino acids [22] and alkyl chains [23] via covalent bonding.

NDs have been found to be biocompatible with various cell lines [15,24,25], and they exhibit lower cytotoxicity than other carbon-based nanomaterials such as single- and multi-walled carbon nanotubes, and carbon black [24,25]. As such, they have been assessed for their ability to act as vectors for the intracellular delivery of drugs and biochemical molecules. It has been shown that the hydrophilic nature of NDs is responsible for improving the aqueous solubility of chemotherapeutic and anti-inflammatory drugs that have initially showed poor solubility in water [26]. Indeed, chemotherapeutic drugs such as doxorubicin [5] and 10-

hydroxycamptothecin [6] have been successfully delivered into cancer cells after being bound to NDs. This carbon nanomaterial has also been envisioned as a suitable vector for gene therapy, and polymer-coated NDs have been shown to improve the delivery of plasmid DNA (pDNA) [16] and small interfering RNA (siRNA) [17] into cellular systems. Contrary to self-assembling nanoparticles, NDs are attractive for use in these applications because of their ability to resist biological environmental changes, which could improve the overall delivery of the attached biomolecules.

Despite the promise NDs show as vectors for delivering small chemical drugs and large biotechnology products, it remains a challenge to obtain nano-sized ND particles in laboratory and industrial settings owing to their strong tendency to assemble into micron-sized aggregates when dispersed in a polar liquid medium. As these aggregates have the potential to block capillaries, which could lead to toxic effects in the body [27], the maintenance of dispersion stability of NDs is a key requirement when developing drug delivery formulations. One way in which dispersion stability can be improved is through the use of chemical modifications such as fluorination [21] and biotinylation [28]. These methods have been shown to reduce the size of ND aggregates from micrometer sizes to 160 [21] and 170 nm [28], respectively. While a variety of mechanical disaggregation approaches have also been explored, stirred media milling and bead-assisted probe sonication were the most successful in achieving high dispersion stability and producing single-digit nanometer particle sizes [29]. However, while primary-sized NDs may be attained by high-energy bead-assisted probe sonication, the potential for the contamination of samples with sonotrode material when using this technique [29] is unacceptable in life science applications. To the authors' knowledge, no previous studies have examined the disaggregation of NDs to particles less than 50 nm in size using a simple mechanochemical technique that can be applied at a laboratory level. Therefore, the purpose of this study was to generate nanosized, amino acid–functionalized particles through the covalent modification of NDs with lysine using conventional bath sonication. These functionalized NDs were found to have the ability to bind nucleic acids through electrostatic interactions and the potential to act as vectors for carrying genetic materials into cellular systems, using aqueous medium.

4.2 Material and Methods

4.2.1 Chemicals

Pharmaceutical-grade (ND98) carboxylic acid–functionalized NDs with an average particle size of 5 nm were purchased from Dynalene Inc (Whitehall, PA). Tosoh Corporation (Grove City, OH) graciously provided YTZ® grinding media (0.05 mm). Dry dimethylformamide (DMF), 4M hydrochloric acid (HCl) (in dioxane) and ethidium bromide solution (~1% in water) were obtained from Sigma-Aldrich (Oakville, ON, Canada). Boc-lysine(Boc)-OH, Fmoc-$NH_2(CH)_3NH_2$·HCl, diisopropylethylamine (DIPEA), piperidine, and HATU [N,N,N′,N′-tetramethyl-O-(7-azabenzotriazol-1-yl)uronium hexafluorophosphate] were obtained from Chem-Impex International, Inc. (Wood Dale, IL). Dichloromethane (DCM) (high-performance liquid chromatography grade) was purchased from Thermo Fisher Scientific (Waltham, MA) and was dried using a solvent purification system (MBraun Incorporated, Stratham, NH). Thionyl chloride was acquired from Alfa Aesar (Ward Hill, MA). The pGTCMV.IFN-GFP plasmid (encoding for interferon gamma and green fluorescent protein genes) [30] was used as a model plasmid for examining the binding properties of NDs. Anti-GFP siRNA was purchased from Ambion® (Life Technologies Inc, Burlington, ON, Canada). Gibco® UltraPure DNase/RNase-free water was obtained from Invitrogen (Life Technologies Inc, Burlington, ON, Canada). All chemicals were at 99% purity.

4.2.2 Preparation and Functionalization of NDs with Lysine

Unless otherwise stated, all reactions (Figure 4.1) were carried out under a nitrogen atmosphere using standard Schlenk techniques. Ultrasonication was performed using a bath sonicator in some steps of the reaction scheme in order to improve the accessibility of chemical reagents to the surfaces of the nano-sized particles.

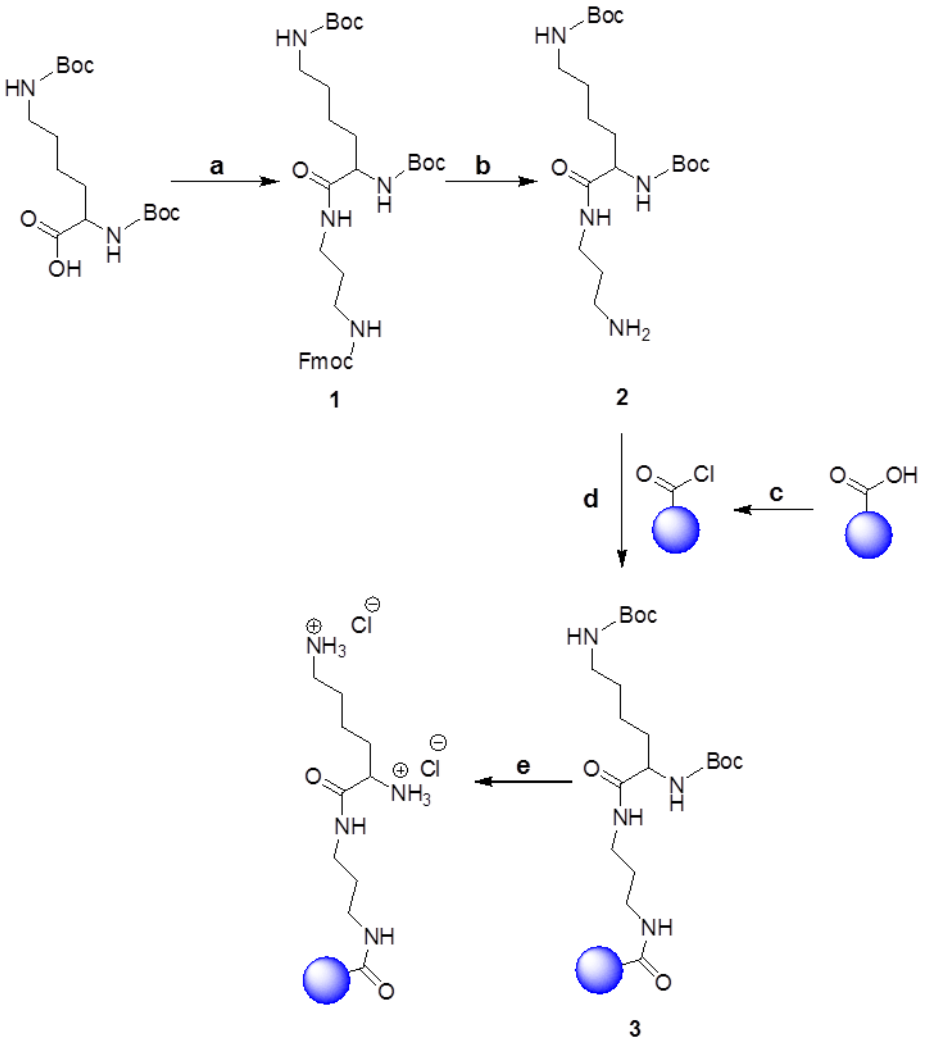

Figure 4.1: Preparation and functionalization of nanodiamonds with lysine in the presence of a 3-carbon-length linker.

Preparation and functionalization of nanodiamonds (NDs) with lysine in the presence of a three-carbon-length linker: (A) synthesis of compound 1 [N′-(N^{α},N^{ε}-bis-Boc-lysyl),N″-(Fmoc)-diaminopropane], reagents, and solvents – Fmoc-NH$(CH2)_3NH_2$ · HCl, HATU [N,N,N′,N′-tetramethyl-O-(7-azabenzotriazol-1-yl) uronium hexafluorophosphate], diisopropylethylamine, and dimethylformamide (DMF); (B) Fmoc deprotection, reagents, and solvents – 50% (v/v) piperidine-DMF; (C) reoxidation of pristine carboxylated NDs, reagents – concentrated sulfuric acid and concentrated nitric acid, and preparation of acid chloride–functionalized NDs, reagents – thionyl chloride; (D) synthesis of Boc-protected lysine-functionalized NDs, solvent – DMF; (E) deprotection of Boc on lysine-functionalized NDs, reagents, and solvents – hydrochloric acid and dichloromethane.

Step A: synthesis of N′-(N^{α},N^{ε}-bis-Boc-lysyl),N″-(Fmoc)-diaminopropane

In a dry Schlenk flask, Boc-lysine(Boc)-OH (8.661 mmol) was dissolved in dry DMF (15 mL), followed by the addition of HATU (10.82 mmol) and DIPEA (17.97 mmol). The reaction mixture was then stirred for 15 minutes before the addition of a 10 mL solution of Fmoc-$NH(CH_2)_3NH_2 \cdot HCl$ (9.925 mmol) and DIPEA (10.92 mmol) in DMF. After 18 hours, DMF was removed from the reaction mixture under high vacuum, and the sample was dissolved in DCM (100 mL) and extracted with a saturated aqueous solution of sodium bicarbonate (4 × 100 mL). The organic phase was dried with sodium sulfate before removing the DCM under vacuum. Upon further purification by column chromatography (Silica Gel 60, EMD Inc, Mississauga, ON, Canada) using a methanol-chloroform (1:9, v/v) solvent system, a pale yellow solid compound, N-(N^{α},N^{ε}-bis-Boc-lysyl),N″-(Fmoc)-diaminopropane (hereafter called compound 1), was obtained with a yield of 79%.

Step B: Fmoc deprotection of compound 1

The removal of Fmoc from compound 1 was carried out using 300 mg of the compound and 10 mL of a 50% (v/v) piperidine-DMF mixture. The recovered compound (hereafter called compound 2) was used in step D without further purification.

Step C: reoxidation of NDs and preparation of acid chloride–functionalized NDs

In order to optimize the surface functionalization of the pristine carboxylated NDs (pNDs), they were reoxidized in a mixture of concentrated nitric and sulfuric acids (1:3, v/v) with overnight ultrasonication [31-33]. The reoxidized NDs (rNDs) were subsequently dialyzed with water using a cellulose membrane with an average pore radius of 2.4 nm until neutral pH was achieved, and then they were freeze-dried. To promote amide bond formation between the NDs and compound 2, the surface carboxylic acid groups of the rNDs were converted into more reactive acyl chloride functional groups using an excess of thionyl chloride [34-36] in the presence of YTZ® grinding media. This mixture was ultrasonicated at a frequency of 25 kHz in a bath sonicator (Transsonic TI-H-5 Ultrasonicator; Elma Hans Schmidbauer GmbH and Co KG, Singen, Germany) for 22 hours, refluxed for 5 hours at 70°C, and ultrasonicated for 48 hours. Finally, the sample was dried overnight under high vacuum.

Steps D and E: preparation of lysine-functionalized NDs

Compound 2 was dissolved in 10 mL of DMF and added to the acid chloride–functionalized NDs (100 mg) suspended in 5 mL of DMF. The heterogeneous mixture was refluxed for 45 minutes at 75°C, ultrasonicated for 72 hours, and lyophilized. Boc removal (step E, Figure 4.1) was achieved by suspending the Boc-protected lysine-functionalized NDs (fNDs) in 10 mL of DCM and 10 equivalents of HCl (4 M in dioxane) [37] for 90 minutes. This produced positively charged fNDs capable of electrostatic interactions with the negatively charged phosphate groups of DNA. The fNDs were dialyzed with ethanol followed by water, using a cellulose membrane with an average pore radius of 2.4 nm, before being freeze-dried.

4.2.3 Nuclear Magnetic Resonance and Mass Spectroscopic Characterization of Compound 1

Proton nuclear magnetic resonance (^{1}H NMR) spectra were recorded on a Bruker 500 MHz Avance spectrometer (Bruker BioSpin, Milton, ON, Canada). Chemical shifts for ^{1}H NMR are reported in ppm in reference to the residual ^{1}H resonances of deuterated chloroform at δ 7.26. Mass spectrum was obtained using the QSTAR® XL MS/MS System with electrospray ionization source (ESI-Q-TOF) (Applied Biosystems, Toronto, ON, Canada).

4.2.4 ND Dispersions

NDs (2 mg/mL) in reverse osmosis-purified water (Millipore, Milford, MA) were ultrasonicated at a frequency of 25 kHz for 4 hours and centrifuged at 5200 g for 6 minutes. The resulting dispersions were used for Raman spectroscopy, atomic force microscopy (AFM), gel electrophoresis, and zeta potential and size distribution measurements. For the dispersion stability experiment, the ND samples were sonicated for 20 minutes and allowed to settle for 3 days at room temperature without centrifugation.

4.2.5 Raman Spectroscopic Measurements

Raman spectroscopic measurements were carried out using a Renishaw Invia Reflex microscope (Renishaw Inc, Chicago, IL) fitted with a 514.5 nm argon ion laser (Spectra-Physics® 163-M42-010 Spectra Physics®, Santa Clara, CA) and 1800 line/mm grating. Aqueous

dispersions of NDs were dropped onto a gold-coated silicon wafer (Platypus Technologies, Madison, WI) and allowed to dry. A Leica N PLAN Objective (Leica Microsystems, Buffalo Grove, IL) 50× with a numerical aperture of 0.75 was used to focus the sample, and backscattered Raman signals were detected using a Peltier-cooled charge-coupled device. Instrument calibration was verified using an internal silicon wafer, measured at 520 cm^{-1}.
The Raman spectra of NDs and compound 1 were acquired in the static scanning mode. Baseline correction was performed using Renishaw WiRE software (v3.2; Renishaw Inc).

4.2.6 Infrared Spectroscopy

Infrared (IR) spectra of all materials were recorded on a Bruker IFS 66v/S Fourier transform spectrometer (Bruker Optics, Billerica, MA) in the mid-IR range using a liquid nitrogen–cooled mercury cadmium telluride detector at the Canadian Light Source, University of Saskatchewan, Saskatoon, SK, Canada. All sample measurements were carried out in the solid state using pelletized, homogeneous powder dispersions of the materials in a potassium bromide matrix. For compound 1, a PIKE MIRacle™ Single Reflection ATR (PIKE Technologies, Madison, WI) accessory was used in order to avoid potential pressure-induced changes. In all cases, 512 individual interferograms were averaged for both the background and the sample measurements from which the absorbance spectra were calculated.

Data analysis was performed with the Bruker OPUS software package (v6.5; Bruker Optics). Baseline correction was performed on all raw absorbance spectra using the built-in concave rubber band correction routine (number of baseline points: 32; number of iterations: 2) to strictly avoid the introduction of any artificial features into the spectra.

4.2.7 Size and Zeta Potential Measurements

Particle size and zeta potential measurements were obtained using a Malvern Zetasizer Nano ZS instrument (Malvern Instruments Ltd, Malvern, Worcestershire, UK). The size distribution of NDs in water was obtained by measuring the light scattered ($\theta = 173°$) by particles (dynamic light scattering, DLS) illuminated with a laser beam, using the CONTIN algorithm to analyze the decay rates that are a function of the translational diffusion coefficients of the particles, D. The measured data are reported in volume distribution. The hydrodynamic

radius, R_H, of the particles was estimated using the Stokes-Einstein equation ($R_H = kT/6\pi\eta D$), where k is the Boltzmann constant, T is the temperature, and η is the viscosity of the solution. This analysis gives an estimate of size based upon the hydrodynamic radius of spherical particles having a translational diffusion coefficient equivalent to the actual particles. Size distribution values were derived from three measurements, each consisting of a minimum of ten individual runs. Zeta potential measurements were based upon laser Doppler electrophoresis and phase analysis light scattering analysis. The reported zeta potentials are the average of three measurements, each derived from a minimum of ten individual runs.

4.2.8 AFM

AFM images were obtained in intermittent contact mode using an atomic force microscope (Agilent 4500; Agilent Technologies, Inc., Chandler, AZ) equipped with a silicon cantilever (T190R; Nanoscience Instruments, Inc., Phoenix, AZ). The specifications of the silicon cantilever include a force constant of approximately 45 N/m and a resonant frequency of approximately 190 kHz. A small volume (25 µL) of ND dispersion samples was dropped onto a freshly prepared poly-L-lysine-coated mica substrate and allowed to incubate for 1 minute. The substrate was then rinsed with purified water and dried gently using a stream of nitrogen gas. The amplitude range was between 1 and 1.5 V for all measurements, while the amplitude ratio for set point to free air oscillation was 0.80. Ambient conditions were maintained throughout the experimental procedure, and the scan rate used for image acquisition ranged from 0.5 to 1 lines per second (512 pixels per line). Line scan profiles were obtained for three particles from each sample, and the reported particle sizes were determined from the particle height (SPIP, v5.1.6; Image Metrology A/S, Lyngby, Denmark).

4.2.9 Thermogravimetric Analysis

Thermogravimetric analysis was carried out using a TGA Q50 (TA Instruments-Waters LLC, New Castle, DE). The furnace tube carrying the sample was heated to 450°C, and the percentage weight loss was obtained as a function of the temperature. The surfaces of the pNDs and rNDs were considered dominated by carboxylic acid functional groups, and surface loading was calculated using the following equation:

$$\text{Surface loading} = \frac{\text{Number of moles}_{\text{lost functional group}}}{\text{Weight}_{\text{total sample}} - \text{Weight}_{\text{lost sample}}} \quad (4.1)$$

Any loss in weight that occurred below 115°C was attributed to water and was excluded from estimates of surface loading.

4.2.10 Agarose Gel Electrophoresis

Electrophoresis was performed in 1% (for pDNA) or 2% (for siRNA) agarose gels prepared with tris-acetate ethylenediaminetetraacetic acid buffer and ethidium bromide at a final concentration of 1 µg/mL. The amounts of pDNA and siRNA in each sample were 500 and 400 ng, respectively. Complexes of fNDs-pDNA and fNDs-siRNA with different weight ratios (fNDs:nucleic acid component ranging from 1:1 to 50:1) were prepared in ultrapure water and incubated for 30 minutes at room temperature. Uncomplexed pDNA and siRNA were used as standards. All samples were loaded into the gel using 30% glycerol and were subjected to electrophoresis at 100 V using a Bio-Rad PowerPac HC electrophoresis apparatus (Bio-Rad Laboratories, Inc., Mississauga, ON, Canada) for 1 hour for pDNA or 45 minutes for siRNA. The gels were then imaged using an AlphaImager® imaging system (Alpha Innotech Corporation, San Leandro, CA) to detect ultraviolet fluorescence.

4.2.11 Size and Zeta Potential Measurements of fND-pDNA and fND-siRNA Complexes

Size and zeta potential measurements of fND-genetic material complexes formed at weight ratios in the range between 1:1 and 50:1 were performed using the Zetasizer Nano ZS (Malvern Instruments Ltd). Different sets of samples were prepared for analysis of size and zeta potential using the same sample preparation technique as described for agarose gel electrophoresis assay. Each reported value was obtained from the Z-average size, and each value is the average of four measurements, each consisting of a minimum of ten individual runs.

4.3 Results and Discussion

4.3.1 Synthesis of fNDs

The synthesis of the lysine linker intermediate (compound 1) and its subsequent covalent functionalization with NDs was performed (Figure 4.1). The ^{1}H NMR spectrum of compound 1 was used to established its structure: ^{1}H NMR (500 MHz, deuterated chloroform) δ 7.76(d, J = 7.5, 2H, fluorenyl), 7.61 (d, J = 7.4, 2H, fluorenyl), 7.39 (t, J = 7.5, 2H, fluorenyl), 7.31 (t, J = 7.4, 2H, fluorenyl), 6.67(s, 1H, NH), 5.48(s, 1H, NH), 5.23(s, 1H, NH), 4.67(s, 1H, NH), 4.38(d, J =7.0, 2H, fluorenyl-CH_2), 4.21(t, J = 7.0, 1H, fluorenyl-CH), 4.04(s, 1H), 3.28 (m, 2H), 3.20(m, 2H), 3.10(m, 2H), 1.63–1.82(m, 4H), 1.48 (m, 2H), 1.43(s, 18H, Boc-$(CH_3)_6$), 1.37(m, 2H) (Figure S 4.1). The successful synthesis of compound 1 was also confirmed by mass spectroscopic measurements: electrospray ionization mass spectrometry mass-to-charge ratio calculated for $C_{34}H_{48}N_4O_7$: 624.3523 [M], found 625.3603 $[M+H]^+$ (Figure S 4.2).

4.3.2 Surface Functionalization Assessed by Raman Spectroscopy, IR Spectroscopy, Zeta Potential, and Thermogravimetric Measurements

To provide evidence of functionalization of NDs with the lysine linker, Raman spectroscopy of pNDs, rNDs, fNDs, and compound 1 was performed (Figure 4.2). The pNDs showed the signature peak of diamond at 1326 cm^{-1}, which is downshifted in frequency compared with the 1332 cm^{-1} Raman peak assigned to bulk diamond [38]. This frequency shift could be attributed to the smaller size of NDs, as explained by the phonon confinement model [39,40]. Furthermore, the existence of the diamond peak at ∼1326 cm^{-1} after the reoxidation process suggests that the intrinsic diamond structure was unaltered by the harsh acidic oxidation conditions. A broad peak was also observed at 1617 cm^{-1} on the pND spectra, which could have arisen because of overlapping signals from the in-plane stretching of the sp^2 carbon (G-mode) at ∼1590 cm^{-1}, oxygen-hydrogen (O-H) bending at ∼1635 cm^{-1}, and carbon-oxygen double bond stretching of the carboxylic acid group at ∼1740 cm^{-1} [41]. The suppression of the D-band of graphitic carbon (∼1410 cm^{-1}) in the Raman spectra of pristine and reoxidized NDs supports the existence of high ratios of sp^3/sp^2 carbon in NDs [42]. After reoxidation, the emergence of a prominent band at ∼1630 cm^{-1} was accompanied by a decrease in the 1590 cm^{-1} band of

graphitic carbon, supporting the use of mineral acids in the oxidation of graphitic carbon. Raman spectroscopy was not used to monitor carboxylic acid vibrations in any of the samples.

The Raman spectrum of compound 1 revealed noticeable peaks of carbon-hydrogen (C-H) deformation at ~1481 cm^{-1}, amide III at ~1295 cm^{-1}, and amide I at ~1611 cm^{-1}, with a weak shoulder representing amide II observed at ~1580 cm^{-1}. It is important to note that the fND spectrum was acquired by a single scan, as additional laser scanning resulted in burning of the fNDs. In comparison with the Raman spectrum of compound 1, the Raman spectrum of the fNDs exhibited amide I (~1612 cm^{-1}), amide II (~1582 cm^{-1}), amide III (~1299 cm^{-1}), and C-H deformation (~1482 cm^{-1}) peaks, indicating that the functionalization had been successful. The Raman peak of fNDs at 1299 cm^{-1} is very broad in comparison with the corresponding peak of compound 1 because of interference from the diamond signal. Furthermore, the covalent modification of the NDs with the lysine linker, which has a much higher mass than carbon, caused a further downshift in the frequency of the diamond signal in fNDs.

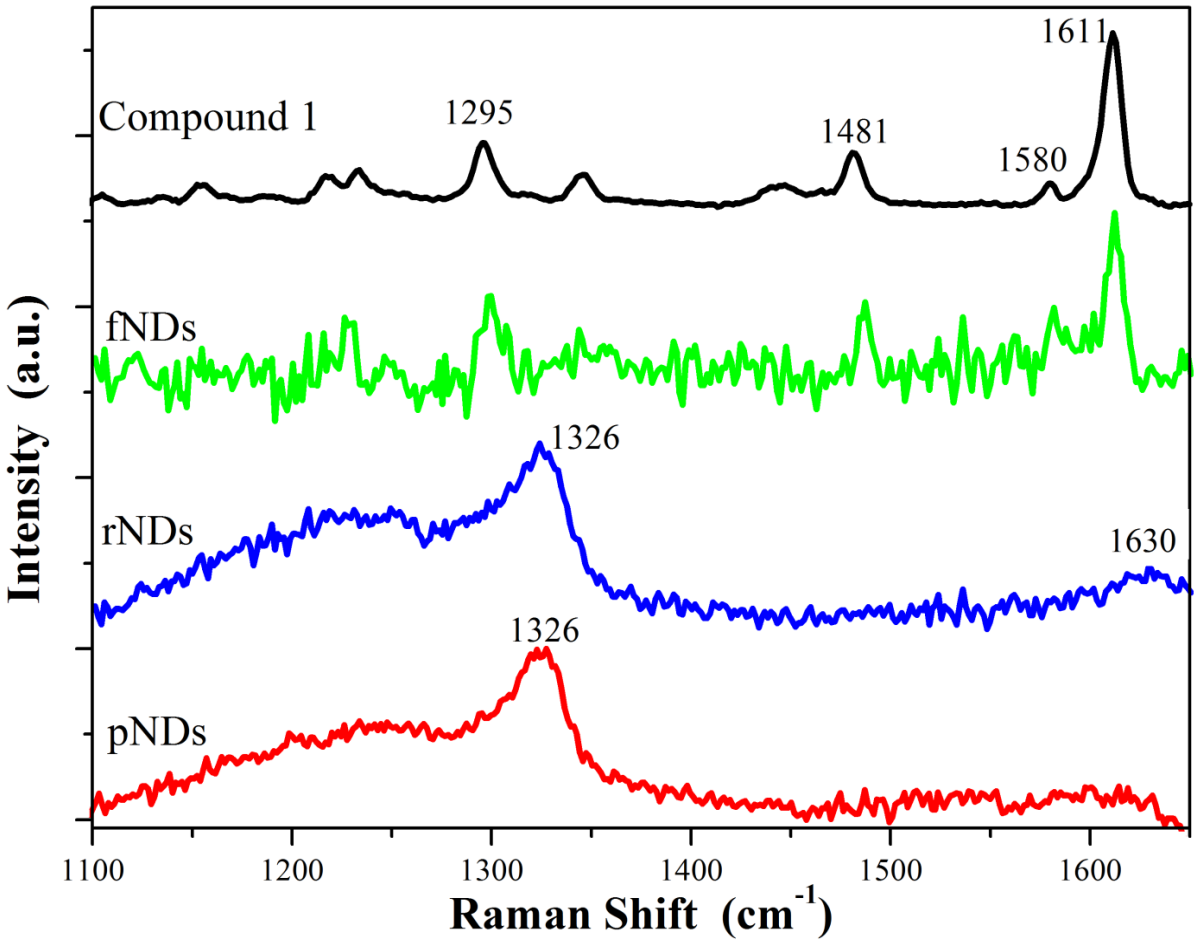

Figure 4.2: Raman spectra of nanodiamonds and compound 1

Baseline-corrected static scan Raman spectra of the pristine carboxylated nanodiamonds (pNDs), reoxidized nanodiamonds (rNDs), lysine-functionalized nanodiamonds (fNDs), and compound 1 [N′-(N^{α},N^{ε}-bis-Boc-lysyl),N″-(Fmoc)-diaminopropane] using a 514.5 nm excitation source. A total of 128 accumulations were collected for pNDs and rNDs, while the spectrum of fNDs was obtained from a single acquisition.

Overall, the Raman spectra obtained in this study support the successful formation of fNDs; however, as the Raman cross section is smaller than the fluorescence cross section, it is likely that fluorescence swamps the Raman signals. Hence, to strengthen the evidence of successful functionalization, IR spectroscopy, a complementary technique to Raman spectroscopy, was performed at various stages of functionalization, including on compound 1 (Figure 4.3A). Band positions are indicated by the second derivative curves (Figure 4.3B). The ND spectra showed that characteristic bands at ~1045 cm^{-1} and ~1262 cm^{-1} due to vibrations of ether-like groups [43] might arise from the covalent bonding of inter-particular carboxylic and/or hydroxyl groups, as well as bands in the C-H stretching region at ~2900 cm^{-1} due to vibrations arising from the C-H bonds present on the surface of the NDs. In fact, a very broad IR spectrum ranging from 1000 to 1500 cm^{-1} is identified as the "fingerprint region" of NDs in the literature [42]. It is important to note that all ND spectra were found to have features in the carbonyl region (~1760 cm^{-1}), suggesting that the raw material was already somewhat oxidized. The peaks at ~1630 cm^{-1} (O-H bending) and ~3400 cm^{-1} (O-H stretching) may have originated because of either the water adsorbed onto the NDs/potassium bromide or the presence of covalently bonded hydroxyl functional groups on the surface of the NDs.

Comparing the spectra of fNDs with those of pNDs and rNDs, it is evident from both the peak height and shape of the band located at ~1630 cm^{-1} that the functionalization reaction was successful. The presence of an amide I band from ~1640 to 1690 cm^{-1} and an amide II shoulder from ~1510 to 1580 cm^{-1} in the fND spectrum provide further evidence of functionalization. These bands were also observed in the compound 1 spectrum at a slightly higher frequency. The peak at ~730 cm^{-1} in the spectra of both fNDs and compound 1 is associated with the rocking mode of hydrocarbons with more than four methylene groups [44], while a methylene deformation band can be observed at ~1465 cm^{-1}. A combination of the spectra of the two starting materials (rNDs and compound 1) was recognizable in the C-H stretching region of the second derivative spectra (Figure 4.3B, red oval shape), further verifying the lysine functionalization of NDs.

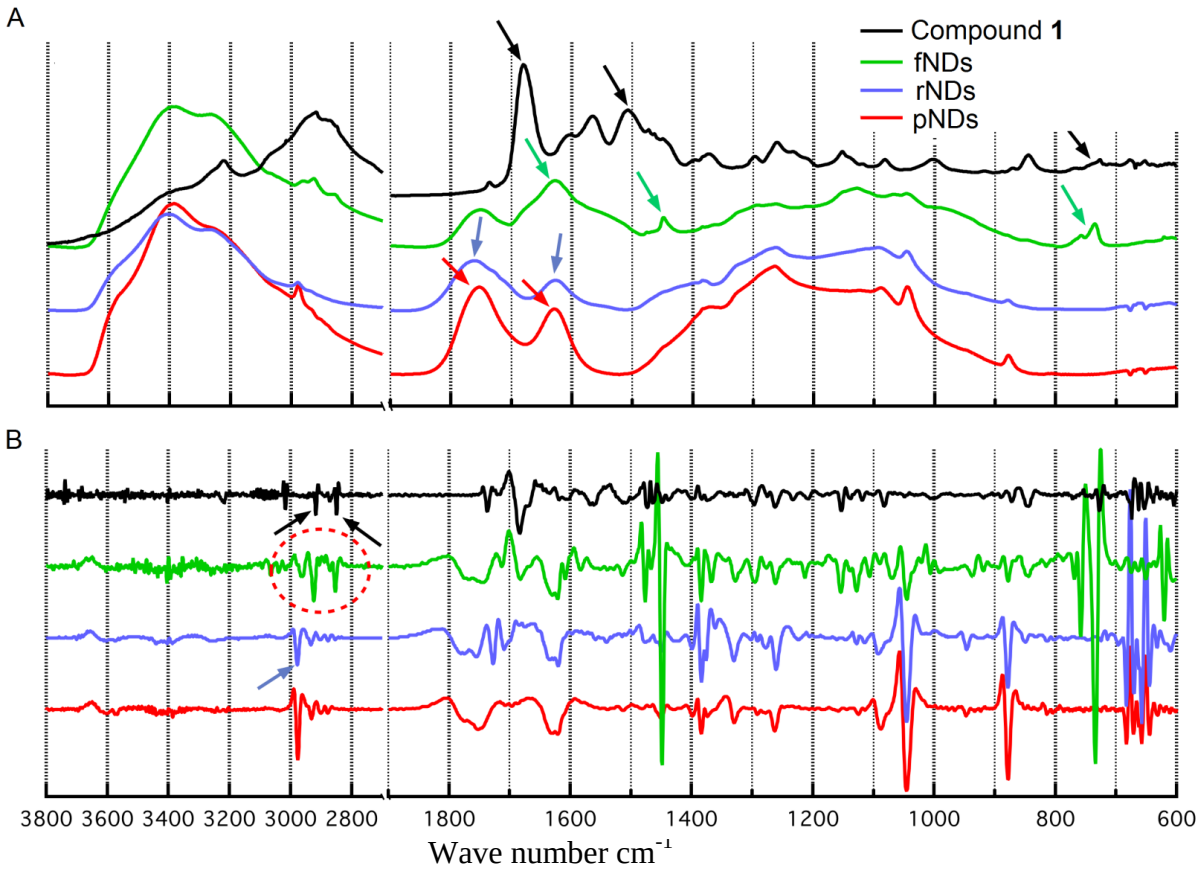

Figure 4.3: Infrared spectra of nanodiamonds and compound 1

Baseline-corrected absorbance and attenuated total reflectance: (A) infrared spectra of the pristine carboxylated nanodiamonds (pNDs), reoxidized nanodiamonds (rNDs), lysine-functionalized nanodiamonds (fNDs), and compound 1 [N′-(N^{α},N^{ε}-bis-Boc-lysyl),N″-(Fmoc)-diaminopropane]; (**B**) second derivatives of all spectra. A total of 512 individual interferograms were collected and averaged for each sample. The featureless region between wave numbers of 2700 and 1900 cm^{-1} is not shown.

The successful functionalization of NDs with lysine was also confirmed by the zeta potential measurements (Table 4.1). The pNDs showed a negative zeta potential of −21.1 mV, suggesting that negatively charged surface functional groups such as carboxylate were present. After reoxidation, the mean zeta potential shifted to −23.7 mV, indicating a slight increase in the density of negatively charged surface groups. As expected, the lysine-modified NDs showed a positive zeta potential of +48.9 mV, demonstrating the predominance of a large number of positively charged (amine) groups on their surfaces.

Thermogravimetric analyses were performed to provide quantitative estimates of the surface loading of functional groups attached to the NDs. The thermograms of the pNDs and rNDs did not show any considerable weight loss in the temperature range of 30°C to 440°C, indicating that NDs are thermally stable in this range (Figure 4.4). The surface loading of the pNDs, rNDs, and fNDs was calculated (Table 4.2) from their respective thermograms. Providing that the surfaces of pNDs and rNDs are dominated by carboxylate groups, the estimated surface coverage was 0.35 mmol g^{-1} for the pNDs and 1.0 mmol g^{-1} for the rNDs, while the fNDs demonstrated surface loading of 1.7 mmol g^{-1} of ND. This coverage is greater than was found in a previously reported study of the covalent functionalization of long-chain alkyl groups on the surface of NDs (0.3–0.4 mmol g^{-1}) [23]. The high surface functionalization confers high nucleic acid–binding capacity to the nanomaterial.

Table 4.1: Zeta potential measurements of nanodiamonds

Sample	Zeta Potential (mV) in Millipore water
pNDs	-21.1 ± 0.2
rNDs	-23.7 ± 0.5
fNDs	+48.9 ± 0.1

Each value represents the mean ± standard deviation of three measurements with $n \geq 10$

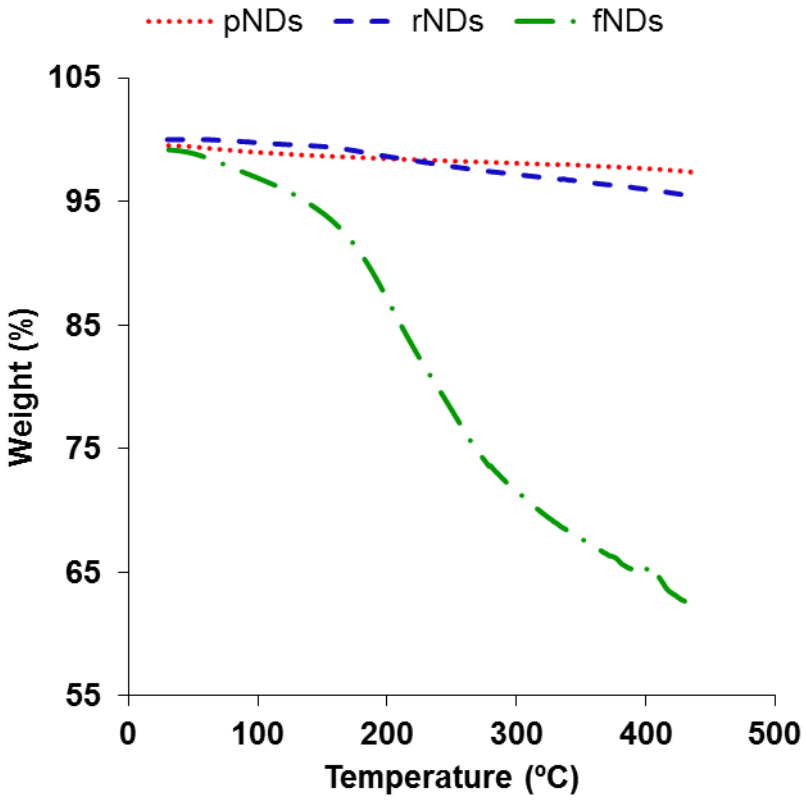

Figure 4.4: Thermograms of samples of nanodiamonds.

Thermograms of pristine carboxylated nanodiamonds (pNDs), reoxidized nanodiamonds (rNDs), and lysine-functionalized nanodiamonds (fNDs) shows highest % weight loss in fNDs followed by rNDs and pNDs.

Table 4.2: Surface loading of nanodiamonds as calculated from their respective thermograms

Sample	Surface Loading (mmol/g)
pNDs	0.35
rNDs	1.00
fNDs	1.70

Note: Weight loss below 115ºC is excluded

4.3.3 Dispersion of NDs in Aqueous Medium and AFM Imaging

For biomedical applications, the stability of the biomaterial in aqueous medium is of paramount importance, as aggregation can lead to toxic effects in biological systems. In this study, the pND, rND, and fND samples were dispersed in water and the stability of the resultant hydrosols was monitored for 3 days. While sedimentation of the pND and rND hydrosols was observed to occur within the first 5 minutes of incubation, fNDs remained stable even after 3 days (Figure 4.5). This was in agreement with the results of the authors' zeta potential measurements, which also indicated that fNDs have colloidal stability in water. According to the DLVO theory (Derjaguin-Landau-Verwey-Overbeek), repulsive forces dominate among particles in systems with a zeta potential higher than 30 mV (49 mV for the fNDs), which prevents aggregation and flocculation of the colloidal system [45].

The high aqueous dispersibility of fNDs may be explained by the greater hydrophilicity of the lysine hydrochloride functional groups found on their surfaces [46], as well as inter-particle repulsion due to the positively charged amine groups of lysine. On the other hand, the sedimentation of pNDs and rNDs is most likely due to van der Waals' forces, dipole-dipole interactions, and/or hydrogen bonding between the surface functional groups. A similar dispersion behavior has been shown to occur with adenosine-functionalized multi-walled carbon nanotubes, which exhibit greater aqueous solubility than pristine, reoxidized forms [32].

Particle size is also considered to be an important parameter in the development of bio-nanomaterials. Therefore, hydrodynamic particle size measurements were carried out in this study to gain more insight into the suitability of fNDs for use in gene delivery applications (Figure 4.6). The pNDs were found to have a very wide size distribution (polydispersity index [PDI] = 0.56) when dispersed in aqueous medium, with a major fraction of the particles having size distributions centered at 1281 nm. Reoxidation did not improve the particle dispersibility considerably; while a shift towards smaller size with a peak at 531 nm was observed, the broadness in the size distribution was maintained (PDI = 0.59). No NDs smaller than 50 nm in diameter were detected in either pND or rND samples.

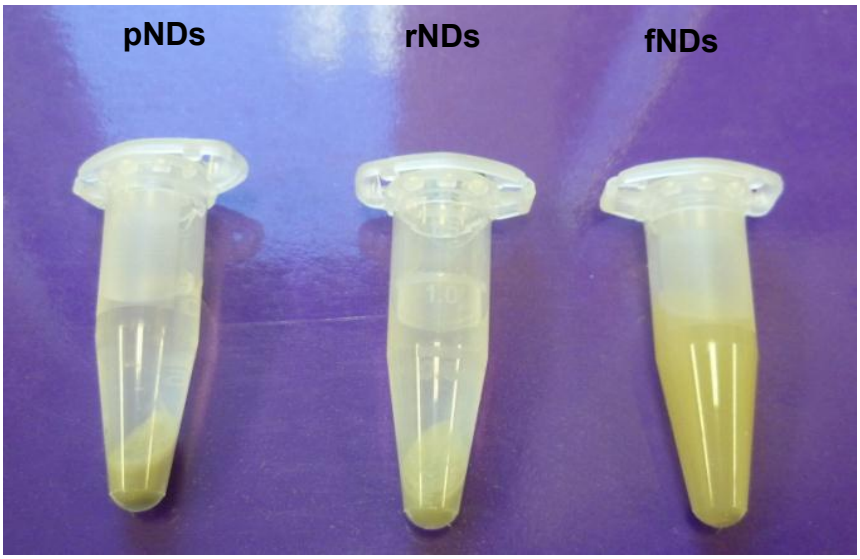

Figure 4.5: Dispersion stability of 2 mg/mL nanodiamonds samples in water.

Dispersion of nanodiamonds (NDs) in water after 20 minutes of conventional bath sonication and a 3-day incubation. From left to right: pristine nanodiamonds (pNDs), reoxidized nanodiamonds (rNDs), and lysine-functionalized nanodiamonds (fNDs).

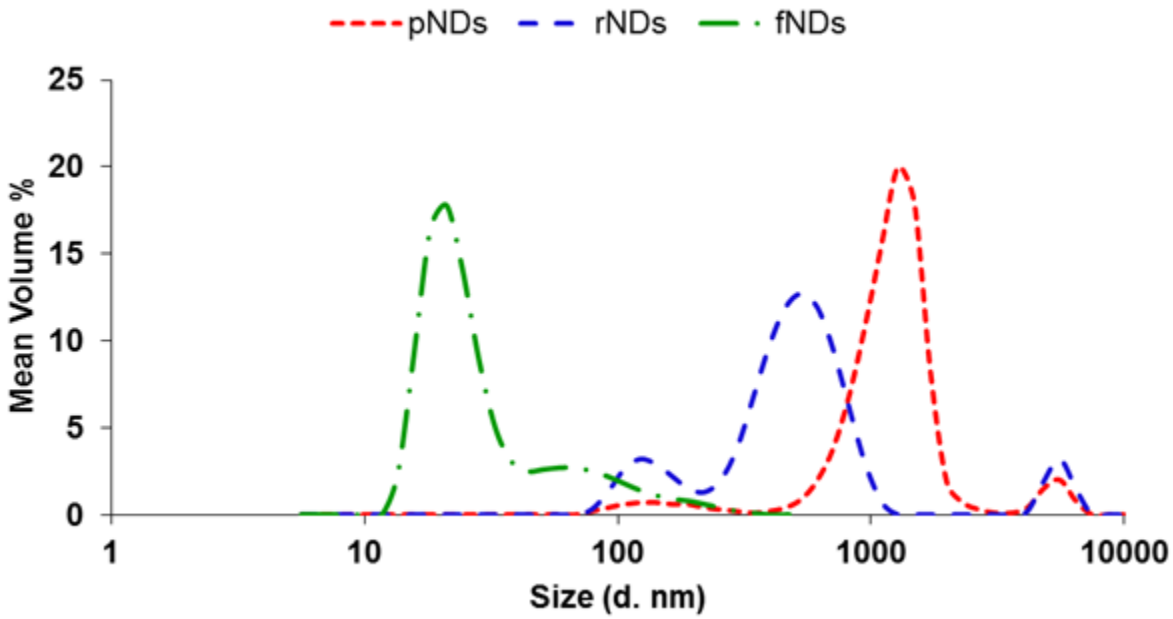

Figure 4.6: Size distribution curves of nanodiamonds samples.

Size distributions of pristine carboxylated (pNDs), reoxidized (rNDs), and lysine-functionalized nanodiamonds (fNDs) in water, as measured by dynamic light scattering. Each curve is derived from three measurements with $n \geq 10$.

In addition to the physical inter-particle interactions that cause agglomeration of pristine and reoxidized NDs, the surface carboxylate groups can also result in the formation of tightly bound aggregates via anhydride bond formation [22]. In contrast, when the size of the fNDs was examined, the surface functionalization was found to result in a remarkable reduction in aggregate size, with the majority of particles centering at 21 nm. A narrower size distribution (PDI =0.25) was also observed when compared with the pND and rND particle distributions. The fNDs in this study were also found to have considerably smaller hydrodynamic radii than those obtained in a previous study that functionalized NDs with glycine through a silane linker (peak at >350 nm) [22]. The disaggregation of fNDs also contributes to their dispersion stability in aqueous media.

AFM was used to determine the topographic features (Figure 4.7A) and size (Figure 4.7B) of pNDs (i), rNDs (ii), and fNDs (iii). Since substrate surface features and drying could cause aggregation of the particles, the height rather than the diameter is reported for particle size. The pNDs formed irregularly shaped aggregates of 40–80 nm, while the rNDs appeared to be round with a comparatively smaller aggregate size of 20–60 nm. In agreement with the DLS measurements, AFM images provided visual evidence for the disaggregation of NDs after their functionalization with the lysine linker (Figure 4.7A, iii). The particles of fNDs were found to be 3–5 nm in size. Besides aggregation on a solid mica surface, the environment of the sample and the principle of the measurement technique can also influence the size determination of particles, as can be observed in the differences in particle sizes determined by DLS and AFM. DLS measures the average hydrodynamic radius of nanoparticles in liquid medium under the assumption that they are spherical in shape, while AFM measures the height and diameter of individual particles devoid of their native environment. The different principles utilized by these two techniques for size determination have also been considered to be a cause of size variation in an earlier study [47].

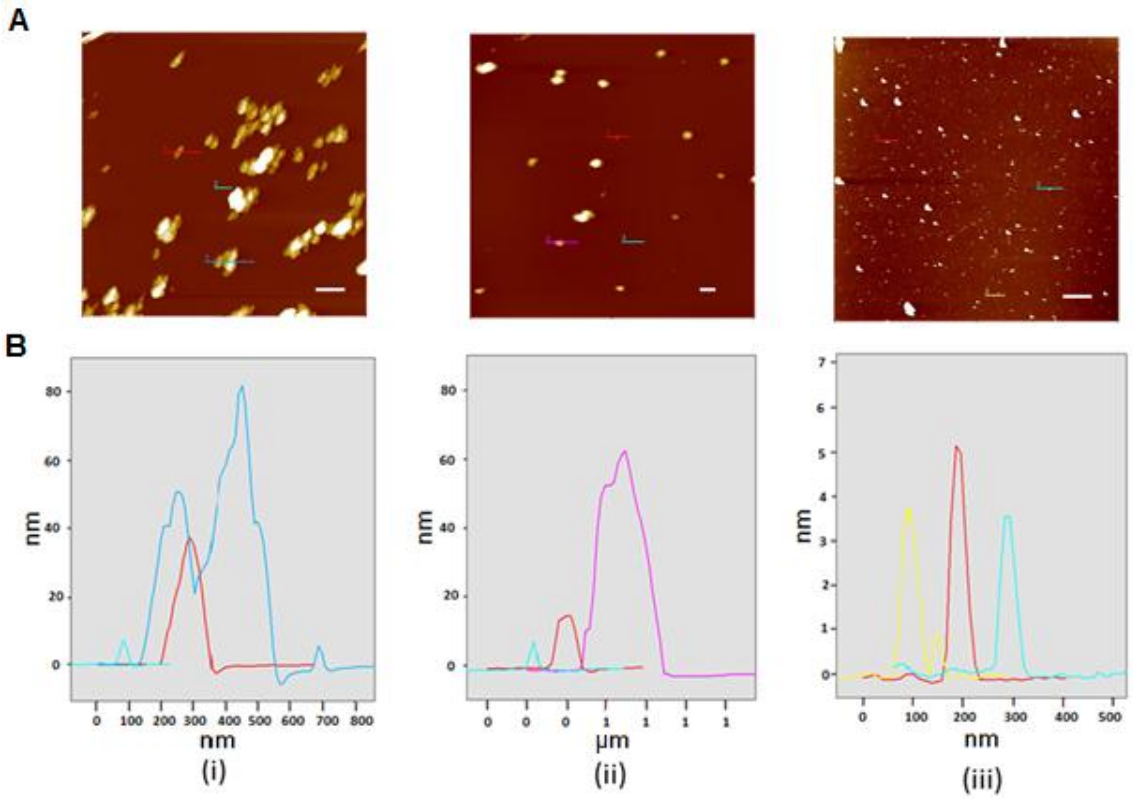

Figure 4.7: Atomic force microscopic images and line-scan profiles of nanodiamonds samples.

(A) Intermittent contact mode atomic force microscopy (AFM) of ND samples and (B) line-scan profiles of the particles indicated in each image. From left to right: (i) pristine nanodiamonds (pNDs), (ii) reoxidized nanodiamonds (rNDs), and (iii) lysine-functionalized nanodiamonds (fNDs). Line scan profiles were obtained for three particles from each sample, and the reported particle sizes were determined from the particle height.

4.3.4 Binding of fNDs to Nucleic Acids

As the nanosize, positive zeta potential, and hydrophilic properties of fNDs suggest that they may be suitable for use in biomedical applications, the applicability of fNDs as non-viral vectors was evaluated by examining their ability to bind and protect pDNA and siRNA. Weak binding can lead to the disruption of vector–nucleic acid complexes by negatively charged protein molecules, leading to inefficient gene delivery [48]. Therefore, the binding stability of complexes is essential for the protection of genetic material against enzymatic degradation and the production of high levels of gene expression in cellular systems [30]. In this study, the binding efficacy of the fNDs for genetic material was examined by carrying out gel electrophoresis assays on a series of fNDs:pDNA (Figure 4.8A) and fNDs:siRNA (Figure 4.8B) weight ratios. The naked pDNA revealed two major bands (Figure 4.8A), corresponding to the two different forms of pDNA: a highly mobile supercoiled form and a lesser mobile band representing the circular form. The complexes obtained by using equal weight ratios of fNDs and pDNA were not stable, as the migration of pDNA was not hindered (Figure 4.8A). However, no pDNA bands were detected at fNDs:pDNA weight ratios of 5:1 and above, indicating that the formation of a complex between the pDNA and the fNDs hampered its migration towards the anode. For siRNA (Figure 4.8B), the trend of binding was found to be similar; however, complex formation was comparatively less efficient than that observed with pDNA, as siRNA was detected in its free form at weight ratios of 5:1 (Figure 4.8B) and 10:1. The band intensity gradually decreased with an increase in the amount of fNDs, and only a negligible amount of siRNA was detected in its free form at weight ratios of 20:1 and higher.

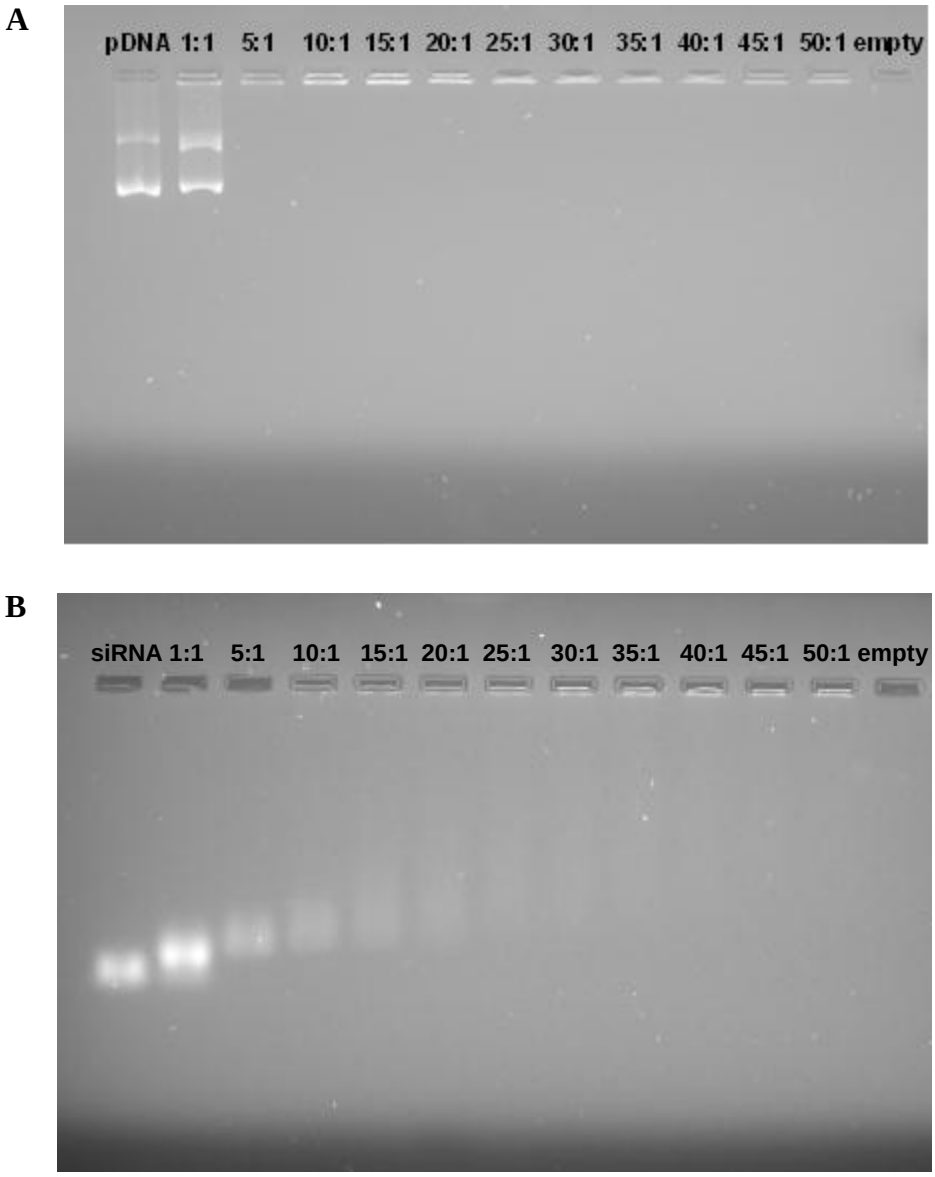

Figure 4.8: Agarose gel electrophoresis of lysine-functionalized nanodiamonds with plasmid DNA and small interfering RNA.

Results of agarose gel electrophoresis of (A) lysine-functionalized nanodiamonds-plasmid DNA (fNDs-pDNA) and (B) lysine-functionalized nanodiamonds-small interfering RNA (fNDs-siRNA) complexes ("diamoplexes") with increasing weight ratios of fNDs to nucleic acid.

As the size of a nanomaterial–nucleic acid complex can also have a pronounced impact on transfection efficacy, a delivery agent should condense genetic material to prevent its degradation by nucleases and promote cellular internalization. A size in the range of 100–300 nm is considered optimal for producing efficient transfection [49]. In addition to appropriate size, the surface charge of transfection complexes also governs the intracellular delivery of transgenes, and an overall positive charge is desired in order to promote internalization across the negatively charged cell surface by means of favorable electrostatic interactions [50]. In order to optimize these parameters, the size and zeta potential of particles formed at various weight ratios of fNDs:pDNA and fNDs:siRNA were measured. An increase in the weight proportion of fNDs to genetic material from 1:1 to 50:1 resulted in a shift in zeta potential from negative to positive, indicating that no free genetic material was available at higher weight ratios. The fND:pDNA particles exhibited considerable aggregation (precipitate) at a 6:1 weight ratio because of neutral zeta potential (Figure 4.9A), while this neutral zeta potential was reached at a much higher weight ratio (20:1) in the fND-siRNA system (Figure 4.9B). With an increase in ratio from 10:1 to 50:1, particle size was found to stabilize around 110 nm for fND-pDNA complexes (Figure 4.9A) and was less than 280 nm for the fND-siRNA complexes (Figure 4.9B). In the case of the fND-pDNA complexes, the zeta potential reached 40–50 mV at ratios of 30:1 and beyond, while a positive zeta potential of nearly 30 mV was attained at a ratio of 50:1 in fND-siRNA complexes. These results demonstrate the ability of fNDs to condense pDNA and form complexes with pDNA and siRNA within the size range suitable for producing efficient transfection. These size and zeta measurements correlate well with those from the gel electrophoresis assay, indicating that the retardation of nucleic acid material coincides with the electroneutrality of the “diamoplexes.”

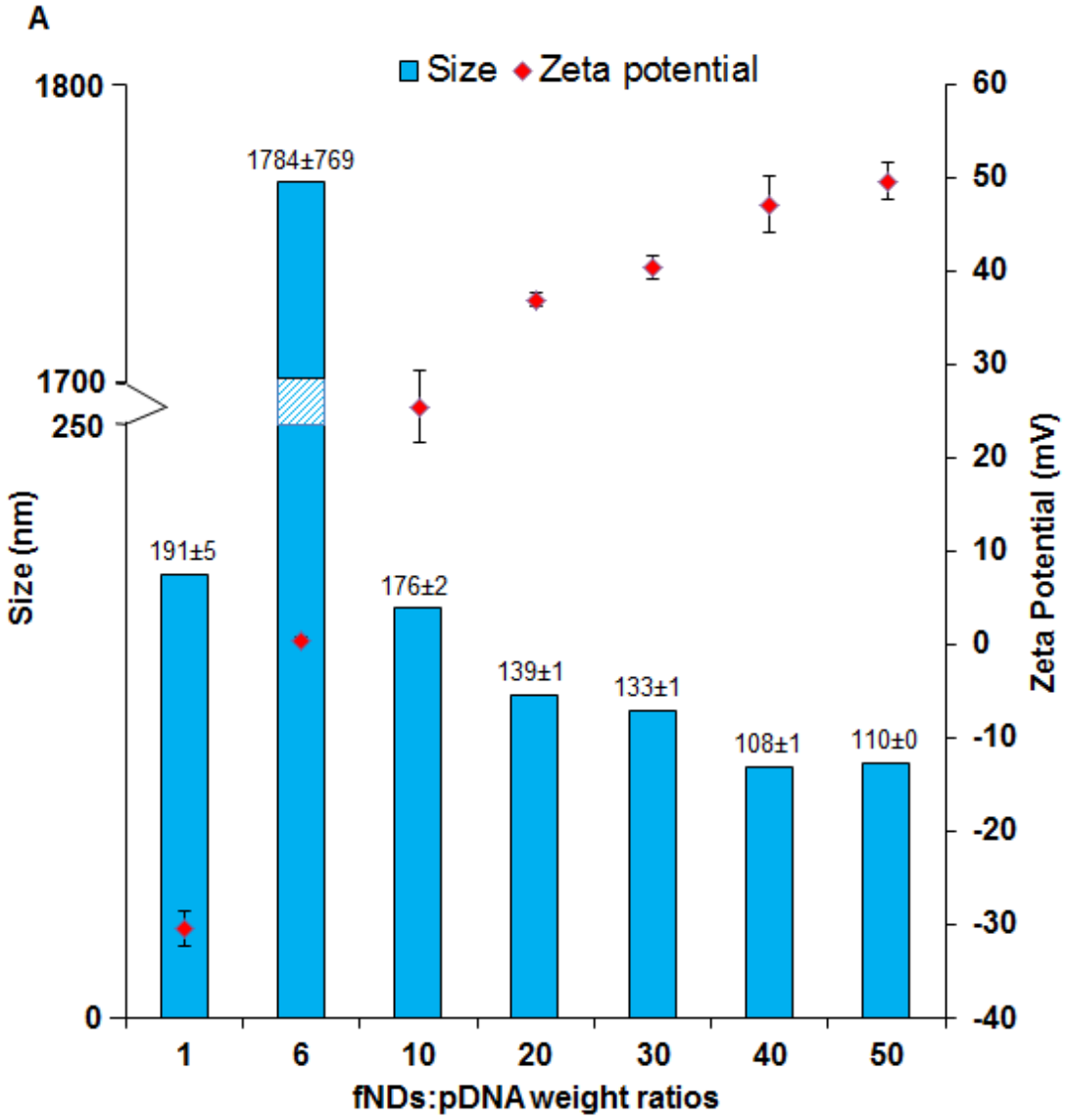
A
Size
Zeta potential
1800
1700
250
0
60
50
40
30
20
10
0
-10
-20
-30
-40
Size (nm)
Zeta Potential (mV)
191±5
1784±769
176±2
139±1
133±1
108±1
110±0
1
6
10
20
30
40
50
fNDs:pDNA weight ratios

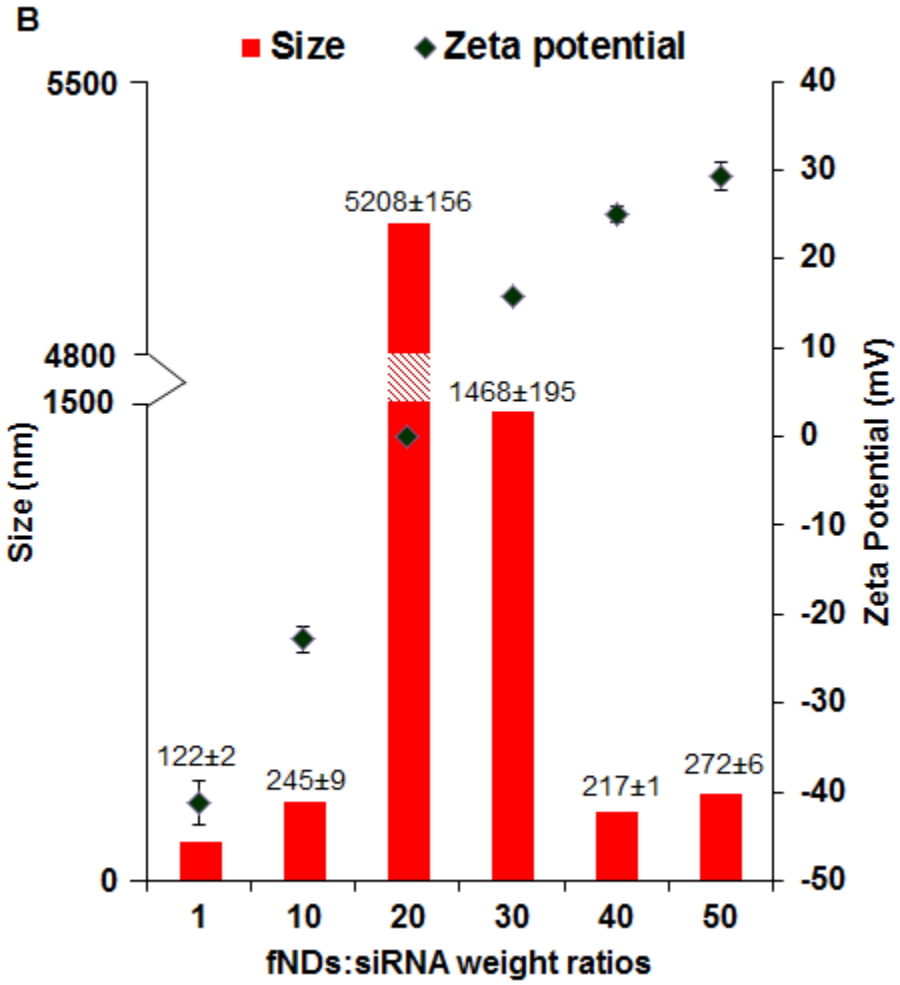

Figure 4.9: Size and zeta potential measurements using various weight ratios of lysine-functionalized nanodiamonds with plasmid DNA and small interfering RNA.

Size and zeta potential measurements using various weight ratios of (A) lysine-functionalized nanodiamonds-plasmid DNA (fNDs:pDNA) and (B) lysine-functionalized nanodiamonds-small interfering RNA (fNDs:siRNA).

In this study, the ratio of lysine linker present per base pair of pDNA and siRNA was also calculated based on the surface loading of the fNDs and the number of base pairs of nucleic acids (Table 4.3). The differences in the binding behavior of these two genetic materials to the fNDs can be attributed to structural differences of the circular pDNA having 5805 base pairs and linear siRNA having only 21 base pairs. The formation of complexes between nanoparticles and siRNA has also been observed to occur at a higher weight ratio than nanoparticles and pDNA in previous studies involving chitosan nanoparticles [51,52]. A suggested model for the formation of complexes between fNDs and pDNA or siRNA, taking into account the binding behavior, size, and zeta potential measurements of the complexes, as well as the structural peculiarities of the genetic materials themselves, is shown in Figure 4.10. In this model, the pDNA is thought to form a spherical nanostructure with positively charged fNDs, while the structural configuration of linear siRNA with fNDs is rather complex, involving several linear siRNA sequences.

Table 4.3: Ratios of lysine residues on the nanodiamonds per base pair of genetic material as calculated from surface loading measurements

Weight ratios of fNDs:genetic material	Calculated lysine per siRNA base pair ratio	Calculated lysine per pDNA base pair ratio
1:1	1.1	1.1
5:1	5.4	NR
6:1	NR	**6.6**
10:1	11	11
20:1	**22**	22
30:1	32	33
40:1	43	44
50:1	54	55

Note: NR, not reported.

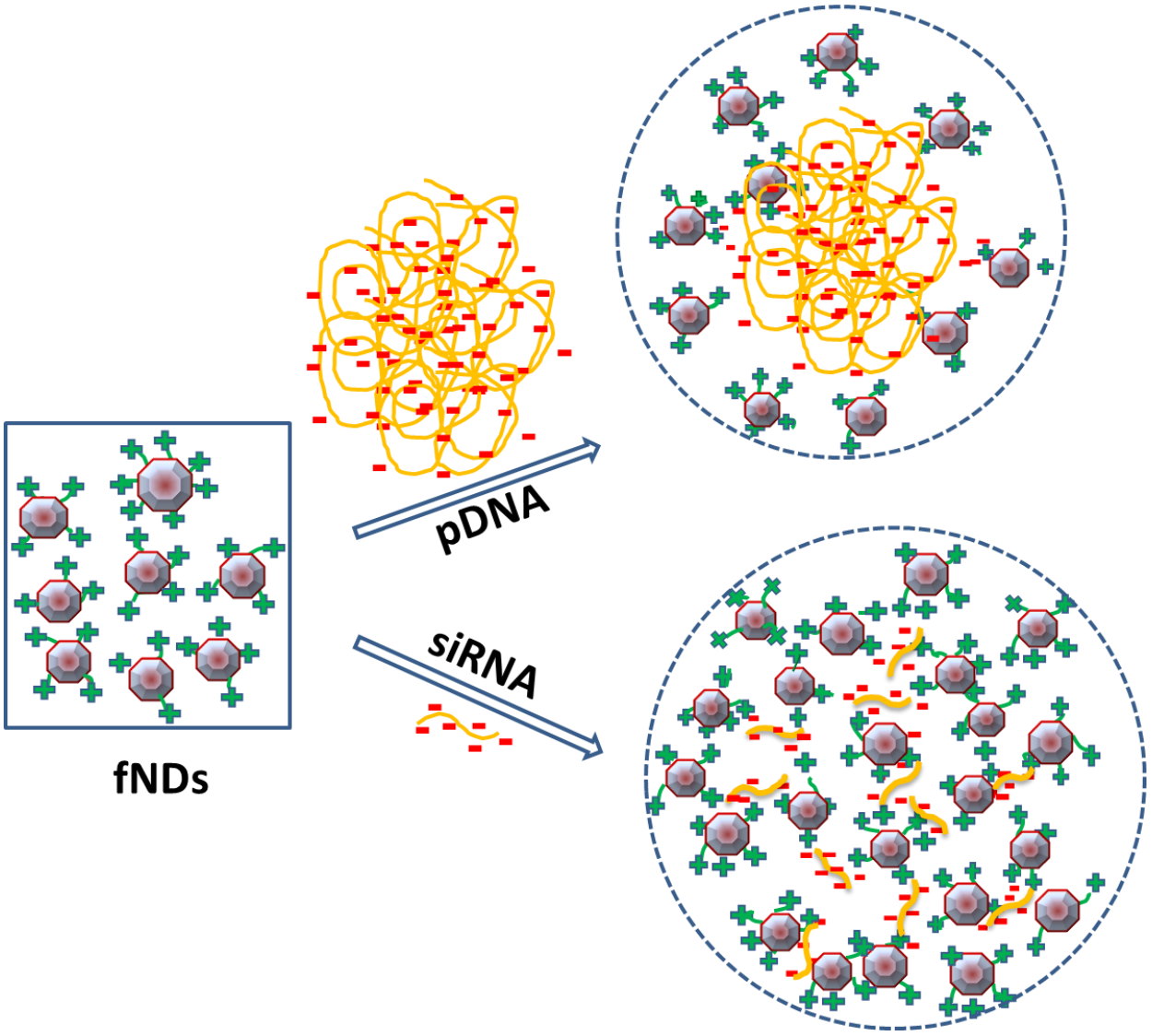

Figure 4.10: Schematic representation of the different binding behavior of plasmid DNA (pDNA) and small interfering RNA (siRNA) to positively charged lysine-functionalized nanodiamonds (fNDs).

4.4 Conclusion

In this study, the surfaces of NDs were covalently functionalized with lysine attached to a three-carbon-length linker. These modified NDs exhibited surface loading of 1.7 mmol g^{-1} and excellent dispersibility in water, as well as showing a considerable reduction in the aggregate size of the particles (21 nm), as measured by DLS. AFM images confirmed the disaggregation of the fNDs in comparison with the carboxylated NDs. The hydrophilicity exhibited by the functionalized NDs in this study also provides an advantage for their use in animal and human systems, as water can be used as a dispersion medium. Finally, the fNDs exhibited an ability to bind pDNA and siRNA by forming nanosized "diamoplexes". This property should be explored further to determine the applicability of fNDs as vectors for the delivery of genetic materials in gene therapy.

4.5 References

1. Schrand AM, Hens SAC, Shenderova OA: Nanodiamond particles: Properties and perspectives for bioapplications. *Critical Reviews in Solid State and Materials Sciences* 2009, 34:18-74.

2. Danilenko VV: On the history of the discovery of nanodiamond synthesis. *Physics of the Solid State* 2004, 46:595-599.

3. Dolmatov VY: Applications of detonation nanodiamond. In *Ultrananocrystalline Diamond: Synthesis, Properties, and Applications*. Edited by Shenderova OA, Gruen DM: William Andrew Publishing; 2006:477-527.

4. Bondar VS, Pozdnyakova IO, Puzyr AP: Applications of nanodiamonds for separation and purification of proteins. *Physics of the Solid State* 2004, 46:758-760.

5. Chow EK, Zhang XQ, Chen M, Lam R, Robinson E, Huang H, Schaffer D, Osawa E, Goga A, Ho D: Nanodiamond therapeutic delivery agents mediate enhanced chemoresistant tumor treatment. *Science Translational Medicine* 2011, 3:73ra21.

6. Li J, Zhu Y, Li W, Zhang X, Peng Y, Huang Q: Nanodiamonds as intracellular transporters of chemotherapeutic drug. *Biomaterials* 2010, 31:8410-8418.

7. Dolmatov VY: Detonation synthesis ultradispersed diamonds: Properties and applications. *Russian Chemical Reviews* 2001, 70:607-626.

8. Shenderova OA, Hens SAC: Detonation nanodiamond particles processing, modification and bioapplications. In *Nanodiamonds: Applications in Biology and Nanoscale Medicine*. Edited by Ho D: Springer; 2010:79-116.

9. Aleksenskii AE, Baidakova MV, Vul AY, Siklitskii VI: The structure of diamond nanoclusters. *Physics of the Solid State* 1999, 41:668-671.

10. Jiang T, Xu K: FTIR study of ultradispersed diamond powder synthesized by explosive detonation. *Carbon* 1995, 33:1663-1671.

11. Krueger A: New carbon materials: Biological applications of functionalized nanodiamond materials. *Chemistry - A European Journal* 2008, 14:1382-1390.

12. Puzyr AP, Purtov KV, Shenderova OA, Luo M, Brenner DW, Bondar VS: The adsorption of aflatoxin B1 by detonation-synthesis nanodiamonds. *Doklady Biochemistry and Biophysics* 2007, 417:299-301.

13. Shimkunas RA, Robinson E, Lam R, Lu S, Xu X, Zhang XQ, Huang H, Osawa E, Ho D: Nanodiamond-insulin complexes as pH-dependent protein delivery vehicles. *Biomaterials* 2009, 30:5720-5728.

14. Wang HD, Niu CH, Yang Q, Badea I: Study on protein conformation and adsorption behaviors in nanodiamond particle-protein complexes. *Nanotechnology* 2011, 22:145703.

15. Huang H, Pierstorff E, Osawa E, Ho D: Active nanodiamond hydrogels for chemotherapeutic delivery. *Nano Letters* 2007, 7:3305-3314.

16. Zhang XQ, Chen M, Lam R, Xu X, Osawa E, Ho D: Polymer-functionalized nanodiamond platforms as vehicles for gene delivery. *ACS Nano* 2009, 3:2609-2616.

17. Chen M, Zhang XQ, Man HB, Lam R, Chow EK, Ho D: Nanodiamond vectors functionalized with polyethylenimine for siRNA delivery. *Journal of Physical Chemistry Letters* 2010, 1:3167-3171.

18. Ida S, Tsubota T, Tanii S, Nagata M, Matsumoto Y: Chemical modification of the diamond surface using benzoyl peroxide and dicarboxylic acids. *Langmuir* 2003, 19:9693-9698.

19. Tsubota T, Tanii S, Ida S, Nagata M, Matsumoto Y: Chemical modification of diamond surface with various carboxylic acids by radical reaction in liquid phase. *Diamond and Related Materials* 2004, 13:1093-1097.

20. Tsubota T, Ohno T, Yoshida H, Kusakabe K: Introduction of molecules containing a NO2 group on diamond surface by using radical reaction in liquid phase. *Diamond and Related Materials* 2006, 15:668-672.

21. Liu Y, Gu Z, Margrave JL, Khabashesku VN: Functionalization of nanoscale diamond powder: Fluoro-, alkyl-, amino-, and amino acid-nanodiamond derivatives. *Chemistry of Materials* 2004, 16:3924-3930.

22. Krüger A, Liang Y, Jarre G, Stegk J: Surface functionalisation of detonation diamond suitable for biological applications. *Journal of Materials Chemistry* 2006, 16:2322-2328.

23. Krueger A, Boedeker T: Deagglomeration and functionalisation of detonation nanodiamond with long alkyl chains. *Diamond and Related Materials* 2008, 17:1367-1370.

24. Schrand AM, Huang H, Carlson C, Schlager JJ, Osawa E, Hussain SM, Dai L: Are diamond nanoparticles cytotoxic? *Journal of Physical Chemistry B* 2007, 111:2-7.

25. Schrand AM, Dai L, Schlager JJ, Hussain SM, Osawa E: Differential biocompatibility of carbon nanotubes and nanodiamonds. *Diamond and Related Materials* 2007, 16:2118-2123.

26. Chen M, Pierstorff ED, Lam R, Li SY, Huang H, Osawa E, Ho D: Nanodiamond-mediated delivery of water-insoluble therapeutics. *ACS Nano* 2009, 3:2016-2022.

27. Faraji AH, Wipf P: Nanoparticles in cellular drug delivery. *Bioorganic and Medicinal Chemistry* 2009, 17:2950-2962.

28. Krueger A, Stegk J, Liang Y, Lu L, Jarre G: Biotinylated nanodiamond: Simple and efficient functionalization of detonation diamond. *Langmuir* 2008, 24:4200-4204.

29. Ozawa M, Inaguma M, Takahashi M, Kataoka F, Krüger A, Osawa E: Preparation and behavior of brownish, clear nanodiamond colloids. *Advanced Materials* 2007, 19:1201-1206.

30. Singh J, Yang P, Michel D, Verrall RE, Foldvari M, Badea I: Amino acid-substituted gemini surfactant-based nanoparticles as safe and versatile gene delivery agents. *Current Drug Delivery* 2011, 8:299-306.

31. Kim B, Sigmund WM: Functionalized multiwall carbon nanotube/gold nanoparticle composites. *Langmuir* 2004, 20:8239-8242.

32. Pham TA, Son SM, Jeong YT: Water-dispersible multi-walled carbon nanotubes and novel hybrid nanostructures. *Synthesis and Reactivity in Inorganic, Metal-Organic and Nano-Metal Chemistry* 2010, 40:216-224.

33. Liu J, Rinzler AG, Dai H, Hafner JH, Kelley Bradley R, Boul PJ, Lu A, Iverson T, Shelimov K, Huffman CB, et al.: Fullerene pipes. *Science* 1998, 280:1253-1256.

34. Kong H, Gao C, Yan D: Functionalization of multiwalled carbon nanotubes by atom transfer radical polymerization and defunctionalization of the products. *Macromolecules* 2004, 37:4022-4030.

35. Philip B, Xie J, Abraham JK, Varadan VK: Polyaniline/carbon nanotube composites: Starting with phenylamino functionalized carbon nanotubes. *Polymer Bulletin* 2005, 53:127-138.

36. Sainsbury T, Erickson K, Okawa D, Zonte CS, Fréchet JMJ, Zettl A: Kevlar functionalized carbon nanotubes for next-generation composites. *Chemistry of Materials* 2010, 22:2164-2171.

37. Han G, Tamaki M, Hruby VJ: Fast, efficient and selective deprotection of the tert-butoxycarbonyl (Boc) group using HCL/dioxane (4 M). *Journal of Peptide Research* 2001, 58:338-341.

38. Solin SA, Ramdas AK: Raman spectrum of diamond. *Physical Review B* 1970, 1:1687-1698.

39. Ager JW 3rd, Veirs DK, Rosenblatt GM: Spatially resolved Raman studies of diamond films grown by chemical vapor deposition. *Physical Review B* 1991, 43:6491-6499.

40. Ganesan S, Maradudin AA, Oitmaa J: A lattice theory of morphic effects in crystals of the diamond structure. *Annals of Physics* 1970, 56:556-594.

41. Mochalin V, Osswald S, Gogotsi Y: Contribution of functional groups to the raman spectrum of nanodiamond powders. *Chemistry of Materials* 2009, 21:273-279.

42. Mochalin VN, Shenderova O, Ho D, Gogotsi Y: The properties and applications of nanodiamonds. *Nature Nanotechnology* 2012, 7:11-23.

43. Osipov VY, Aleksenskiy AE, Shames AI, Panich AM, Shestakov MS, Vul AY: Infrared absorption study of surface functional groups providing chemical modification of nanodiamonds by divalent copper ion complexes. *Diamond and Related Materials* 2011, 20:1234-1238.

44. Bellamy LJ: Alkanes. In *Advances in Infrared Group Frequencies*. Edited by: Methuen; 1968:1-20.

45. Kim T, Lee K, Gong MS, Joo SW: Control of gold nanoparticle aggregates by manipulation of interparticle interaction. *Langmuir* 2005, 21:9524-9528.

46. Dishun Z, Qian L, Erhong D, Hongsheng L, Xiaobing S: Solubility of L-lysine hydrochloride in dimethyl sulfoxide,methanol, ethanol,water,and glycol between (283 and 323) K. *Journal of Chemical and Engineering Data* 2009, 54:2126-2127.

47. Zanetti-Ramos BG, Fritzen-Garcia MB, Creczynski-Pasa TB, Oliveira CSD, Pasa AA, Soldi V, Borsali R: Characterization of polymeric particles with electron microscopy, dynamic light scattering, and atomic force microscopy. *Particulate Science and Technology* 2010, 28:472-484.

48. Singh J, Michel D, Chitanda JM, Verrall RE, Badea I: Evaluation of cellular uptake and intracellular trafficking as determining factors of gene expression for amino acid-substituted gemini surfactant-based DNA nanoparticles. *Journal of Nanobiotechnology* 2012, 10.

49. Donkuru M, Badea I, Wettig S, Verrall R, Elsabahy M, Foldvari M: Advancing nonviral gene delivery: lipid- and surfactant-based nanoparticle design strategies. *Nanomedicine (London, England)* 2010, 5:1103-1127.

50. Akinc A, Lynn DM, Anderson DG, Langer R: Parallel synthesis and biophysical characterization of a degradable polymer library for gene delivery. *Journal of the American Chemical Society* 2003, 125:5316-5323.

51. Katas H, Alpar HO: Development and characterisation of chitosan nanoparticles for siRNA delivery. *Journal of Controlled Release* 2006, 115:216-225.

52. Lee DW, Yun KS, Ban HS, Choe W, Lee SK, Lee KY: Preparation and characterization of chitosan/polyguluronate nanoparticles for siRNA delivery. *Journal of Controlled Release* 2009, 139:146-152.

4.6 Supplemental Data

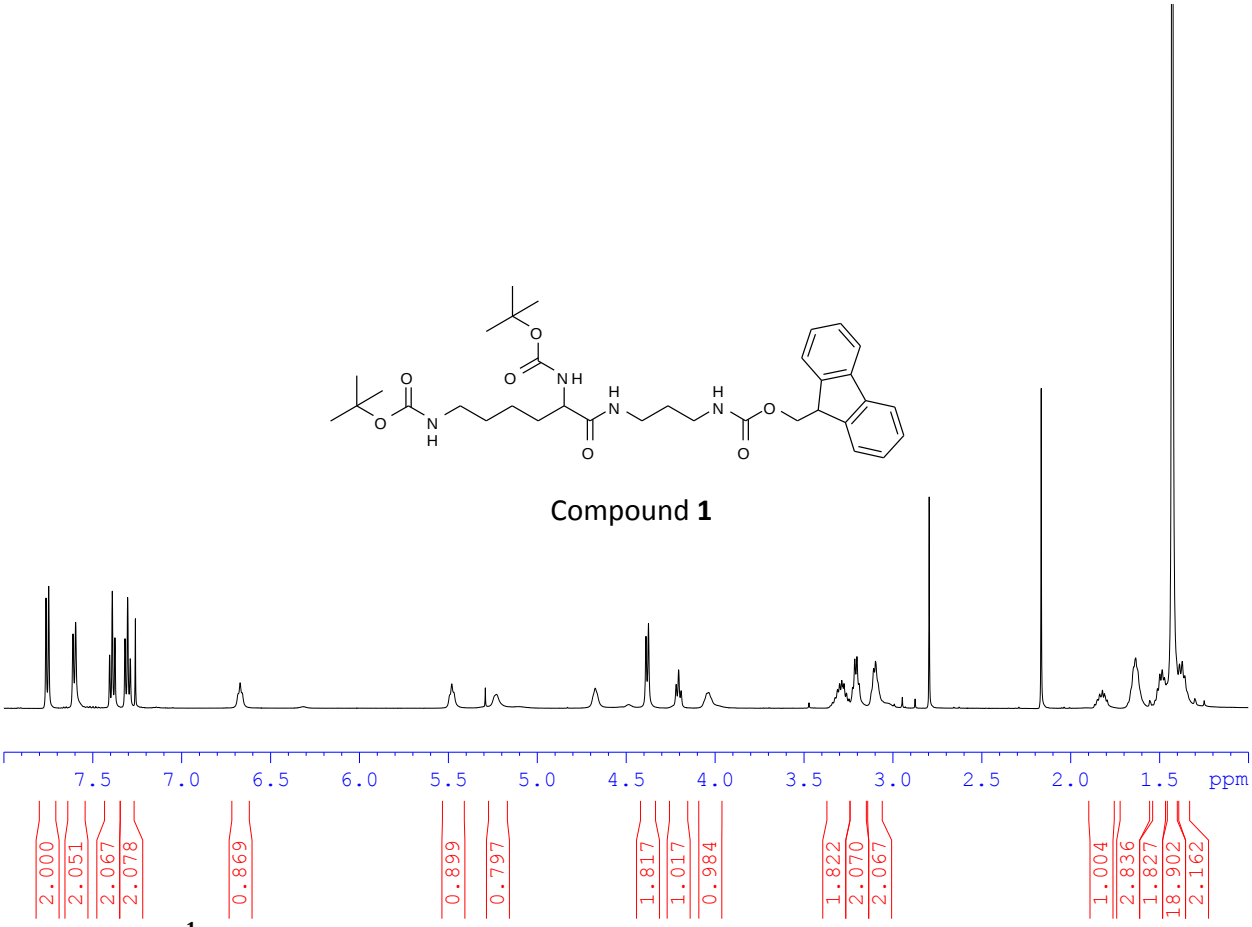

Figure S 4.1: ^{1}H NMR spectra of compound 1 at 500 MHz.

Proton nuclear magnetic resonance spectra of compound 1 [N′-(N$^{\alpha}$,N$^{\varepsilon}$-bis-Boc-lysyl),N″-(Fmoc)-diaminopropane] at 500 MHz.

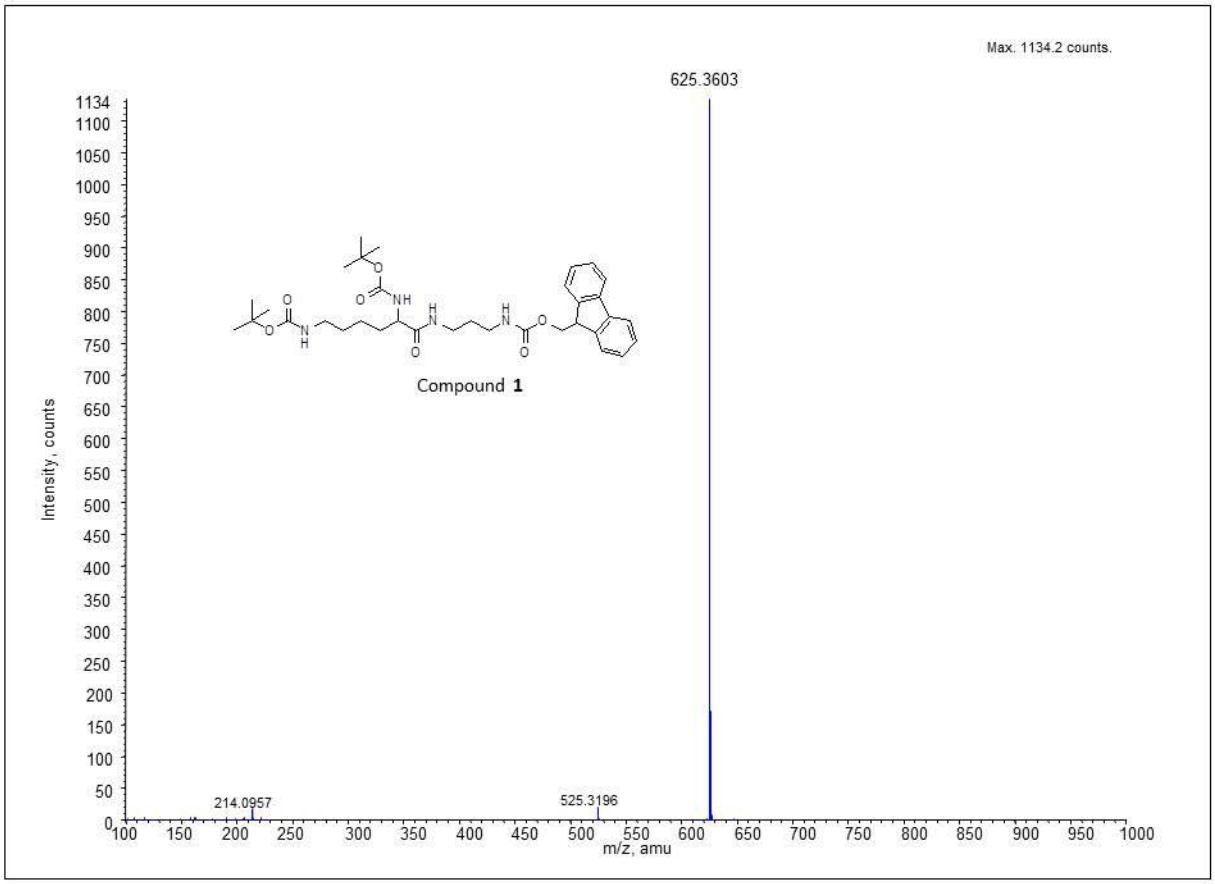

Figure S 4.2: Mass spectrum of compound 1.

Mass spectrum of compound 1 [N′-(N^{α},N^{ε}-bis-Boc-lysyl),N″-(Fmoc)-diaminopropane].

Chapter 5

CELLULAR STUDIES ON NANODIAMONDS: INTERACTION WITH MAMMALIAN CELLS, TOXICITY AND ABILITY TO DELIVER SMALL INTERFERING RNA

Abstract

Nanodiamonds (NDs) are carbon based nanomaterials with an inert sp^3 hybridized carbon core. The potential of lysine-functionalized NDs (fNDs) as nucleic acid delivery vehicle is demonstrated in the previous chapter, however, their cellular association, toxicity and ability to deliver siRNA needs to be assessed *in vitro*. In this study, Raman-fluorescence, backscattering and laser scanning confocal microscopy was employed to examine the cellular interaction of NDs. MTT cytotoxicity assay investigated the viability of cells after incubating with NDs for 24 hours. Fluorescence activated cell sorter was used to evaluate the intracellular siRNA delivering efficacy of fNDs. The fNDs demonstrated successful cellular association, while remaining biocompatible to the cells from 4 to 250 μg/mL concentration. However, fNDs generated in this study were unable to improve the overall intracellular delivery of siRNA. Although fNDs showed cellular interaction and negligible cytotoxicity, their superior siRNA delivering ability remains to be established in this study.

5.1 Introduction

One of the basic requirements for the consideration of a material for use in delivering therapeutic agents into biological systems is their cellular interaction, leading to successful internalization. Previous studies demonstrated the ability of nanodiamonds (NDs) to be internalized by mammalian cells via passive diffusion, clathrin-mediated endocytosis and macropinocytosis [1,2]. In this study, Raman-fluorescence and elastic light scattering mapping were applied to explore the interaction of NDs with the human cells. The feasibility of laser scanning confocal microscopy to identify the localization of NDs in a human cell line using the autofluorescence of NDs as a detection marker was also investigated. The advantages and disadvantages of employing these techniques as tools for *in vitro* tracking of NDs are discussed.

In addition to the cellular interaction and consequent internalization, another crucial requirement of the delivery agent to be used in biological systems is their biocompatibility [3,4]. Although earlier studies have demonstrated negligible *in vitro* toxicity of NDs [3,5-9], the cell

type, size, surface properties and shape of nanoparticles can influence the biocompatibility [10]. Therefore, the cytotoxicity of pristine carboxylated nanodiamonds (pNDs) and lysine-functionalized nanodiamonds (fNDs), with and without serum, was again tested using human cell line. Finally, flow cytometry was used to assess the efficacy of fNDs to deliver anti-green fluorescent protein (GFP) small interfering RNA (siRNA) in mammalian cells expressing GFP.

5.2 Materials

Hela cells (human cervical cancer cells), Eagle's Minimum Essential Medium (EMEM), and Dulbecco's Modified Eagle Medium (DMEM) were obtained from American Type Culture Collection, VA, USA. Hela cells expressing GFP (Hela/GFP) were acquired from Cell Biolabs, CA, USA. Fetal bovine serum (FBS) and 0.1 mM MEM Non-Essential Amino Acids were acquired from Gibco, ON, Canada. Lipofectamine^{TM} RNAiMAX and (Dimethylthiazol-2-yl)-2,5-diphenyltetrazolium bromide (MTT) reagent were purchased from Invitrogen, ON, Canada. Trypsin and antibiotics were obtained from Sigma Aldrich, ON, Canada, and anti GFP siRNA was purchased from Ambion, ON, Canada. Cell culture plates and polystyrene petri dishes were purchased from Falcon BD, ON, Canada. Gold-coated silicon wafer was supplied by Platypus Technologies, WI, USA and coverslips were purchased from VWR International, ON, Canada.

5.3 Methods

5.3.1 Cell Culture

Hela cells were grown in EMEM supplemented with 10% FBS and 1% antibiotic/antimycotic agents. The growth medium for Hela/GFP cells was DMEM supplemented with 10% FBS, 0.1 mM non-essential amino acids and 1% antibiotic/antimycotic agents. All the cells were grown to 70-80% confluency at 37°C in a humidified incubator supplied with 5% CO_2. Second passage from the initiation of the frozen cell line was used for all the experiments. In general, no more than 12 passages from the original population were used for any of the experiment. In all the assays, the media of cells was replaced with fresh unsupplemented media one hour prior to the treatment and the cells were incubated at 37°C and 5% CO_2 in a humidified incubator.

5.3.2 ND Dispersion Preparation

Unless stated, the dispersions of NDs for all the assays were prepared in unsupplemented media with 4 hours of bath sonication at a frequency of 25 kHz without heating.

5.3.3 Imaging of NDs with Cells using Raman-Fluorescence and Backscattering Mode Microspectroscopic Mapping

Raman-fluorescence and backscattering mode mapping of cells incubated with NDs was carried out using a Renishaw Invia Reflex microscope. Pieces of the gold-coated silicon wafer were washed with double distilled water and 70% ethanol, and placed in the wells of 48-well plate. Hela cells, at the density of 10,000 cells per well were allowed to adhere to the gold substrate 24 hours prior to ND treatment. Then the media of each well were replaced with 200 µl of the ND dispersion prepared at the concentration of 200 µg/mL. After 7 hours, the media was supplemented with FBS to a final concentration of 10%. The cells were incubated with NDs for 24 hours, and then washed three times with sterile phosphate buffer saline (PBS) (5 minutes each) using a plate shaker to remove non-internalized NDs. Gold wafers with cells were placed in polystyrene Petri dish containing 2 mL of PBS. Raman-fluorescence and backscattering mode mapping of the cells was carried out with 514.5 nm (1800 lines/mm grating) and 1060 nm (1200 lines/mm grating) lasers, respectively. Long working-distance 50X objective allowed the measurements of the cells in PBS. The instrument was calibrated using Silicon wafer measuring at 520 cm^{-1}. The laser intensity during the Raman-fluorescence mapping was 100%, while the backscattering mapping was performed with 0.1% (pNDs treated cells and control) and 0.05% (fNDs treated cells and control) laser intensity. The lower and upper intensity limits of the Look Up Table, used to create the map of control and treated cells, were set manually from 3400 to 4000 (Raman-fluorescence maps), 13500 to 38000 (backscattering maps using 0.1% laser intensity) and 3153 to 5594 (backscattering maps using 0.05% laser intensity). The Raman-fluorescence maps were constructed using signal to axis intensity values from 1315 to 1345 cm^{-1}. The intensity of the laser at 1058.22 nm was used for constructing the backscattering maps. Rainbow color scheme is chosen for representing the intensity in the maps, where violet represents the lowest intensity and red represents the highest intensity of the scattered light.

5.3.4 Imaging of NDs with Cells using Laser Scanning Confocal Microscopy

To evaluate whether NDs can be detected in the cells based upon their intrinsic fluorescence, laser scanning confocal microscopy was performed. Hela cells seeded at the density of 40,000 cells per well were allowed to adhere to coverslip placed in 12-well plate, for 24 hours. The media of cells were replaced with 1 mL of NDs dispersion prepared at a concentration of 50 µg/mL. After 6 hours, FBS was added to the media of the cells at the final concentration of 10%. The cells were incubated for a total of 24 hours and then washed three times with PBS (5 minutes each). Slides of the live cells were prepared and imaged with a Leica TCS SP5 laser scanning confocal microscope (Leica Microsystems Inc., Benshein, Germany; WCVM, University of Saskatchewan, Saskatoon, Canada) using 63X oil immersion objective. The sample excitation was carried out with 476 nm argon laser source and the emission was collected from 492 to 677 nm. A total of 44 z-sections of cells were imaged, each with the step size of 0.38 µm.

5.3.5 MTT Assay

The cytotoxicity of pNDs and fNDs in serum and serum free medium was evaluated in Hela cells by MTT assay. The stock dispersions of pNDs and fNDs at a concentration of 250 µg/mL were prepared in serum and serum-free EMEM. A two-fold serial dilution from the stock preparation of NDs was carried out to reach a concentration of 4 µg/mL. The cells were plated in 96-well cell culture plates at the density of 5,000 cells per well (100 µL volume) and allowed to adhere for 24 hours. The media of the cells were replaced with 100 µl volume of each dilution of NDs (with serum and without serum). After 24 hours, the treatments were removed from the cells followed by PBS washing. The cells were incubated for another 48 hours to perform MTT assay. 10 µl of sterile MTT stock solution (5 mg/mL of MTT in PBS) diluted in 90 µl of supplemented EMEM was added to each well, and the plates were incubated at 5% CO_2/37ºC for 45 minutes. Thereafter, the supernatant containing excess MTT solution was removed and the plates were dried gently. The formazan crystals resulting from the reduction of MTT were extracted in DMSO by shaking the plates for 10 minutes on a plate shaker. The plates were incubated at 37ºC for 10 minutes to remove any air bubbles formed during shaking. To prevent

any interference in reading absorbance that may occur due the ND particles, the plates were centrifuged at 160 g for 10 minutes. The supernatant from the each well was transferred to the new 96-well plates and the absorbance was read at 550 nm using microplate reader (BioTek® Microplate Synergy HT, VT, U.S.A.). The cells grown under the same conditions without ND treatment were used as controls. The mean absorbance of the control cells was set to 100% and consequently, the cellular viability was calculated as percent viability based on the formula:

$$\text{.....\% Cell viability} = \frac{\text{Absorbance}_{\text{treated}}}{\text{Absorbance}_{\text{control}}} * 100 \text{.....(5.1)}$$

5.3.6 Fluorescence Activated Cell Sorting (FACS)

FACS was used to evaluate the transfection ability of fNDs-siRNA complex. Hela/GFP cells were seeded in a 6-well plate at the density of 1×10^5 cells per well and allowed to adhere for 24 hours. The fNDs-siRNA complex was prepared at the weight ratio of 35:1 fNDs:siRNA as described in Chapter 4, section 4.2.10. Lipofectamine was used as a positive control for delivering the siRNA to the cells and cells with no siRNA treatment were used as a control. The cells were treated with fNDs-siRNA, Lipofectamine-siRNA and naked siRNA at a final siRNA concentration of 60 nM. After 7 hours, the Lipofectamine-siRNA treatment was removed (due to high toxicity of Lipofectamine) and fresh supplemented media was added to the wells. On the remaining wells, after 7 hours of treatment, the media was supplemented with FBS to the final concentration of 10%. After 24 hours of treatment, the media from all the wells were aspirated and replaced with the fresh supplemented media, and the plates were incubated for another 48 hours.

Thereafter, the cells were washed three times with PBS (5 minutes each), harvested using trypsin (0.25%)-EDTA, and resuspended in supplemented EMEM media (10% FBS). The cell suspension was transferred into a 5-mL flow cytometry tube and GFP knockdown was measured by BD FACSCalibur™ (BD Biosciences, CA, USA) flow cytometer using a 488-nm excitation laser. A total of 10,000 events were recorded per sample. The GFP fluorescence was measured using 585/42 nm (FL2) band pass filters with the detector voltage set to 392 V. The signals were amplified using logarithmic mode with the amplification gain of 1. The forward scatter (volatge-E1, mode-linear, amplitude gain-3.35) and side scatter (voltage-334, mode-linear, amplitude

gain-1.00) excluded the cell debris. Data were analyzed using BD CellQuest^{TM} Pro software (version 6.0). To quantify the GFP knockdown, the histogram (GFP intensity versus number of events) was divided into four equal quadrants, and assigned low, mild, moderate and high GFP fluorescence intensity regions. The relative percentage GFP intensity shown by the treatment groups was determined by combining the populations of moderate and high GFP intensity quadrants, and then comparing those with the untreated cells.

5.3.7 Statistical Analyses

MTT results are expressed as the mean of n=3 ± S.E.M, where each n is derived from the average of 3 individual measurements. Scheffé post-hoc multiple comparison tests was used for statistical analyses when the sample variance was homogenous. In case of non-homogenous variance, Dunnett's T3 post-hoc multiple comparison test was used. The significant differences were considered at $p<0.05$ level. SPSS program version 19.0 was used.

5.4 Results and Discussion

5.4.1 Interaction of NDs with Human Cells

The cellular interaction of NDs was examined using the techniques of Raman-fluorescence and backscattering mode microspectroscopic mapping.

5.4.1.1 Raman-Fluorescence Microspectroscopic Mapping

Raman microspectroscopy has the potential to detect the NDs by identifying the unique diamond signal at 1332 cm^{-1} [8] with an advantage of lateral spatial resolution of 1-2 μm, greater than infrared (5 μm) [11]. The high fluorescence of NDs observed during their Raman spectral acquisition (Chapter 4, section 4.3.2, Figure 4.2) led to the hypothesis that the Raman spectrum obtained from the regions of the cells with NDs would show higher signal intensity with respect to the axis (fluorescence) compared to the cellular regions devoid of NDs. Therefore, the Raman maps of the cells in this experiment were constructed using the signal to axis intensity from 1315 to 1345 cm^{-1} wavenumbers. This could theoretically provide information about interaction of NDs with the cells.

The Raman-fluorescence maps of pNDs (Figure 5.2B) and fNDs (Figure 5.3B) treated cells when compared with the control cells (Figure 5.1B), revealed very high signal to axis intensity (red region). Green and blue colored areas near the membrane of the NDs treated cells can also be observed (Figure 5.2B and 5.3B), which might indicate the interaction of NDs with cell membranes. The green color was more prevalent in the fNDs-treated cells (Figure 5.3B) compared to the cells treated with the pNDs (Figure 5.2B) in the selected intensity range. This might to be attributed to the higher fluorescence or cellular interaction ability of fNDs compared to the pNDs. The cationic fNDs might have interacted with the negatively charged cellular membrane more favorably than the negatively charged pNDs, which could ultimately lead to cellular internalization of fNDs. The white light images of the control (Figure 5.1A), pNDs treated (Figure 5.2A) and fNDs treated (Figure 5.3A) cells are also shown.

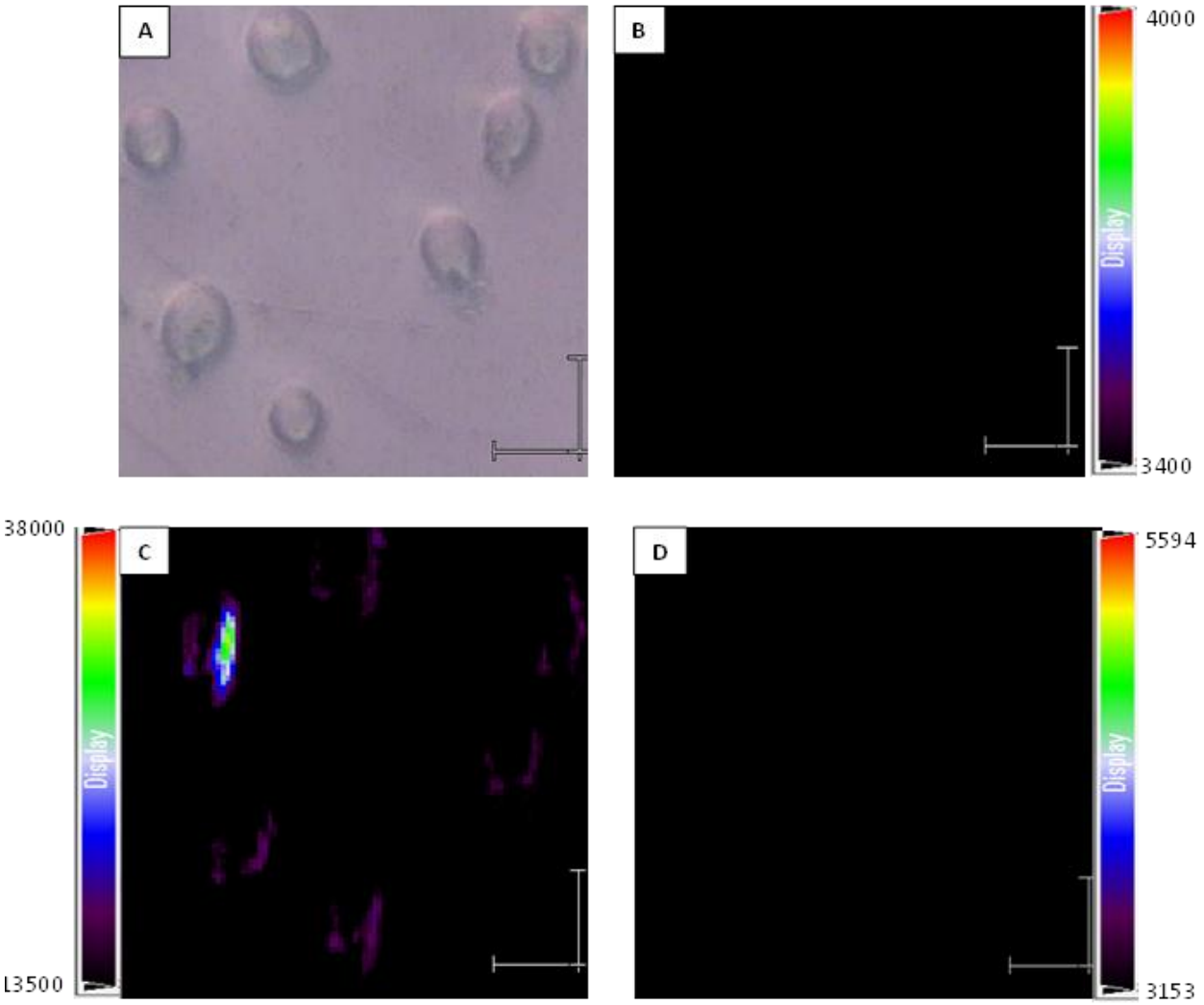

Figure 5.1: Raman-fluorescence and backscattering mode maps of untreated cells.

Untreated cells: (A) white light image; (B) Raman-fluorescence map constructed using the signal to axis intensity from 1315−1345 cm^{-1} region; (C) backscatter map constructed using the intensity of elastically scattered light at 1058.22 nm using 0.1% laser intensity source (D) backscatter map constructed using the intensity of elastically scattered light at 1058.22 nm using 0.05% laser intensity source. No Raman and backscattering signals are observed in the intensity range of 3400 to 4000 and 3153 to 5594, respectively. The colors range from violet (lowest intensity) to red (highest intensity). Each scale bar is 20 µm.

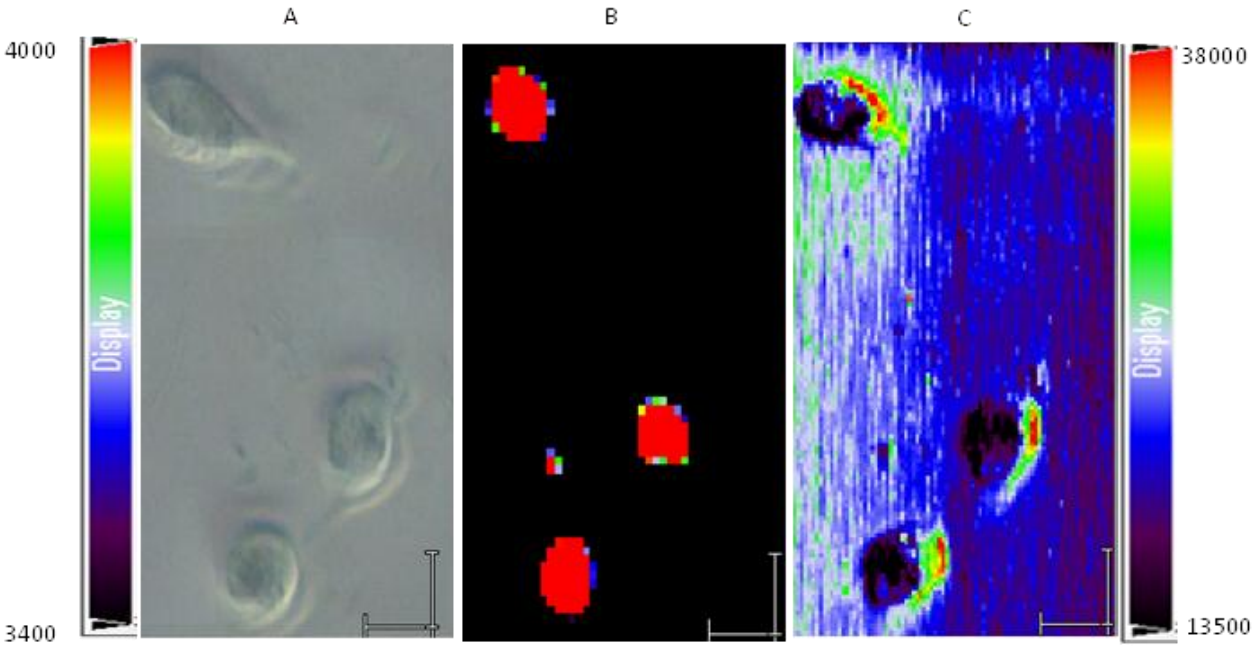

Figure 5.2: Raman-fluorescence and backscattering mode maps of pristine carboxylated nanodiamond treated cells.

Pristine carboxylated nanodiamond treated cells: (A) white light image; (B) Raman-fluorescence map constructed using the signal to axis intensity from 1315−1345 cm^{-1} region; (C) backscatter map constructed using the intensity of elastically scattered light at 1058.22 nm using 0.1% laser intensity source. The colors range from violet (lowest intensity) to red (highest intensity). Each scale bar is 20 µm.

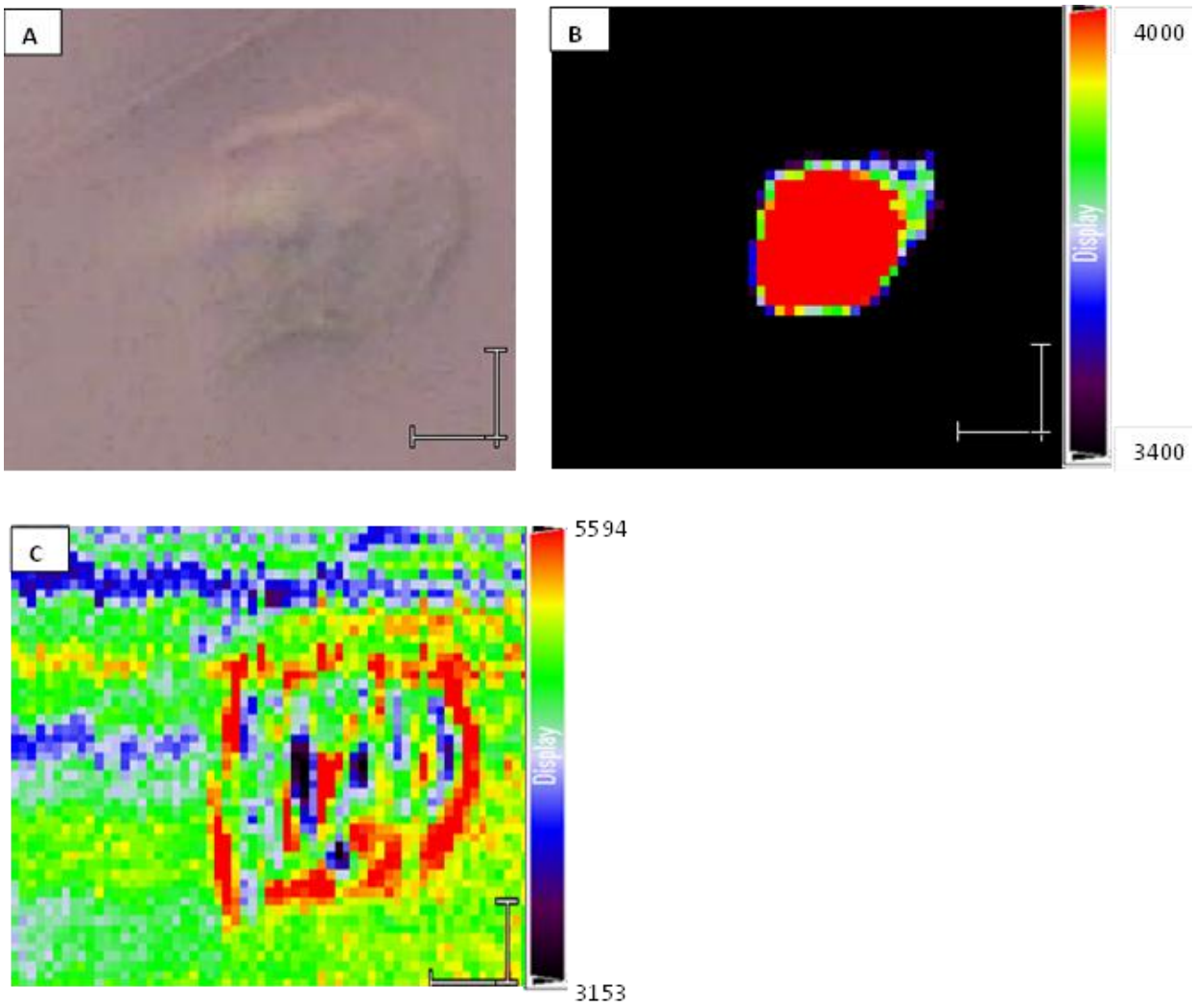

Figure 5.3: Raman-fluorescence and backscattering mode maps of lysine-functionalized nanodiamond treated cell.

Lysine-functionalized nanodiamond treated cell: (A) white light image; (B) Raman-fluorescence map constructed using the signal to axis intensity using 1315−1345 cm^{-1} region; (C) backscatter map constructed from the intensity of elastically scattered light at 1058.22 nm using 0.05% laser intensity source. The colors range from violet (lowest intensity) to red (highest intensity). Each scale bar is 10 µm. Representative data. Other analyzed cell also showed cellular interaction of lysine-functionalized nanodiamonds with a somewhat different pattern (red region located inside rather than near the cellular membrane).

However, the Raman maps of pNDs and fNDs treated cells were equivocal with regards to the cellular association of NDs for two reasons. Firstly, the detection of the diamond Raman signal of NDs with cells was challenging due to the intrinsic fluorescence exhibited by the cells and NDs, as shown in the Raman-fluorescence spectra obtained from one of the highest intensity region of cells treated with pNDs (Figure S 5.1) and fNDs (Figure S 5.2). Moreover, the Raman intensity of diamond signal became weak with the decrease in the size of diamond [12], contributing to the challenges of identifying the diamond peak embedded in the fluorescence with a single spectral acquisition. Secondly, the Raman-fluorescence maps did not reveal the existence of the individual ND particles or aggregates of NDs in the cells, rather, the entire cell showed high signal to axis intensity, bringing ambiguity to the results. It is important to mention here that the fNDs used in this study emitted fluorescence upon excitation with blue, green and red light sources as detected with conventional fluorescence microscope.

Therefore, it became important to apply another technique, which in corroboration with the Raman maps can provide a better insight on the cellular interaction ability of the NDs.

5.4.1.2 Backscattering mode Mapping

Considering the high refractive index of diamonds (2.4), it could be possible to identify these particles in the cells by measuring the intensity of elastically scattered light. NDs scatter the light elastically with a higher intensity than the same-sized cellular structures [13] since the refractive indices of cellular materials is almost half (~1.35 to ~1.7) of the diamond [14]. Synthetic diamond nanocrystals (55 nm) have been identified in the cells using differential interference contrast microscopy and have shown potential to act as scattering label [15].

Hence with an aim of identifying the cellular association of detonation NDs, the same area of the gold substrate with cells that was scanned for Raman spectroscopic measurements, was scanned to measure elastically scattered light. The backscatter map of the pNDs treated cells showed high intensity red region (surrounded by the green region) only near one end of the cells (Figure 5.2C), when compared to the control cells (Figure 5.1C). No red color was observed in any other region of the cells. However a clearly distinct blue colored region accompanied by the indigo colored region can be observed near the inner cellular membrane, in contrast to the central region of cells that showed violet color (least intensity). The backscatter map of the fND-treated cells (Figure 5.3C) demonstrated clear distinct red regions near the cellular membrane and also towards the center of the cells, when compared with the controlled cells (Figure 5.1D).

Hence, the backscattering mode mapping demonstrated the interaction of fNDs with the cells. It should be noted that no NDs were observed in the white light images of NDs treated cells, which could be attributed either due to the smaller size of NDs that is beyond the resolution power of Raman microspectroscopy or due to the cellular internalization of NDs themselves. Although the backscattering maps provided evidence of cellular interaction of fNDs with cells, however, it was not clear if the NDs were present inside the cells or on the surface of cells.

5.4.1.3 Laser Confocal Scanning Microscopy

With an aim of examining the cellular internalization ability of fNDs, laser scanning confocal microscopy was carried out on Hela cells cultured in the media containing fNDs. As the NDs used in this study did not show bright fluorescence emission at a particular wavelength, therefore the images was collected over a wide emission range [16]. The brightfield (A), fluorescence (B) and overlay of brightfield and fluorescence (C) images of the top, middle and bottom z-positions of fND treated Hela cell are shown (Figure 5.4). The top, middle and bottom section corresponds to the 44^{th}, 22^{nd} and 1^{st} section, respectively. An overlay of brightfield and fluorescence image of middle slice of fND treated live cell revealed internalization of few fND particles, as marked by the red circle (Figure 5.4C, middle). These particles appear to be localized near the nucleus of the cell. However the fluorescence of these particles in the middle z-section was not distinctly identified due to the interference originating from cellular autofluorescence. The overlay of fluorescence and brightfield image of four consecutive slices from the middle (21^{st}) towards the bottom of the cell revealed more distinct fND fluorescence emission, since the autofluorescence from the cell was less dominating towards the bottom of the cell (Figure 5.5C).

It was revealed that the NDs used in this study had their own fluorescence, but the emission was not bright enough to be detected distinctly by the confocal fluorescence microscopy. It should be noted that these detonation NDs were not irradiated and annealed, which might create the (N-V) color centers emitting bright fluorescence with high photostability [17,18]. Therefore, in the future studies it will be necessary to irradiate the NDs with high energy sources such as proton, electron or helium ions, followed by thermal annealing to create the bright color centers in the NDs, which could be detected by the confocal microscopy. However, from this preliminary study, it could be suggest that the fNDs are able to internalize into the cells, although not at a high rate.

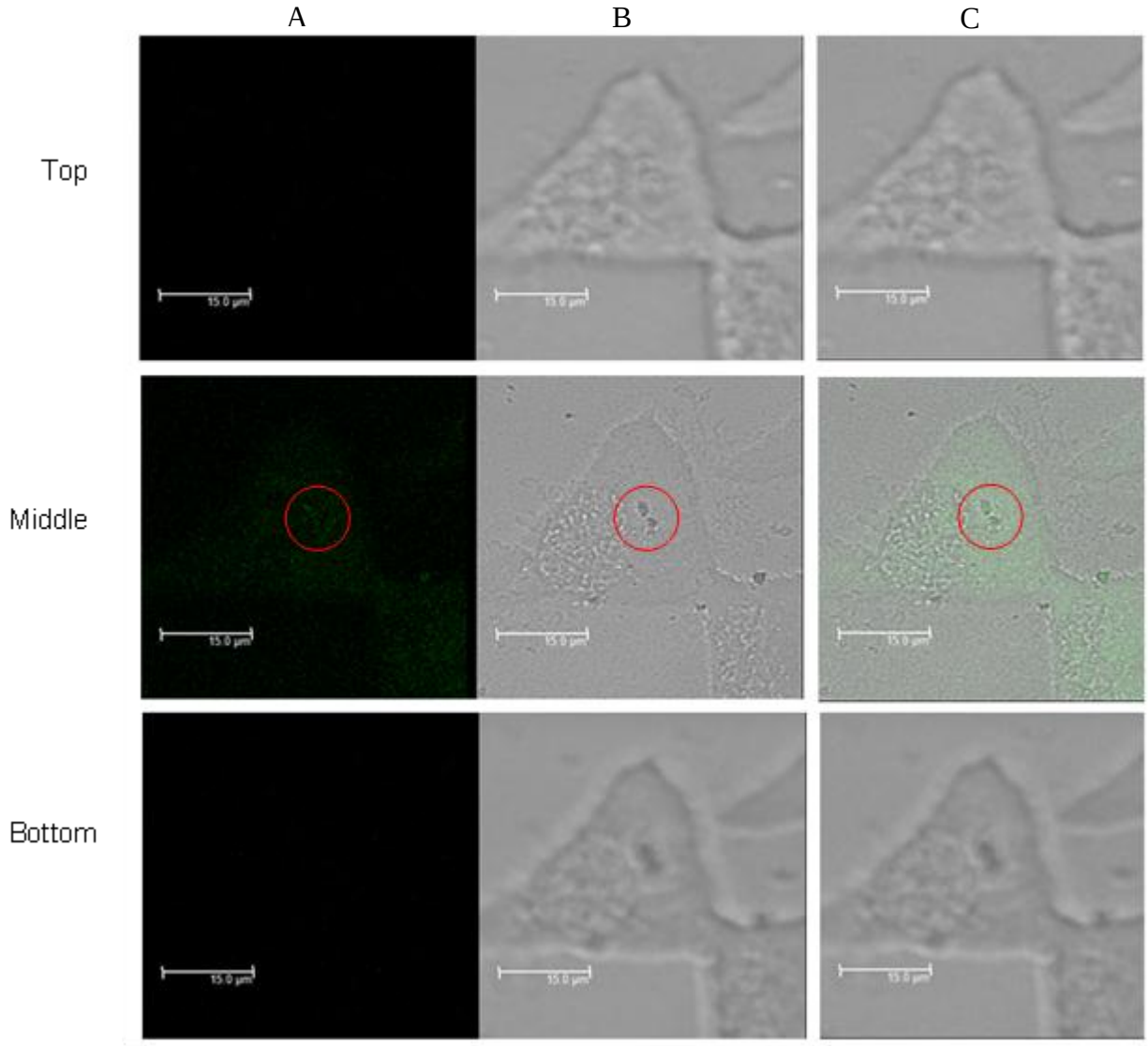

Figure 5.4: Laser scanning confocal microscopic images of the live cell treated with lysine-functionalized nanodiamonds.

Laser scanning confocal microscopic of Hela cells incubated with lysine-functionalized nanodiamonds for 24 hours: From left to right- (A) fluorescence images, (B) bright field images and (C) overlay of fluorescence and bright field images. Excitation was performed using 476 nm laser and emission was collected from 492 to 677 nm. A total of 44 slices were images with 0.38 µm intervals.

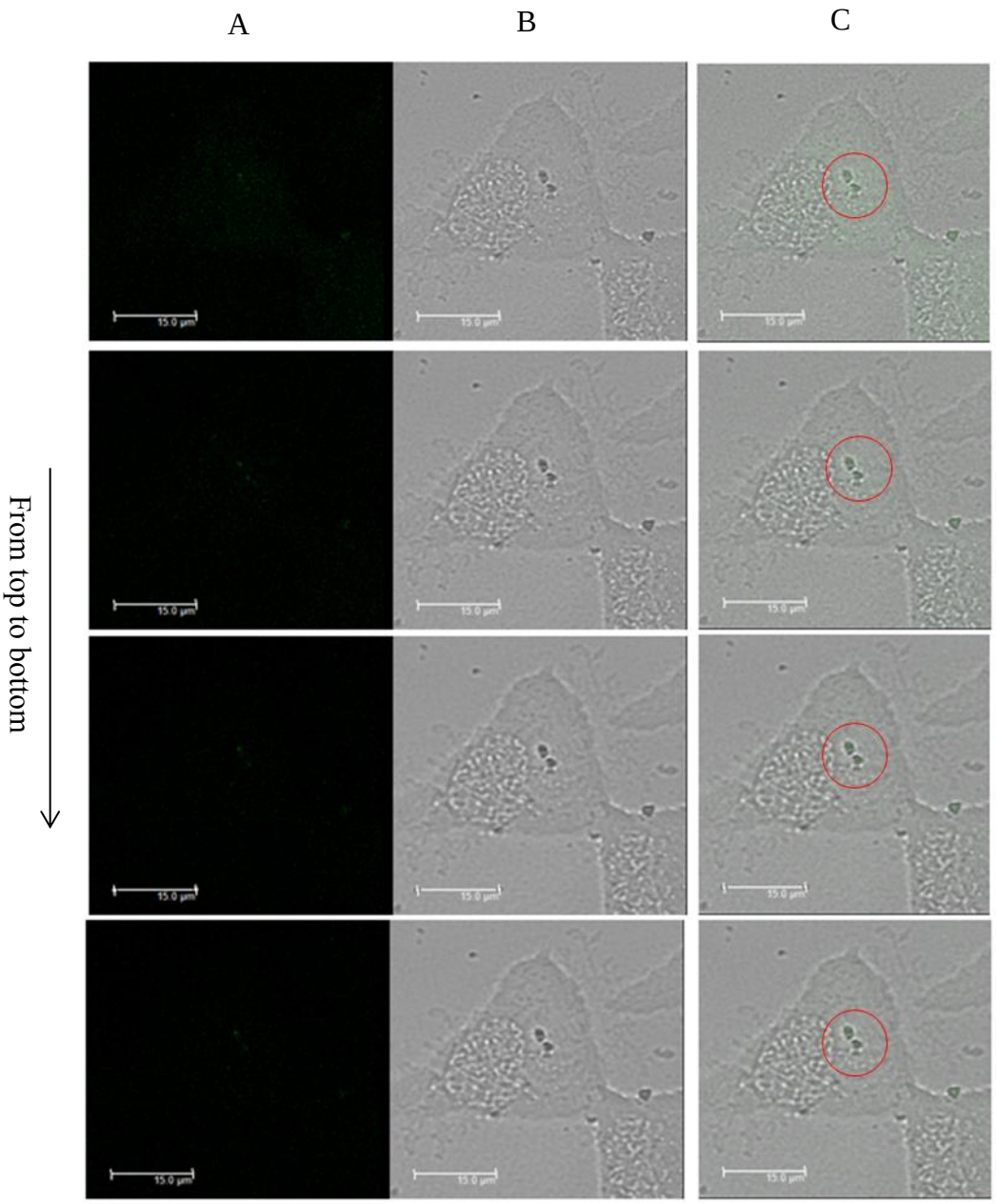

Figure 5.5: Laser scanning confocal microscopic images of four consecutive sections from middle towards the bottom of the cell treated with lysine-functionalized nanodiamonds.

Laser scanning confocal microscopic of four consecutive sections from the middle towards bottom of the Hela cells incubated with lysine-functionalized nanodiamonds for 24 hours. From left to right; (A) fluorescence images, (B) bright field images and (C) overlay of fluorescence and bright field images. From top to bottom; sections 21, 20, 19 and 18 (intervals of 0.38 μm). Excitation was performed using 476 nm laser and emission was collected from 492 to 677 nm.

5.4.2 Cytotoxicity Assay

It is crucial to test the cytotoxicity of the delivery agent before proceeding to the optimization of its transfection efficacy. Using Hela cell line, cytotoxic effects of seven different concentrations of NDs, ranging from 4 to 250 μg/mL incubated with cells for 24 hours, in the presence and absence of serum, were studied. In these experiments, none of the examined concentrations of pNDs showed statistically significant differences in cellular viabilities compared to control and 4 μg/mL pNDs treated cells (Scheffé post-hoc multiple comparison test, $p<0.05$), indicating biocompatibility of pNDs towards the Hela cells (Figure 5.6). In addition, the presence or absence of serum during the treatment did not contribute to any considerable changes in the cellular viabilities (Figure 5.6). The overall mean cellular viabilities after treatment with pNDs in the absence of serum ranged from 88.70 to 102.27%, while the cells incubated with pNDs in presence of serum showed a mean cellular viability from 100.79 to 108.87%. This indicates, that although not significant, the pNDs with serum have a proliferative effect on the cells since the observed mean cellular viability was greater than 100% with all the tested concentrations, in agreement with Schrand et al [10]. However, the cytotoxicity results are in disagreement with Li et al who demonstrated that NDs in the absence of serum in cell culturing media cause extreme toxicity to the cells [4].

The fNDs also had negligible cytotoxic effects on Hela cells as none of the tested concentration showed significant differences in cell viabilities compared to control and 4 μg/mL fND treated cell population, both in presence and in absence of the serum in the cell culture medium (Figure 5.7, Dunnett's T3 post-hoc multiple comparison test, $p<0.05$). The mean cellular viability ranged from 86.61 to 105.24% in fNDs treated cells with serum, which decreased slightly to 84.44 to 99.50% when the serum was excluded from the treatment medium. Overall, the percentage viability of the cells incubated with fNDs (Figure 5.7) was a little lower than that observed with pNDs (Figure 5.6). This can be attributed to the highly positive surface charge of the fNDs (+48.9 mV) [19].

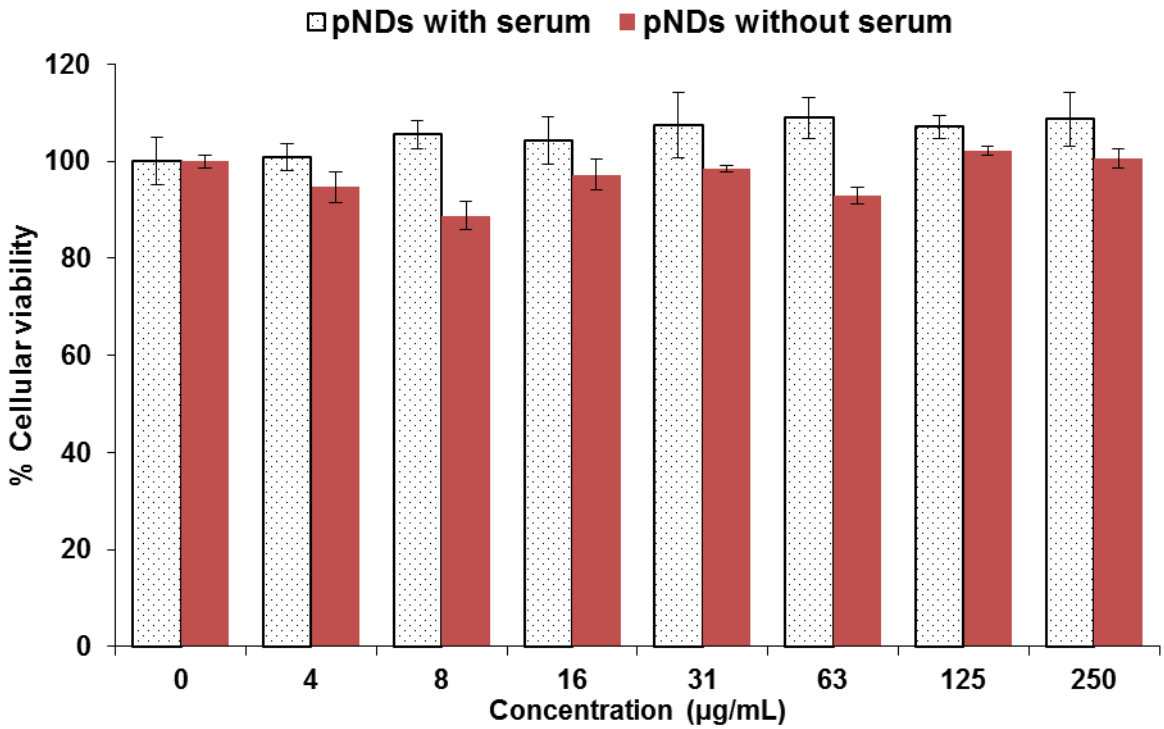

Figure 5.6: MTT cytotoxicity assay of Hela cells treated with pristine carboxylated nanodiamonds with and without serum.

Evaluation of Hela cell viability after incubation with 0-250 µg/mL of pristine carboxylated nanodiamonds in the cell culture medium with and without serum for 24 hours as determined by MTT assay. Cells cultured without nanodiamonds were used as controls. Cells treated with pristine carboxylated nanodiamonds did not elicit significant cytotoxic effects when compared to control cells (Scheffé's post-hoc multiple comparison test, $p<0.05$). Results are expressed as mean ± S.E.M., n=3.

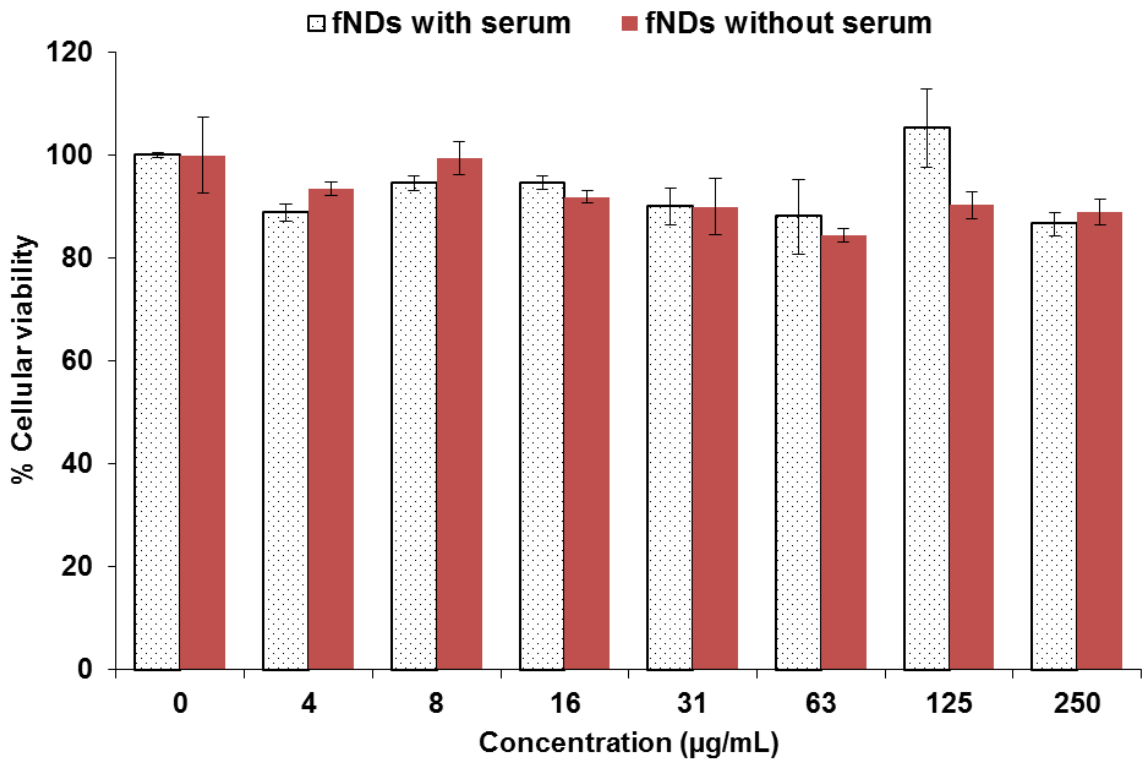

Figure 5.7: MTT cytotoxicity assay of Hela cells treated with lysine-functionalized nanodiamonds with and without serum.

Evaluation of Hela cell viability after incubation with 0-250 µg/mL of lysine-functionalized nanodiamonds in the cell culture medium with and without serum for 24 hours as determined by MTT assay. Cells cultured without nanodiamonds were used as control group. Cells treated with lysine-functionalized nanodiamonds did not elicit significant cytotoxic effects when compared to control cells (Dunnett's T3 post-hoc multiple comparison test, $p<0.05$). Results are expressed as mean ± S.E.M., n=3.

This cytotoxicity assay demonstrated that the NDs do not possess inherent cellular toxicity as supported by other studies [2,3,9], when used in the concentration range from 4 to 250 µg/mL. However, these results cannot be generalized as many other factors such as type of cell line, impurities, functionalization and size of nanoparticles can ultimately affect the behavior of NDs in biological systems [20]. However, the NDs used in this study exhibit high biocompatibility towards Hela cell line.

5.4.3 fNDs as siRNA Delivery Agents

The siRNA is a double stranded fragment of RNA possessing 21-23 nucleotides that has recently gained interest for silencing the specific gene expression [21]. After being internalized into the cells, one strand of siRNA assembles into RNA induced silencing complex (RISC) depending upon the structural features of siRNA [22]. Argonaute 2, a catalytic element of RNA induced silencing complex, activates the RISC complex by cleaving the sense strand of siRNA [23,24], which subsequently releases its antisense strand free to degrade the complementary mRNA released from the nucleus into the cytoplasm of the cell [25]. The activated RISC continues its silencing effect until it undergoes degradation or a significant dilution below the therapeutic level [26]. RNA-interference mediated silencing induced by siRNA has early found early applications in treating hepatitis B [27], cancer [28,29], ocular neovascularization [30] and acute liver failure [31]. Therefore the key of success for silencing gene expression is in delivering siRNA efficiently into the cytoplasm of the cell and making it available for cleaving the complementary post-transcriptional mRNA. As described in chapter-1 (section 1.2), the anionic nature of siRNA provide barrier for its effective internalization across the negatively charged cellular surface, bringing the need for a carrier that could effectively deliver siRNA into the cytoplasm of cells.

The fNDs demonstrated potential to act a siRNA delivery agent (Chapter 4, section 4.3.4), therefore its efficacy to deliver anti GFP-siRNA in Hela/GFP cells was evaluated by flow cytometry. The majority of the gated untreated Hela/GFP cells were found in the moderate (42%) followed by the high GFP (30%) intensity quadrants, while the mild and low GFP intensity regions consisted of only 17% and 11% of the gated events, respectively (Figure 5.8A). Lipofectamine, a commercially available transfecting agent, when used as a siRNA delivery

agent substantially shifted the Hela/GFP cell population towards the lower GFP intensity regions, with only 2% and 22% of the gated cells remaining in the high and moderate GFP intensity quadrants, respectively (Figure 5.8B). The fNDs:siRNA (35:1,w/w/) as a transfection complex also shifted the cell population towards the lower GFP intensity, with 15% and 39% cells appearing in low and mild GFP intensity quadrants, respectively (Figure 5.8C). But a similar shift was also observed in the naked siRNA treated Hela/GFP cells, which showed 30% and 31% of cell population in the low and mild GFP intensity regions, respectively (Figure 5.8D). Overall, the Lipofectamine-siRNA (positive control) knocked the GFP intensity down by 66% (Figure 5.9) relative to the untreated group. The fNDs-siRNA knocked down the GFP intensity by 36%, which was 9% less than that observed with naked siRNA treated cells (45%).

This indicates that fNDs might not be able to release the siRNA efficiently from the fNDs-siRNA complex into the cytoplasm, limiting the GFP knockdown efficiency of the siRNA. The higher number of cells in mild GFP and fewer in low GFP intensity quadrant in fND-siRNA treated cells (Figure 5.8C) compared to the naked siRNA treated cells (Figure 5.8D) also indicates the inability of fNDs to release siRNA efficiently from the fNDs-siRNA complex. This brings forward the need of grafting a moiety on NDs surface that can facilitate the cytoplasmic release of siRNA from the fNDs. In addition, another methodology such as real time polymerase chain reaction or western blotting could be explored to quantitate the mRNA level of the cells.

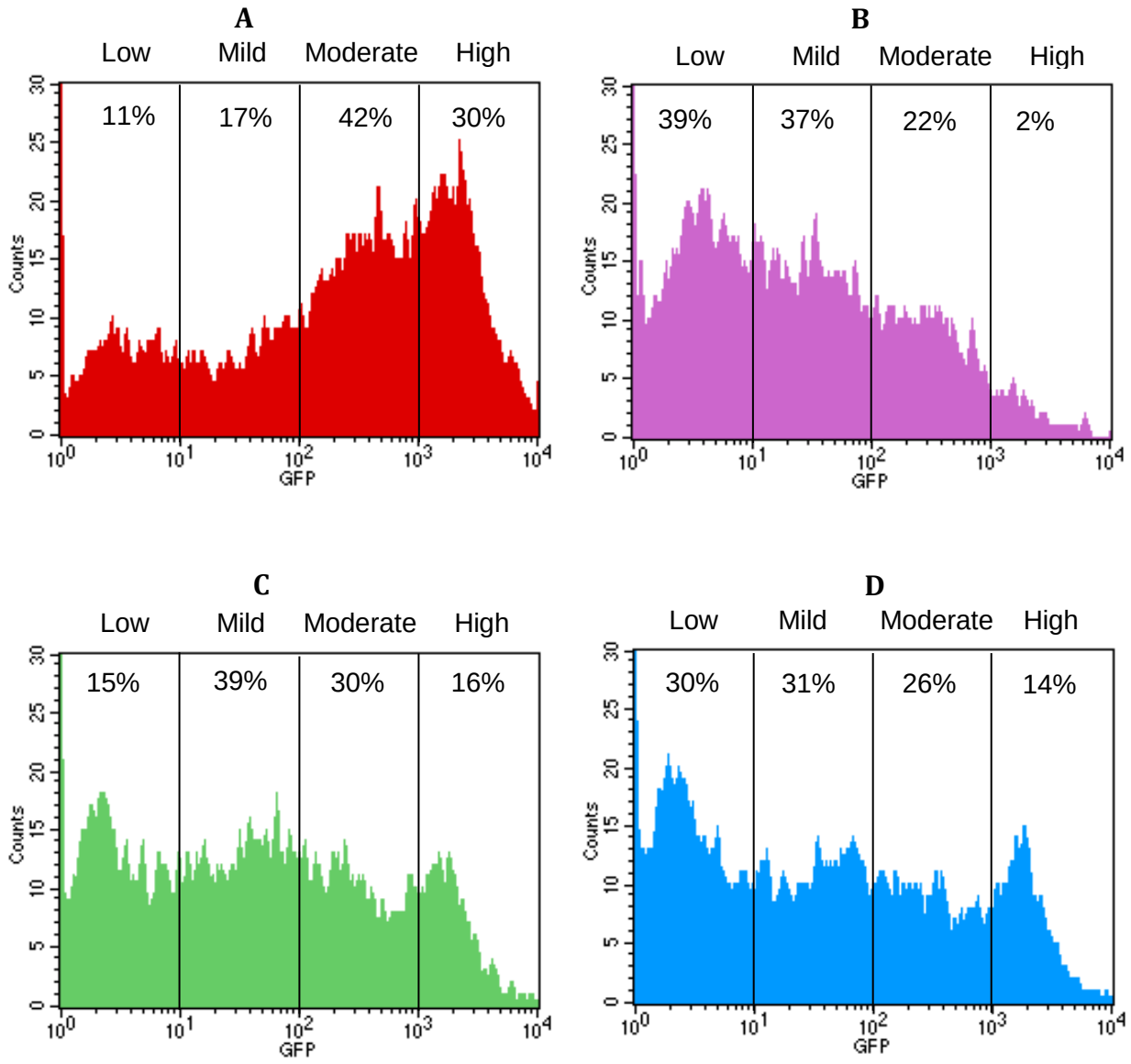

Figure 5.8: Flow cytometer histograms indicating the GFP fluorescence intensity trend in untreated and treated cell populations.

Fluorescence activated cell sorting histograms of (A) control; (B) Lipofectamine:siRNA transfected; (C) fNDs:siRNA (35:1,w/w) transfected; (D) naked siRNA transfected Hela/GFP cells.

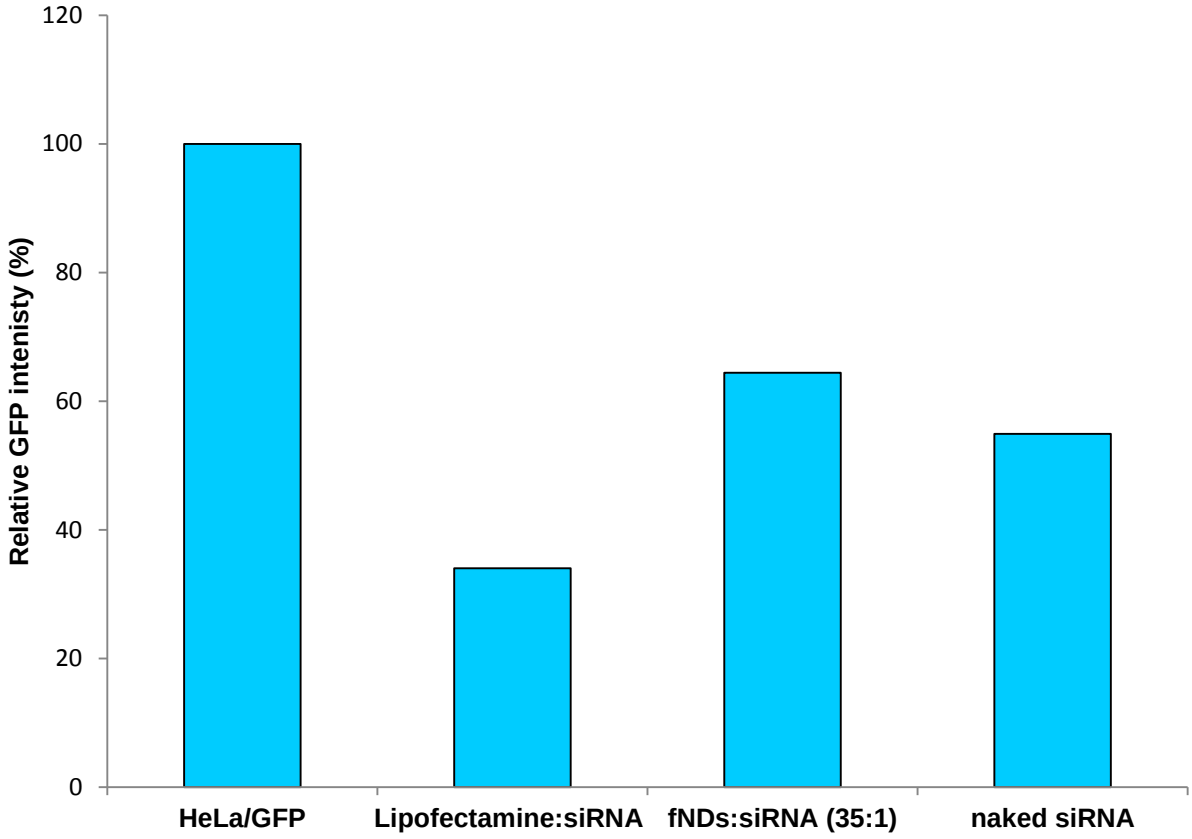

Figure 5.9: The effect of using lysine-functionalized nanodiamonds to deliver small interfering RNA.

Percentage GFP intensity of control Hela/GFP cells, Lipofectamine:siRNA, fNDs:siRNA (35:1) and naked siRNA transfected Hela/GFP cells. The fluorescence intensity of green fluorescent protein was measured by flow cytometer and is expressed as a percentage relative to the untreated Hela/GFP cells. The lower knockdown by lysine-functionalized nanodiamonds-siRNA complex indicates the inefficient intracellular release of siRNA from the complex.

5.5 Conclusions

In this study, the high fluorescence of NDs and cells limited the use of Raman microspectroscopy in detecting the diamond signal of NDs interacting with the cells. However, the maps constructed by measuring the elastically scattered light have higher potential for identification of the NDs in the cells. The comparison of fluorescence and backscattering maps of fND-treated and untreated cells provided a clear evidence of interaction of fNDs with cells. Laser scanning confocal microscopic measurements suggested the internalization of few particles of fNDs. The pNDs and fNDs demonstrated high biocompatibility in Hela cells up to 250 μg/mL concentration, with no considerable alterations in cell viability by the presence or absence of serum in the treatment media. siRNA interference suggested that the binding of fNDs to the siRNA might be to too strong to release the nucleic acid efficiently in the cytoplasm of the cells, suggesting the need for optimization of the formulation.

5.6 References

1. Faklaris O, Joshi V, Irinopoulou T, Tauc P, Sennour M, Girard H, Gesset Cl, Arnault J-C, Thorel A, Boudou J-P, et al.: Photoluminescent Diamond Nanoparticles for Cell Labeling: Study of the Uptake Mechanism in Mammalian Cells. *ACS Nano* 2009, 3:3955-3962.

2. Liu KK, Wang CC, Cheng CL, Chao JI: Endocytic carboxylated nanodiamond for the labeling and tracking of cell division and differentiation in cancer and stem cells. *Biomaterials* 2009, 30:4249-4259.

3. Schrand AM, Dai L, Schlager JJ, Hussain SM, Osawa E: Differential biocompatibility of carbon nanotubes and nanodiamonds. *Diamond and Related Materials* 2007, 16:2118-2123.

4. Li J, Zhu Y, Li W, Zhang X, Peng Y, Huang Q: Nanodiamonds as intracellular transporters of chemotherapeutic drug. *Biomaterials* 2010, 31:8410-8418.

5. Schrand AM, Huang H, Carlson C, Schlager JJ, Osawa E, Hussain SM, Dai L: Are diamond nanoparticles cytotoxic? *Journal of Physical Chemistry B* 2007, 111:2-7.

6. Yu SJ, Kang MW, Chang HC, Chen KM, Yu YC: Bright fluorescent nanodiamonds: No photobleaching and low cytotoxicity. *Journal of the American Chemical Society* 2005, 127:17604-17605.

7. Liu KK, Cheng CL, Chang CC, Chao JI: Biocompatible and detectable carboxylated nanodiamond on human cell. *Nanotechnology* 2007, 18:325102.

8. Chao JI, Perevedentseva E, Chung PH, Liu KK, Cheng CY, Chang CC, Cheng CL: Nanometer-sized diamond particle as a probe for biolabeling. *Biophysical Journal* 2007, 93:2199-2208.

9. Huang H, Pierstorff E, Osawa E, Ho D: Active nanodiamond hydrogels for chemotherapeutic delivery. *Nano Letters* 2007, 7:3305-3314.

10. Schrand AM, Johnson J, Dai L, Hussain SM, Schlager JJ, Zhu L, Hong Y, Osawa E: Cytotoxicity and Genotoxicity of Carbon Nanomaterials. *Safety of Nanoparticles: From Manufacturing to Medical Applications* 2009:159-187.

11. Krafft C, Knetschke T, Siegner A, Funk RHW, Salzer R: Mapping of single cells by near infrared Raman microspectroscopy. *Vibrational Spectroscopy* 2003, 32:75-83.

12. Chung PH, Perevedentseva E, Cheng CL: The particle size-dependent photoluminescence of nanodiamonds. *Surface Science* 2007, 601:3866-3870.

13. Colpin Y, Swan A, Zvyagin AV, Plakhotnik T: Imaging and sizing of diamond nanoparticles. *Optics Letters* 2006, 31:625-627.

14. Tuchin VV: Methods and algorithms for the measurement of the optical parameters of tissues. In *Tissue Optics: Light Scattering Methods and Instruments for Medical Diagnosis*, edn 2. SPIE; 2007:143-256.

15. Smith BR, Niebert M, Plakhotnik T, Zvyagin AV: Transfection and imaging of diamond nanocrystals as scattering optical labels. *Journal of Luminescence* 2007, 127:260-263.

16. Kompan ME, Terukov EI, Gordeev SK, Zhukov SG, Nikolaev YA: Photoluminescence spectra of ultradisperse diamond. *Physics of the Solid State* 1997, 39:1928-1929.

17. Fu CC, Lee HY, Chen K, Lim TS, Wu HY, Lin PK, Wei PK, Tsao PH, Chang HC, Fann W: Characterization and application of single fluorescent nanodiamonds as cellular biomarkers. *Proceedings of the National Academy of Sciences of the United States of America* 2007, 104:727-732.

18. Weng MF, Chiang SY, Wang NS, Niu H: Fluorescent nanodiamonds for specifically targeted bioimaging: Application to the interaction of transferrin with transferrin receptor. *Diamond and Related Materials* 2009, 18:587-591.

19. McNeil SE: Nanoparticle therapeutics: a personal perspective. *Wiley interdisciplinary reviews. Nanomedicine and nanobiotechnology* 2009, 1:264-271.

20. Lewinski N, Colvin V, Drezek R: Cytotoxicity of nanoparticles. *Small* 2008, 4:26-49.

21. Dykxhoorn DM, Novina CD, Sharp PA: Killing the messenger: Short RNAs that silence gene expression. *Nature Reviews Molecular Cell Biology* 2003, 4:457-467.

22. Schwarz DS, Hutvágner G, Du T, Xu Z, Aronin N, Zamore PD: Asymmetry in the assembly of the RNAi enzyme complex. *Cell* 2003, 115:199-208.

23. Matranga C, Tomari Y, Shin C, Bartel DP, Zamore PD: Passenger-Strand Cleavage Facilitates Assembly of siRNA into Ago2-Containing RNAi Enzyme Complexes. *Cell* 2005, 123:607-620.

24. Rand TA, Ginalski K, Grishin NV, Wang X: Biochemical identification of Argonaute 2 as the protein required for RNA-induced silencing complex activity. *Proceedings of the National Academy of Sciences of the United States of America* 2004, 101:14385-14389.

25. Ameres SL, Martinez J, Schroeder R: Molecular Basis for Target RNA Recognition and Cleavage by Human RISC. *Cell* 2007, 130:101-112.

26. Bartlett DW, Davis ME: Insights into the kinetics of siRNA-mediated gene silencing from live-cell and live-animal bioluminescent imaging. *Nucleic Acids Research* 2006, 34:322-333.

27. McCaffrey AP, Nakai H, Pandey K, Huang Z, Salazar FH, Xu H, Wieland SF, Marion PL, Kay MA: Inhibition of hepatitis B virus in mice by RNA interference. *Nature Biotechnology* 2003, 21:639-644.

28. Filleur S, Courtin A, Ait-Si-Ali S, Guglielmi J, Merle C, Harel-Bellan A, Clezardin P, Cabon F: SiRNA-mediated inhibition of vascular endothelial growth factor severely limits tumor resistance to Antiangiogenic thrombospondin-1 and slows tumor vascularization and growth. *Cancer Research* 2003, 63:3919-3922.

29. Yang G, Thompson JA, Fang BL, Liu JS: Silencing of H-ras gene expression by retrovirus-mediated siRNA decreases transformation efficiency and tumorgrowth in a model of human ovarian cancer. *Oncogene* 2003, 22:5694-5701.

30. Reich S, Fosnot J, Kuroki A, Tang WX, Yang XY, Maguire A, Bennett J, Tolentino M: Small interfering RNA (siRNA) targeting VEGF effectively inhibits ocular neovascularization in a mouse model. *Molecular Vision* 2003, 9:210-216.

31. Zender L, Hütker S, Liedtke C, Tillmann HL, Zender S, Mundt B, Waltemathe M, Gösling T, Flemming P, Malek NP, et al.: Caspase 8 small interfering RNA prevents acute liver failure in mice. *Proceedings of the National Academy of Sciences of the United States of America* 2003, 100:7797-7802.

5.7 Supplemental Data

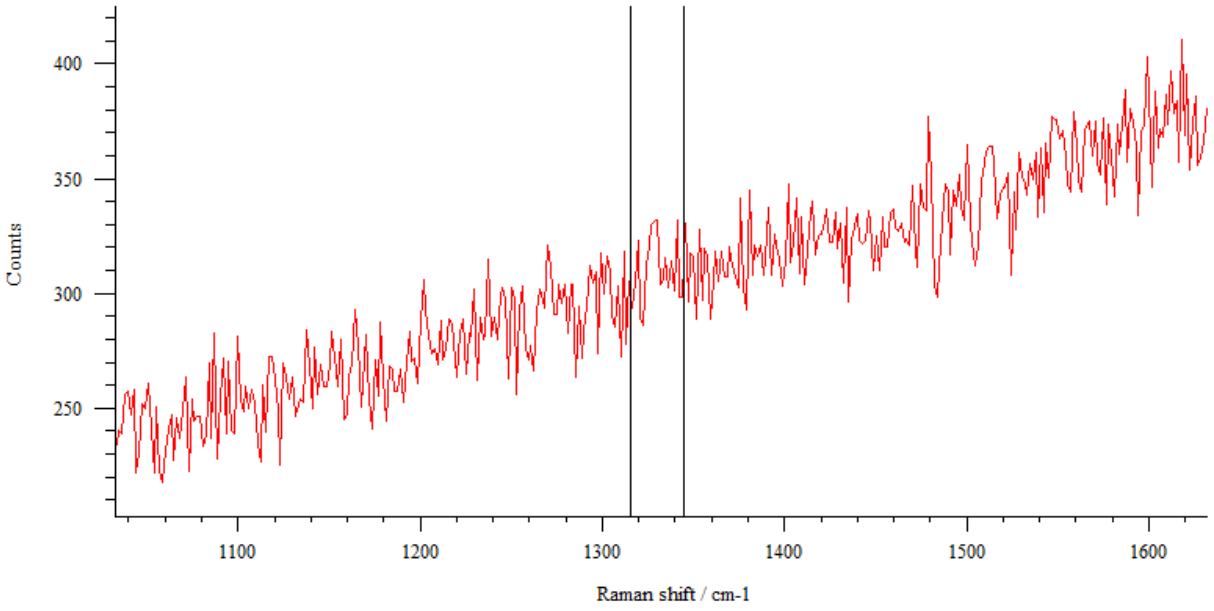

Figure S 5.1: The Raman spectra obtained from a high intensity region of pNDs treated cells.

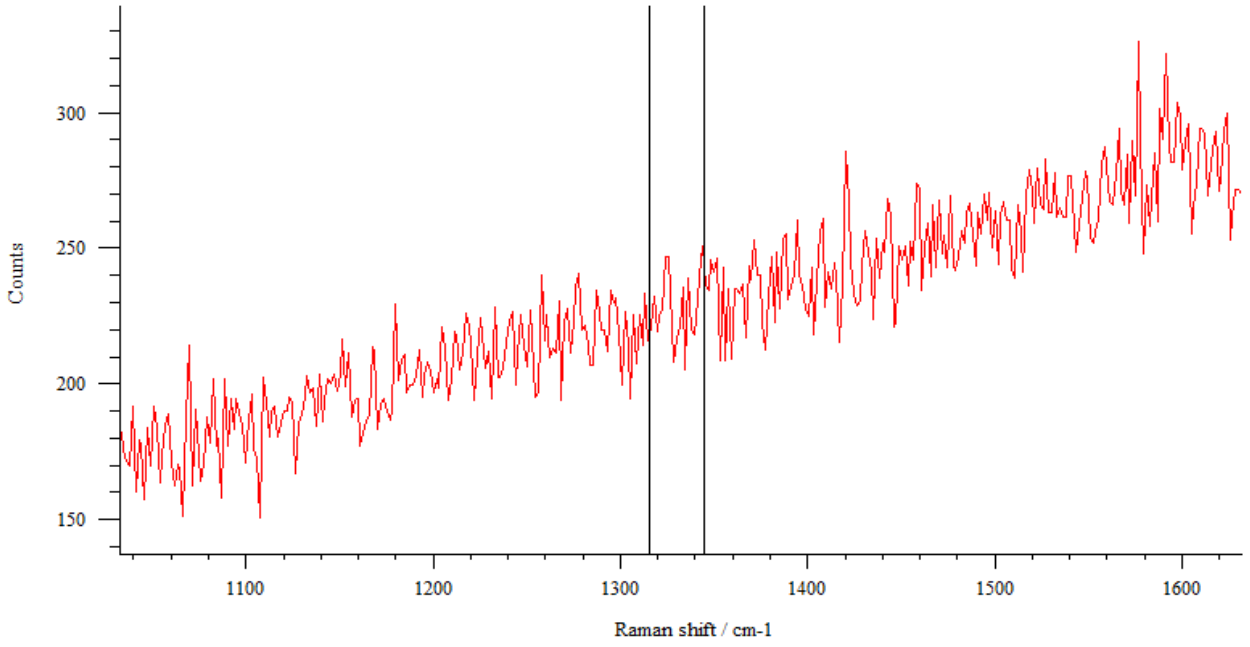

Figure S 5.2: The Raman spectra obtained from a high intensity region of fNDs treated cells.

Chapter 6 CONCLUSIONS AND FUTURE DIRECTIONS

6.1 Overall Conclusions

The present study has probed two main dimensions for developing nanodiamonds (NDs) as a vector for improving the cellular delivery of nucleic acids. The first phase consisted of functionalization, physiochemical characterization and evaluation of potential of NDs for delivering genetic materials into the cell. The second phase probed the interactions of this novel delivery agent with the human cellular systems.

Phase I

NDs have potential to act as a superior delivery agent over many currently available carriers but remained unnoticed for several years due to their strong aggregation tendency. Recently, the techniques using high energy such as bead-assisted probe sonication and milling have been put forth to achieve single-digit-sized nanoparticles; however contamination, re-aggregation as well as structural alterations remain the issue. The mechanochemical disaggregation approach used in this study successfully generated highly stable lysine-functionalized NDs (fNDs) with size less than 50 nm. Not only these nanoparticles showed high stability in the water, which is considered to be biologically most suitable formulation dispersal medium, but were also resistant to re-aggregation upon solvent removal.

The suitability of fNDs generated in this study as nucleic acid delivery agent is reflected by their ability to bind plasmid DNA and small interfering RNA by forming complexes with a size and surface charge favorable for cellular internalization. In the drug delivery studies, generally, the efficacy shown by a carrier for one particular type of genetic material is applied for other nucleic acids as well. However, from this study, it can be clearly concluded that even though all the nucleic acids are negatively charged, their interactions with positively charged solid-core carriers are peculiar depending mainly upon dimensions of the nucleic acids.

Phase II

NDs, both carboxylated and lysine-modified, used in this study were non-cytotoxic towards mammalian cells, therefore potentially suitable for *in vivo* formulation development. Backscattering microscopic mapping revealed the successful interaction of this material either with the cellular surface or intracellular region, or both. The fluorescence emission from the fNDs was weak to be detected efficiently by confocal microscopy; however, the evidence of

internalization of few particles was present. High cellular interaction accompanied by the low cytotoxicity of fNDs supports the use of these nanoparticles as a delivery vehicle. However fND particles obtained in this study were not able to improve the delivery efficacy of small interfering RNA in human cervical cancer cells as studied by using fluorescence activated cell sorting.

In conclusion, fND particles developed in this study have potential to emerge as a suitable candidate for delivering nucleic acids; however efficacy remains to be seen.

6.2 Future Directions

This study was the first attempt by our research group for developing amino acid-functionalized NDs as potential gene delivery agent. The successful disaggregation/functionalization approach established by this study paved the way for future studies on this carbon material. Moreover, this study explored various techniques for *in vitro* detection of ND particles, from which the best techniques would be used directly for future studies.

The future directions will focus on two major aspects of NDs as delivery agent:

6.2.1 Cellular Uptake Studies on NDs

The internalization of pristine carboxylated and fNDs will be tested in human cell line using laser scanning confocal microscopy. For future studies, the NDs will be irradiated with proton, electron or helium ion beam, and then annealed at 800℃, to create bright photoluminescent nitrogen vacancy color centers able to be detected effectively by confocal fluorescence microscopy. In addition, for more comprehensive cellular internalization investigations, synchrotron directed scanning transmission X-ray spectromicroscopy (STXM) will also be carried out based upon its feasibility to distinguish NDs from the cellular composition, as evidenced by a pilot study (Appendix B)

6.2.2 Quantification of mRNA Level in fNDs-Delivered siRNA

Real-time polymerase chain reaction assay or western blotting will be carried out in future to quantitate the gene knockdown effect shown by fNDs-siRNA formulation. These techniques can measure the actual cellular GFP-mRNA level reduction; therefore will be more specific and selective than measuring the overall cellular fluorescence intensity. Based upon these results, the optimization of NDs formulation will be carried out, if required. Incorporation of the lipids such as 1,2-di-(9-octadecenoyl)-glycero-3-phosphoethanolamine (DOPE) and 1,2-dioleoyl-3-trimethylammonium-propane (DOTAP) could be considered if fNDs will be confirmed to have too strong binding with siRNA. Addition of DOPE to the gemini surfactants, synthesized by our research group, has increased the transfection efficacy of plasmid DNA.

APPENDIX A
PRELIMINARY ATTEMPTS TO ACHEIVE DISGGREGATION OF NDs

Following is the summary of the attempts made to disaggregate pristine carboxylated NDs (pNDs), using bath sonication, probe sonication, grinding media and surfactants, before proceeding to the lysine functionalization.

The pNDs at the concentration of 2 mg/mL was dispersed in water and sonicated for 4 hours in a bath sonicator. No decrease in the aggregate size of pNDs was observed (A.1). Dispersion of pNDs prepared in 0.5% aqueous solution of benzalkonium chloride, at a concentration of 2 mg/mL, with 4 hours of bath sonication experienced a decrease in aggregate size of pNDs showing a peak at 255 nm (A.2). However the size distribution was very broad ranging from 90 to 1000 nm (A.2). Keeping all the other parameters same, dispersion of pNDs was also prepared in 2% aqueous solution of Tween 80, but with no improvement in the particle size (A.3). The sonication of pNDs dispersed in water was carried out in presence of 0.05 mm YTZ® grinding media, which also did not result any considerable disaggregation of pND aggregates (A.4). A summary of the Z-Average size, polydispersity index and zeta potential of all these attempts is provided in A.5.

Further efforts were made to disaggregate pND aggregates using high power probe sonication. To observe, if there is any time dependent effect of sonication in achieving disaggregation of pNDs, probe sonication of aqueous dispersions of pNDs was carried out from 5 to 45 minutes (A.6). A summary of Z-Average size, polydispersity index and zeta potential achieved through this technique is presented in A.7. Similarly, the probe sonication was also performed for pNDs dispersed in 1% Tween 80, in the presence of 0.05 mm YTZ®, at various time intervals (A.8). None of these attempts resulted in a considerable disaggregation of pNDs.

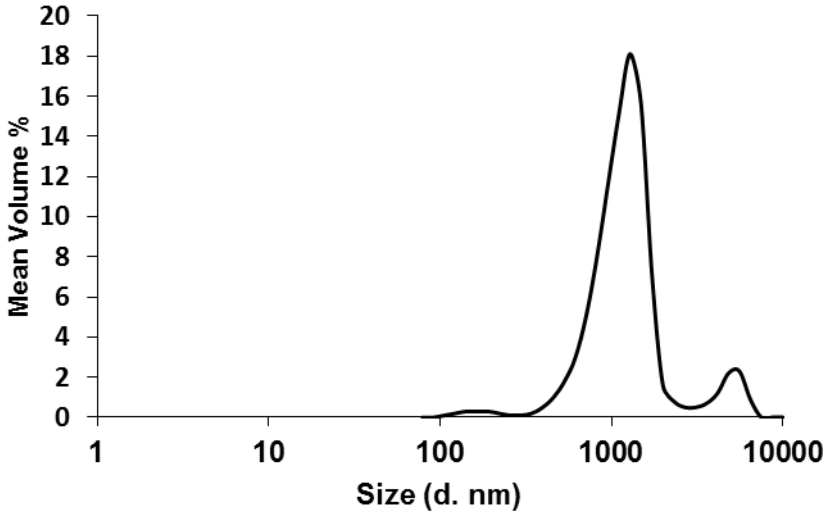

A.1: Size distribution graph of pristine carboxylated nanodiamonds dispersed in water (2 mg/mL) with 4 hours of bath sonication.

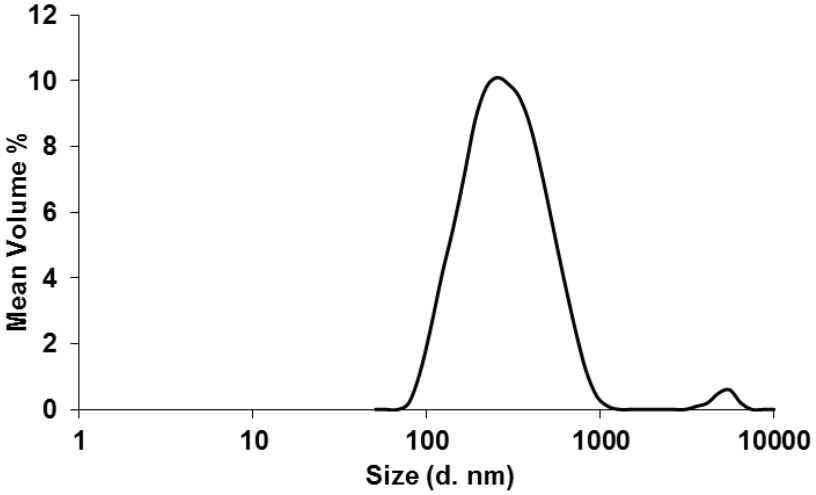

A.2: Size distribution graph of pristine carboxylated nanodiamonds (2 mg/mL) dispersed in 0.5% aqueous solution of benzalkonium chloride with 4 hours of bath sonication.

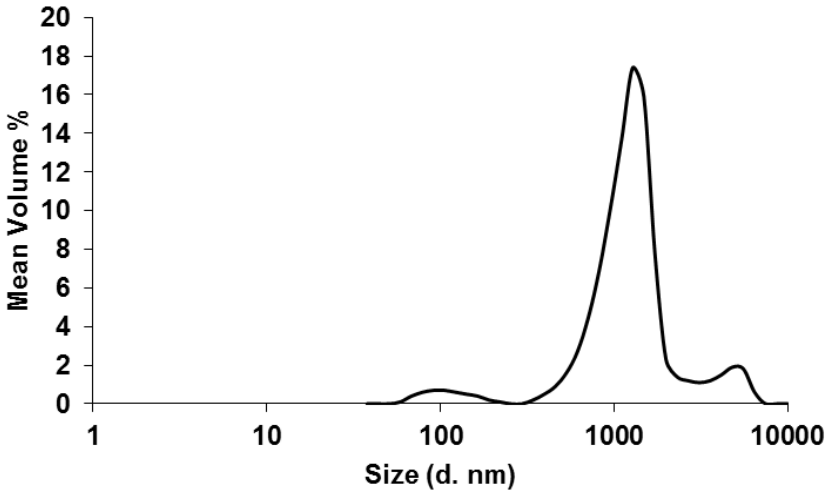

A.3: Size distribution graph of pristine carboxylated nanodiamonds (2 mg/mL) dispersed in 2% aqueous solution of Tween 80 with 4 hours of bath sonication.

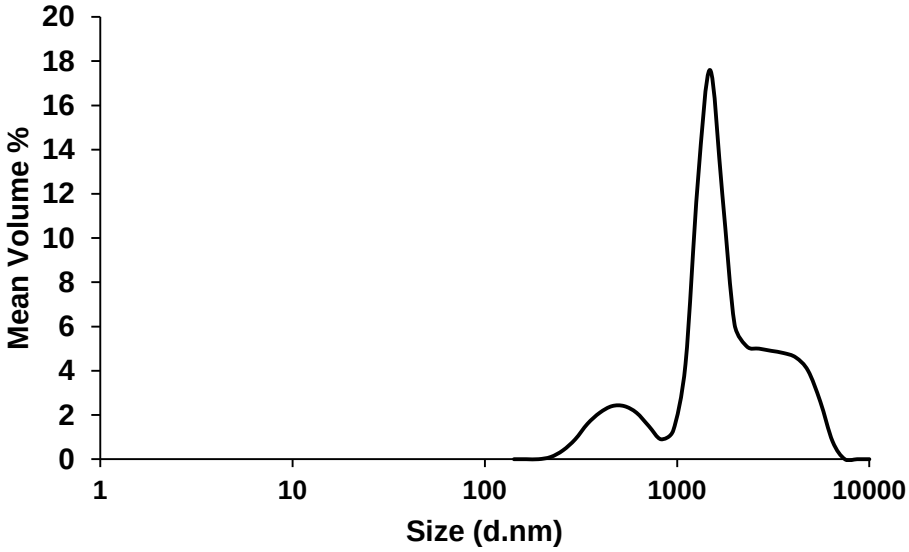

A.4: Size distribution graph of pristine carboxylated nanodiamonds (2 mg/mL) dispersed in water with 4 hours of bath sonication in presence of 0.05 mm YTZ® grinding media.

A.5: Size, polydispersity index and zeta potential measurement of pristine carboxylated nanodiamond samples obtained after bath sonication

Sample	Z-Average size (nm)	Polydispersity index	Zeta Potential (mV)
pNDs (2 mg/mL) dispersed in water with 4 hours of sonication	880.1	0.45	-18.7
pNDs (2 mg/mL) dispersed in 0.5 % aqueous solution of benzalkonium chloride with 4 hours of sonication	241.9	0.18	46.3
pNDs (2 mg/mL) dispersed in 2% aqueous solution of Tween 80 with 4 hours of sonication	716.8	0.64	-12.7
pNDs (2 mg/mL) dispersed in water with 4 hours of bath sonication in presence of 0.05 mm YTZ® grinding media	1100	0.57	-20.2

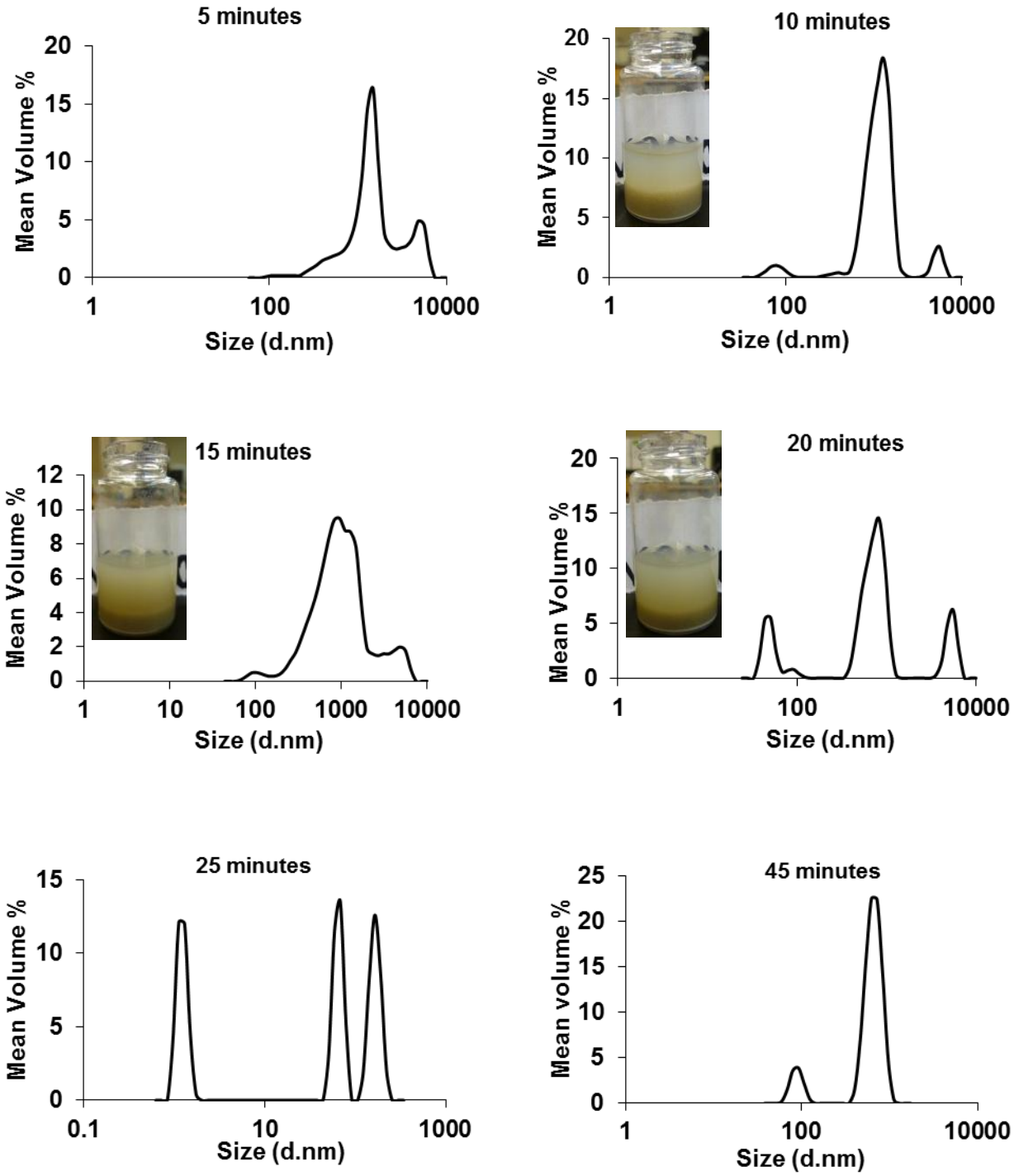

A.6: Aqueous dispersions of pristine carboxylated nanodiamonds (2 mg/mL) obtained by probe sonication at various time intervals.

A.7: Size, polydispersity index and zeta potential measurement of aqueous dispersions of pristine carboxylated nanodiamonds (2 mg/mL) at various time intervals obtained by probe sonication in the presence of 0.05 mm YTZ® grinding media

Sonication time (minutes)	Z-Average size (nm)	Polydispersity index	Average zeta potential (mV)
5	957.5	0.71	-20.4
10	1857	0.92	-16.4
15	563.6	0.46	-21.8
20	2028	0.87	-15.3
25	5137	1.00	-8.24
45	2071	1.00	-20.0

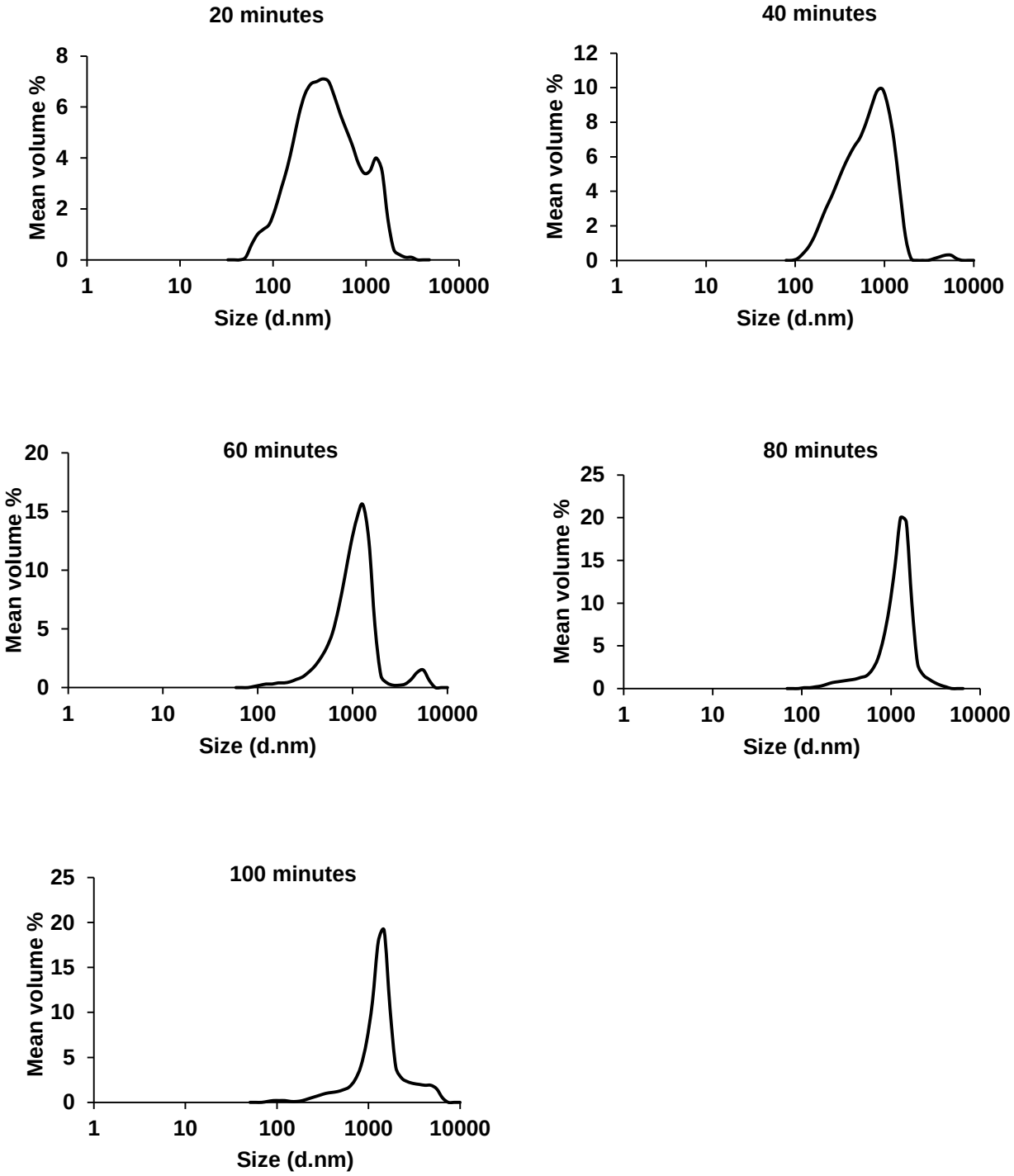

A.8: Pristine carboxylated nanodiamonds (2 mg/mL) dispersed in 1% Tween 80 at various time intervals using probe sonication in the presence of 0.05 mm YTZ®.

APPENDIX B

A PILOT STUDY TO EVALUATE THE FEASIBILITY OF SCANNING TRANSMISSION X-RAY SPECTROMICROSCOPY TO IDENTIFY NANODIAMONDS IN THE MAMMALIAN CELLS

Soft X-ray spectromicroscopy of the cells incubated with fNDs was carried out using scanning transmission X-ray spectromicroscope (STXM) at the beamline 10ID-1 of the Canadian Light Source (University of Saskatchewan, Saskatoon, SK, Canada). The advantages associated with STXM include high spatial resolution (less than 50 nm) [1,2], non-interference from the fluorescence of cells or NDs, and no need of staining the cellular structures. A375 cells were plated on silicon nitride windows, placed in a 24-well cell culture plate, at the density of 10,000 cells per well, and allowed to adhere for 24 hours. After treating with NDs for 2 hours, the samples were sent to CLS for the soft X-Ray microscopic measurements.

To fulfill the requirements for the identification inside the cells, the NDs should possess a unique identifiable STXM spectrum. Spectra from the four different regions of NDs (B.1A) at the C 1s edge were recorded to examine the possibility of identifying these nanoparticles in the cells in the future studies. All the spectra were same with same absorption peaks at C 1s edge (B.1B), supporting the potential of STXM in detecting NDs in the cells. Measurements at the C 1s edge from six different regions of a single cell treated with NDs (B.2A) revealed three different spectral patterns (B.2B and C). In stack 1 (B.2B), the green and blue colored spectra were identical; while pink spectra showed absorption peaks at somewhat different energy range. The blue and green colored spectral pattern were assigned to proteins, while the pink colored pattern arose due to the lipids present in the cells, as discussed in other studies [1,3,4]. The spectra shown in stack 2 (B.2C) were identical to the spectra obtained from NDs alone (B.1B). Therefore, these spectra indeed can be assigned to the NDs. Subsequently by fitting these spectra, the presence of NDs (B.3A), lipids (B.3B) and proteins (B.3C) was revealed, indicated by the brighter regions in the respective figures. The constructed color image of the scanned cellular region clearly revealed the cellular composition and association of NDs (B.4); where blue colored region corresponds to the lipids of the cell, green indicates the cellular proteins and red demonstrates NDs. The magenta color observed in the cells is due to the overlap of the red and blue colors, indicating the association of lipids with NDs.

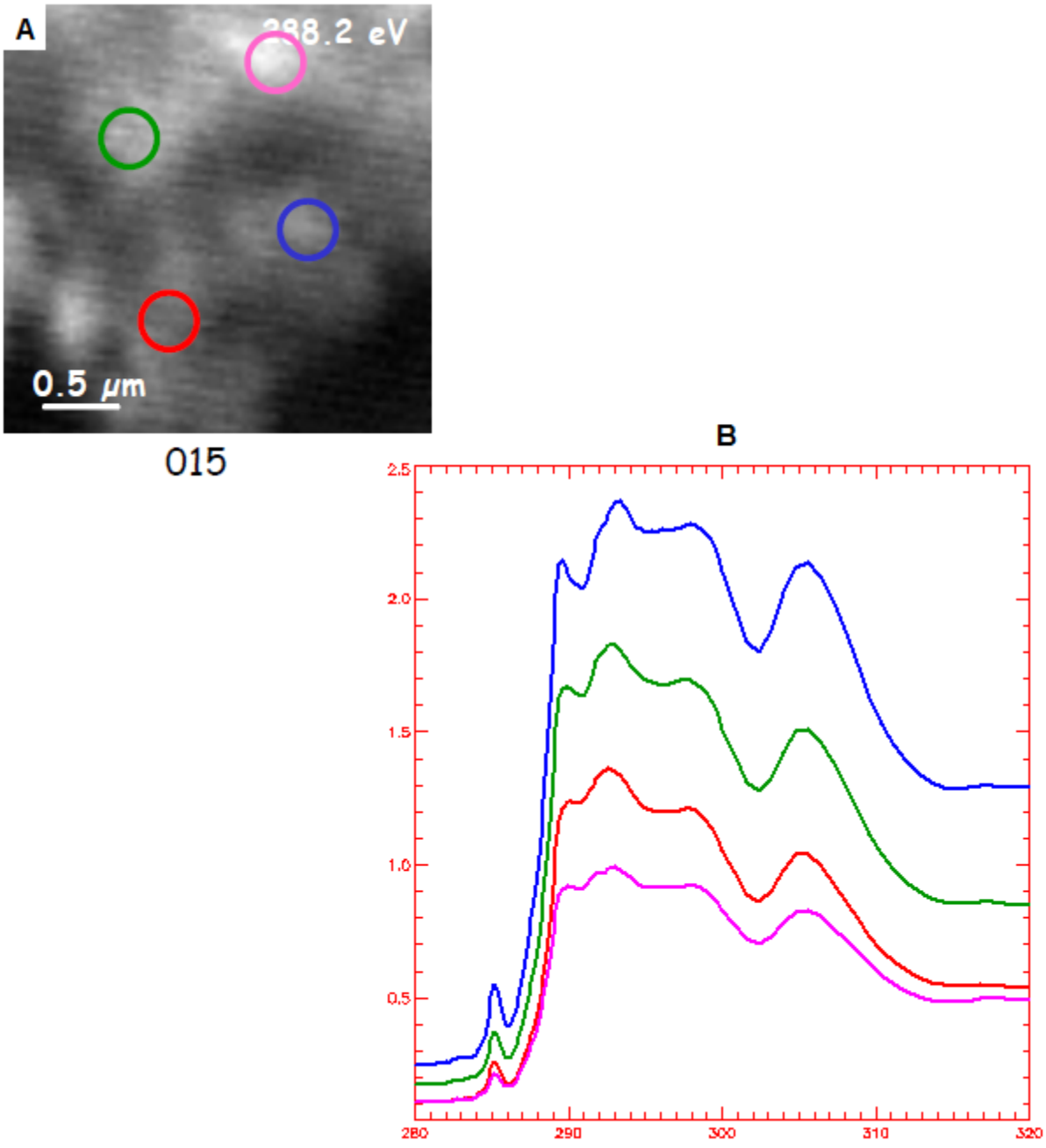

B.1: X-ray absorption C 1s-edge spectra of nanodiamonds.

(A) Scanning transmission X-Ray microscopic image of nanodiamonds; (B) X-ray C 1s-edge spectra of the marked areas recorded by scanning transmission X-Ray microscope. The spectra obtained from four different regions of nanodiamonds showed same spectral pattern.

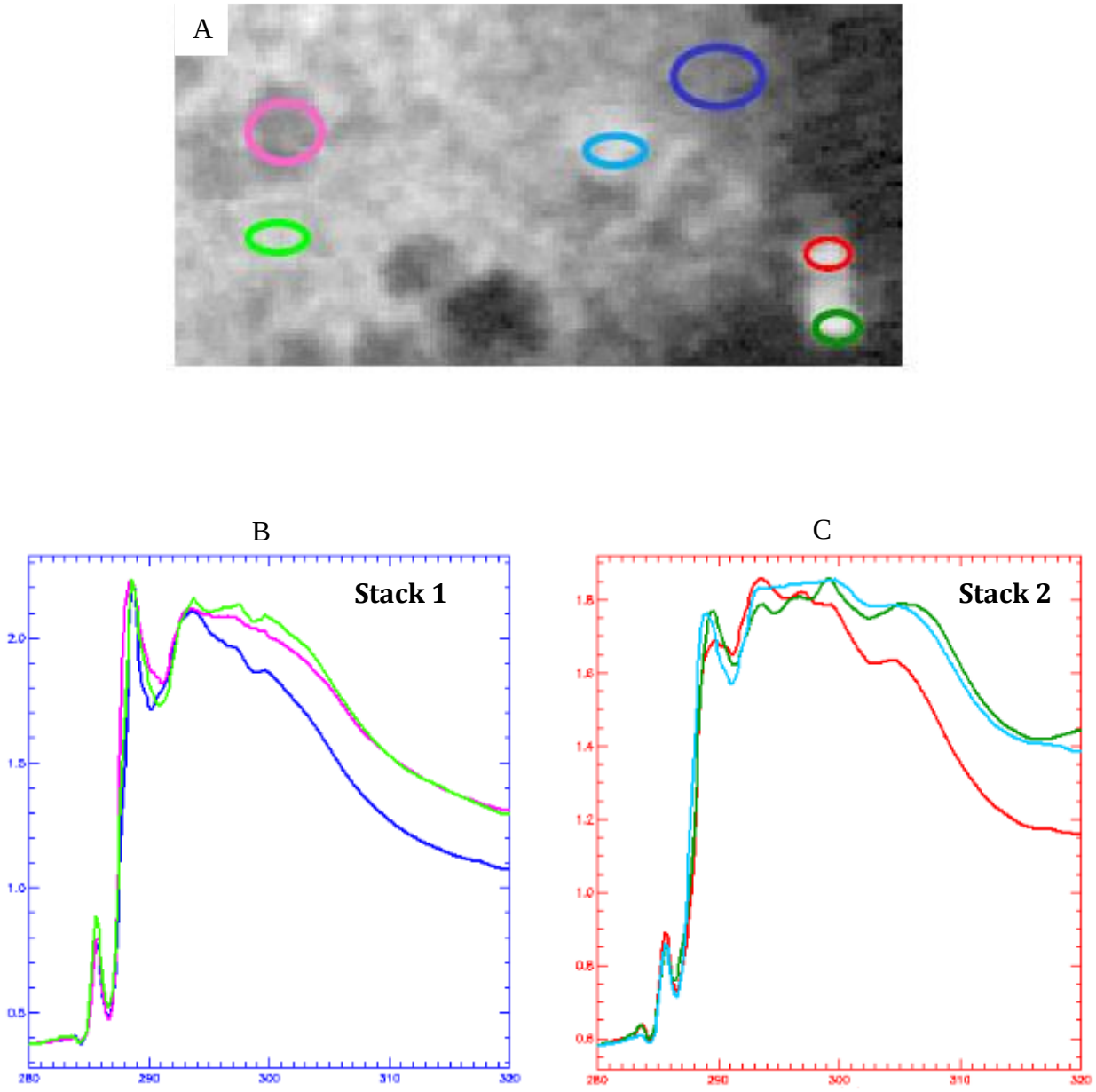

B.1: X-ray absorption C 1s-edge spectra of nanodiamond treated cell.

(A) Scanning transmission X-Ray microscopic image of a single A375 cell incubated with nanodiamonds; (B) and (C) C 1s-edge spectra of the marked areas recorded by scanning transmission X-ray microscope revealing association of nanodiamonds with cell.

A

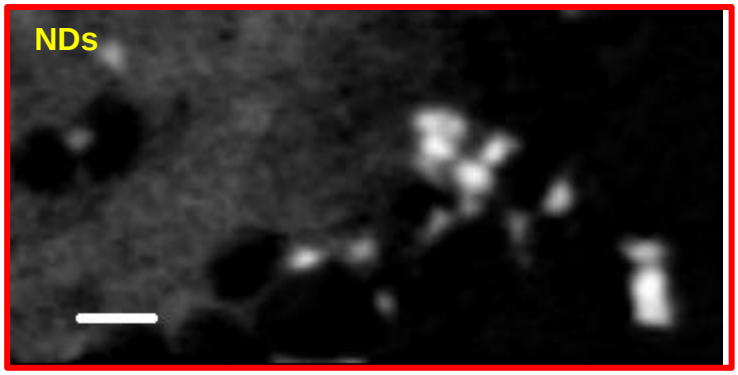

B

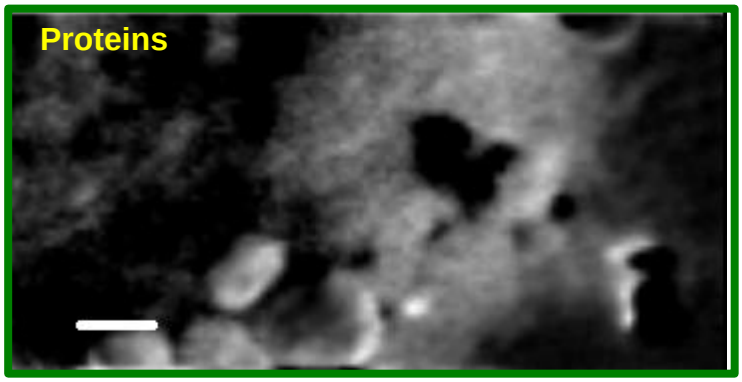

C

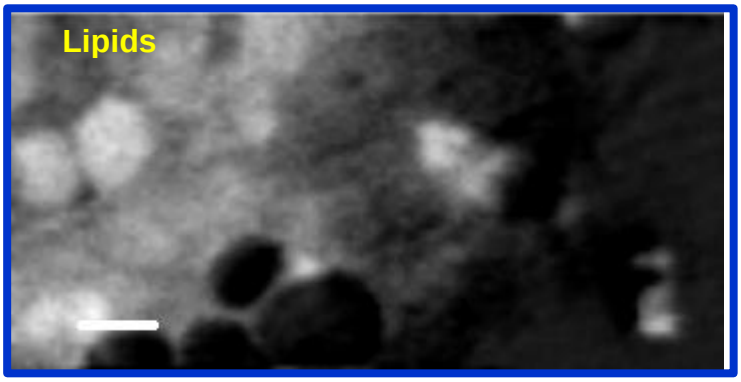

B.2: Grey scale scanning transmission X-Ray microscopic map of a single A375 cell treated with nanodiamonds.

The brighter region indicates the distribution of (A) nanodiamonds; (B) proteins; (C) lipids.

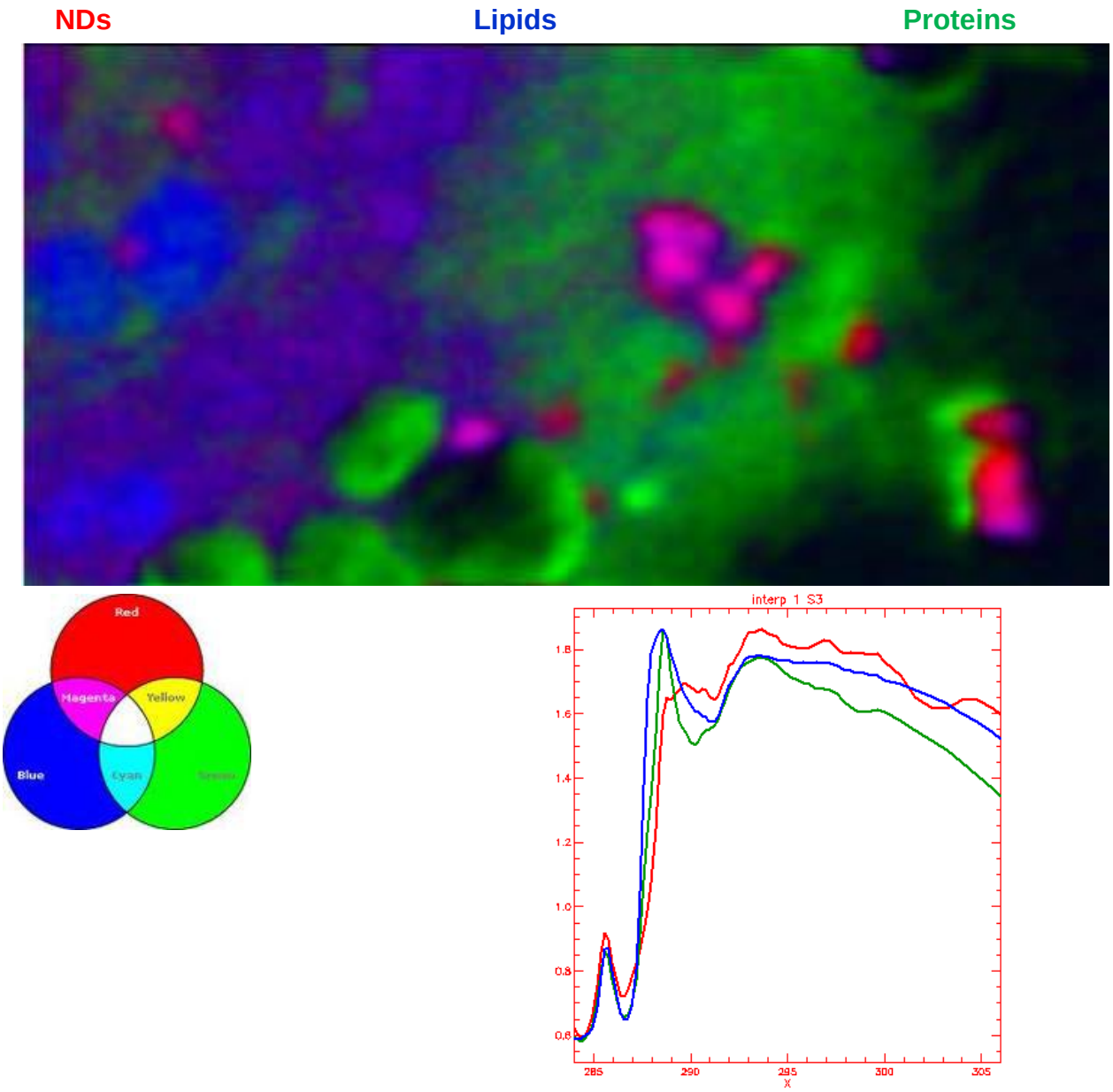

B.3: Color coded scanning transmission X-ray microscopic composite map of a single A375 cell treated with nanodiamonds.

(Upper) Color coded scanning transmission X-Ray microscopic composite map of nanodiamond treated A375 cell revealing lysine-functionalized nanodiamonds, proteins and lipids; (Bottom) C 1s-edge X-ray absorption spectra as recorded by scanning transmission X-ray microscope. Red, nanodiamonds; green, protein; blue, lipids; magenta, nanodiamonds associated with lipids.

Therefore, STXM has the potential to identify the NDs and will be used in future studies to reveal the origin of ND signals, after optimization of the sample preparation.

References

1. Lawrence JR, Swerhone GDW, Leppard GG, Araki T, Zhang X, West MM, Hitchcock AP: Scanning transmission X-ray, laser scanning, and transmission electron microscopy mapping of the exopolymeric matrix of microbial biofilms. *Applied and Environmental Microbiology* 2003, 69:5543-5554.

2. Hitchcock AP, Dynes JJ, Johansson G, Wang J, Botton G: Comparison of NEXAFS microscopy and TEM-EELS for studies of soft matter. *Micron* 2008, 39:311-319.

3. Dynes JJ, Lawrence JR, Korber DR, Swerhone GDW, Leppard GG, Hitchcock AP: Quantitative mapping of chlorhexidine in natural river biofilms. *Science of the Total Environment* 2006, 369:369-383.

4. Lawrence JR, Dynes JJ, Korber DR, Swerhone GDW, Leppard GG, Hitchcock AP: Monitoring the fate of copper nanoparticles in river biofilms using scanning transmission X-ray microscopy (STXM). *Chemical Geology* 2012, 329:18-25.

.

APPENDIX C
PERMISSION LETTERS FOR REPRODUCING FIGURES

C.1: Permission to reproduce Figure 2.2A

AMERICAN INSTITUTE OF PHYSICS LICENSE TERMS AND CONDITIONS

Aug 05, 2012

All payments must be made in full to CCC. For payment instructions, please see information listed at the bottom of this form.

License Number	2962710619248
Order Date	Aug 05, 2012
Publisher	American Institute of Physics
Publication	Journal of Applied Physics
Article Title	Elastic, mechanical, and thermal properties of nanocrystalline diamond films
Author	J. Philip, P. Hess, T. Feygelson, J. E. Butler, et al.
Online Publication Date	Feb 15, 2003
Volume number	93
Issue number	4
Type of Use	Thesis/Dissertation
Requestor type	Student
Format	Print and electronic
Portion	Figure/Table
Number of figures/tables	1
Title of your thesis / dissertation	Lysine-Functionalized Nanodiamonds: Synthesis, Characterization and Potential as Gene Delivery Agents
Expected completion date	Nov 2012
Estimated size (number of pages)	189
Total	0.00 USD

Terms and Conditions

American Institute of Physics -- Terms and Conditions: Permissions Uses

American Institute of Physics ("AIP") hereby grants to you the non-exclusive right and license to use and/or distribute the Material according to the use specified in your order, on a one-time basis, for the specified term, with a maximum distribution equal to the number that you have ordered. Any links or other content accompanying the Material are not the subject of this license.

1. You agree to include the following copyright and permission notice with the reproduction of the Material: "Reprinted with permission from [FULL CITATION]. Copyright [PUBLICATION YEAR], American Institute of Physics." For an article, the copyright and permission notice must be printed on the first page of the article or book chapter. For photographs, covers, or tables, the copyright and permission notice may appear with the Material, in a footnote, or in the reference list.
2. If you have licensed reuse of a figure, photograph, cover, or table, it is your responsibility to ensure that the material is original to AIP and does not contain the copyright of another entity, and that the copyright notice of the figure, photograph, cover, or table does not indicate that it was reprinted by AIP, with permission, from another source. Under no circumstances does AIP, purport or intend to grant permission to reuse material to which it does not hold copyright.

3. You may not alter or modify the Material in any manner. You may translate the Material into another language only if you have licensed translation rights. You may not use the Material for promotional purposes. AIP reserves all rights not specifically granted herein.
4. The foregoing license shall not take effect unless and until AIP or its agent, Copyright Clearance Center, receives the Payment in accordance with Copyright Clearance Center Billing and Payment Terms and Conditions, which are incorporated herein by reference.
5. AIP or the Copyright Clearance Center may, within two business days of granting this license, revoke the license for any reason whatsoever, with a full refund payable to you. Should you violate the terms of this license at any time, AIP, American Institute of Physics, or Copyright Clearance Center may revoke the license with no refund to you. Notice of such revocation will be made using the contact information provided by you. Failure to receive such notice will not nullify the revocation.
6. AIP makes no representations or warranties with respect to the Material. You agree to indemnify and hold harmless AIP, American Institute of Physics, and their officers, directors, employees or agents from and against any and all claims arising out of your use of the Material other than as specifically authorized herein.
7. The permission granted herein is personal to you and is not transferable or assignable without the prior written permission of AIP. This license may not be amended except in a writing signed by the party to be charged.
8. If purchase orders, acknowledgments or check endorsements are issued on any forms containing terms and conditions which are inconsistent with these provisions, such inconsistent terms and conditions shall be of no force and effect. This document, including the CCC Billing and Payment Terms and Conditions, shall be the entire agreement between the parties relating to the subject matter hereof.

This Agreement shall be governed by and construed in accordance with the laws of the State of New York. Both parties hereby submit to the jurisdiction of the courts of New York County for purposes of resolving any disputes that may arise hereunder.

If you would like to pay for this license now, please remit this license along with your payment made payable to "COPYRIGHT CLEARANCE CENTER" otherwise you will be invoiced within 48 hours of the license date. Payment should be in the form of a check or money order referencing your account number and this invoice number RLNK500832383.
Once you receive your invoice for this order, you may pay your invoice by credit card. Please follow instructions provided at that time.

Make Payment To:
Copyright Clearance Center
Dept 001
P.O. Box 843006
Boston, MA 02284-3006

For suggestions or comments regarding this order, contact RightsLink Customer Support: customercare@copyright.com or +1-877-622-5543 (toll free in the US) or +1-978-646-2777.

Gratis licenses (referencing $0 in the Total field) are free. Please retain this printable license for your reference. No payment is required.

C.2: Permission to reproduce Figure 2.2B

AMERICAN PHYSICAL SOCIETY
One Physics Ellipse, College Park, MD 20740 · http://www.aps.org

August 20, 2012

Randeep Kaur
College of Pharmacy and Nutrition
University of Saskatchewan
Room G16, Thorvaldson Building
110 Science Place, Saskatoon
SK, S7N 5C9, Canada

Ref # 20543

Thank you for your permission request dated Aug. 8, 2012. We are pleased to grant you a non-exclusive, non-transferable permission, English rights, limited to **print and electronic format**, provided you meet the criteria outlined below. Permission is for a one-time use and does not include permission for future editions, updates, databases, translations, or any other matters. Permission must be sought for each additional use. This permission does not include the right to modify APS material.

Please print the required copyright credit line on the first page that the material appears: "Reprinted (abstract/excerpt/figure) with permission from [FULL REFERENCE CITATION] as follows: authors names, journal title, volume number, page number and year of publication. Copyright (YEAR) by the American Physical Society.

The following language must appear somewhere on the website: "Readers may view, browse, and/or download material for temporary copying purposes only, provided these uses are for noncommercial personal purposes. Except as provided by law, this material may not be further reproduced, distributed, transmitted, modified, adapted, performed, displayed, published, or sold in whole or part, without prior written permission from the American Physical Society."

Provide a hyperlink from the reprinted APS material (the hyperlink may be embedded in the copyright credit line). APS's link manager technology makes it convenient and easy to provide links to individual articles in APS journals. For information, see: http://link.aps.org/.

You must also obtain permission from at least one of the authors for each separate work, if you haven't done so already. The author's name and address can be found on the first page of the published Article.

Use of the APS material must not imply any endorsement by the American Physical Society.

Permission is granted for use of the following APS material only:
Fig. 2a, Phys. Rev. B 76, 235429 (2007)

Permission is limited to the single title specified or single edition of the publication as follows:
A thesis entitled, "Lysine-functionalized nanodiamonds: synthesis, characterization and potential as gene delivery agents," to be published by the University of Saskatchewan.

If you have any questions, please refer to the Copyright FAQ at: http://publish.aps.org/copyrightFAQ.html or send an email to assocpub@aps.org.

Sincerely,

Melissa Overton

Melissa Overton
Publications Marketing Coordinator

Re: Thesis: Requesting permission to reproduce a figure

Robert Carpick [carpick@seas.upenn.edu]
Sent: Monday, August 06, 2012 8:10 AM
To: Kaur, Randeep

Dear Randeep -

you have my permission.

sincerely,
Rob Carpick

On 8/5/12 8:06 PM, Kaur, Randeep wrote:

> Dear Dr. Caprick,
>
> August 5,2012
> I am preparing my thesis to be submitted to University of Saskatchewan. I would appreciate permission to reproduce the following item in both print and electronic edition
>
> 1. Title of journal : PHYSICAL REVIEW B
> 2. Title of article: Surface chemistry and bonding configuration of ultrananocrystalline diamond surfaces and their effects on nanotribological properties
> 3. Name of author: A. V. Sumant, D. S. Grierson, J. E. Gerbi, J. A. Carlisle, O. Auciello,2,3 and R. W. Carpick
> 4. Volume number, page number (or article identifier), year: 76, 235429, 2007
> 5. Indicate if you are requesting to republish in print, online, CD-ROM, and/or other format: Print and electronic
> 6. Indicate if you wish to republish all or portion of article; if a portion describe the specific material, e.g., figure numbers, excerpt: Figure 2a
> 7. Indicate how the material will be used, e.g., in a book, journal, proceeding, thesis, etc.: Thesis
> 8. Indicate the name of the publication in which your work will appear: University of Saskatchewan
> 9. Indicate the name of the publisher- University of Saskatchewan
> 10. Indicate whether or not a fee will be charged for the publication: No
>
> Would you please let me know if I need to request permission to reproduce this figure from any other author of this article.
> Thank you for your prompt attention to this request.
> Sincerely
> Randeep Kaur
> M.Sc. candidate in Pharmacy
> Address: College of Pharmacy and Nutrition,University of Saskatchewan,
> Room G16, Thorvaldson Building, 110 Science Place, Saskatoon,
> SK, S7N 5C9, Canada
> Tel +1 306 966 6348
> Fax +1 306 966 6377

--
Robert W. Carpick, Professor and Department Chair,
Mechanical Engineering & Applied Mechanics, University of Pennsylvania
carpick@seas.upenn.edu, http://www.me.upenn.edu/faculty/carpick.html

Mail: 229 Towne Bldg., 220 S. 33rd St., Philadelphia, PA, USA, 19104-6315
Office: 251 Towne Bldg., 215-898-4608
Lab: 112 Towne Bldg., 215-898-4591
Fax: 215-573-6334
Office Manager and Assistant to the Chair: Sue Waddington-Pilder, 215-898-2770, waddingt@seas.upenn.edu

Use the Nanoprobe Network, a resource for scanning probe researchers: http://www.nanoprobenetwork.org

C.3: Permission to reproduce Figure 2.3

To: permissions [permissions@iop.org] <permissions@iop.org>,
Cc:
Bcc:
Subject: Thesis-permission to reproduce the figure
Fr 8/2012 22:19
1 attachmer

Dr.Vul and Dr.Baidakova-Phase diagram.pdf

Date: August 5, 2012

To Whom It May Concern

I am preparing my thesis to be submitted to University of Saskatchewan. I would appreciate permission to reproduce the following item in both print and electronic editions. Also, could you please let me know if I can delete some of the numbering such as 2,3 and 4 from the figure (I attached the figure without that numbering, would you please advise me if these deletions are possible)

Figure 1, DOI:10.1088/0022-3727/40/20/S14, title of article: New prospects and frontiers of nanodiamond clusters, authors: Marina Baidakova and Alexander Vul', Journal title: Journal of Physics D: Applied Physics, Volume number: 40, Issue number 20, page number: 6300-6311, publishing date: 5 October 2007, publisher: IOP PUBLISHING

Title of work in which IOP material will appear: Lysine-functionalized nanodiamonds : synthesis, characterization and potential as gene delivery agents
Authors of work: Randeep Kaur
Affiliation of author: Drug Design and Discovery Research Group, College of Pharmacy and Nutrition, University of Saskatchewan,
Publisher of work: University of Saskatchewan
Unless you indicate otherwise, I will use the complete reference given below as the credit line in the reference list.
New prospects and frontiers of nanodiamond clusters. Marina Baidakova and Alexander Vul' 2007 *J. Phys. D: Appl. Phys.* **40** 6300 doi:10.1088/0022-3727/40/20/S14
Thank you for your prompt attention to this request.

Sincerely
Randeep Kaur
M.Sc. candidate in Pharmacy
Address: College of Pharmacy and Nutrition,University of Saskatchewan,
Room G16, Thorvaldson Building, 110 Science Place, Saskatoon,
SK, S7N 5C9, Canada
Tel +1 306 966 6348
Fax +1 306 966 6377

PERMISSION TO REPRODUCE AS REQUESTED IS GIVEN PROVIDED THAT:

(a) the consent of the author(s) is obtained
(b) the source of the material including author, title of article, title of journal, volume number,

issue number (if relevant), page range (or first page if this is the only information available), date and publisher is acknowledged.
(c) for material being published electronically, a link back to the original article should be provided (via DOI).

IOP Publishing Ltd
Temple Circus
Temple Way
BRISTOL
BS1 6BE

06/08/2012
Date

Sarah Ryde
Rights & Permissions

RE: Request for permission to reproduce a Figure

Kaur, Randeep
Sent: Tuesday, August 14, 2012 9:27 AM
To: Alexander Vul [AlexanderVul@mail.ioffe.ru]

Dear Dr. Vul',

I am grateful to you for accepting my request.

Thanks

--
Randeep Kaur
M.Sc. candidate
College of Pharmacy and Nutrition

From: Alexander Vul' [AlexanderVul@mail.ioffe.ru]
Sent: Saturday, August 11, 2012 6:28 AM
To: Kaur, Randeep
Cc: Baidakova Marina
Subject: Re: Request for permission to reproduce a Figure

Dear Mr. Kaur,
You can use this figure in your thesis after the publishing permission. Concerning to the numbering I would advice you to keep the numbering or give detailed explanation in figure caption.
Best regards, Alexander Vul

Alexander VUL
Professor, Head of lab "Physics for Cluster Structures"
Ioffe Physical-Technical Institute
St.Petersburg, Russia

Monday, August 6, 2012, 12:58:30 AM, you wrote:

> Dear Drs. Vul and Baidakova,

Thanks again for accepting my previous request to reproduce the figure. Previously, I requested the permission to use one of the figure appearing in your article for my upcoming review article, which is in progress. I would like to use the same figure in my thesis. Also, could you please let me know if I can delete some of the numbering such as 2,3 and 4 from the figure (I attached the figure without that numbering, would you please advise me if these deletions are possible both for my thesis and review article).

Authors of thesis: Randeep Kaur
Affiliation of author: Drug Design and Discovery Research Group, College of Pharmacy and Nutrition, University of Saskatchewan,
Publisher of work: University of Saskatchewan

I would appreciate permission to reproduce the following item in both print and electronic. Unless you indicate otherwise, I will use the complete reference given below as the credit line.

New prospects and frontiers of nanodiamond clusters. Marina Baidakova and Alexander Vul' 2007 *J. Phys. D: Appl. Phys.* **40** 6300

Figure 1, DOI:10.1088/0022-3727/40/20/S14, title of article: New prospects and frontiers of nanodiamond clusters, authors: Marina Baidakova and Alexander Vul', Journal title: Journal of Physics D: Applied Physics, Volume number: 40, Issue number 20, page number: 6300-6311, publishing date: 5 October 2007, publisher: IOP PUBLISHING

For material being published electronically a link to the version of record will be provided back to the original article via DOI.

Thank you for your prompt attention to this request. Permission is being requested of the publisher separately.

Yours sincerely

Randeep Kaur
M.Sc. candidate in Pharmacy
University of Saskatchewan

C.4: Permission to reproduce Figure 2.8

RE: Requesting permission to reproduce a figure

PNAS Permissions [PNASPermissions@nas.edu]
Sent: Monday, August 06, 2012 2:53 PM
To: Kaur, Randeep

Dear Prof. Kaur,

Permission is granted for your use of the figure as described in your message below. Please cite the full journal references and "Copyright (copyright year) National Academy of Sciences, U.S.A."

Please let us know if you have any questions!

Best regards,
Kat Rodenhizer for
Diane Sullenberger
Executive Editor
PNAS

From: Kaur, Randeep [mailto:rak823@mail.usask.ca]
Sent: Sunday, August 05, 2012 2:39 PM
To: PNAS Permissions
Subject: Requesting permission to reproduce a figure

Date: Aug 5,2012

To whom it may concern

I am preparing my thesis to be submitted to University of Saskatchewan. I would appreciate permission to reproduce the following item in both print and electronic editions.
PNAS volume number: 104
Issue number: 3
Issue date: 2007
PNAS article title: Characterization and application of single fluorescent nanodiamonds as cellular biomarkers
PNAS authors' names: Fu, C.C., Lee, H.Y., Chen, K., Lim, T.S., Wu, H.Y, Lin, P.-, Wei, P.K, Tsao, P.H., Chang, H.C
Page numbers of items to be reprinted: 730
Figure number: 5 A
Title of work in which PNAS material will appear: Lysine-functionalized nanodiamonds : synthesis, characterization and potential as gene delivery agents
Author of work: Randeep Kaur
Publisher of work: University of Saskatchewan
Unless you indicate otherwise, I will use the complete reference given below as the credit line in the reference list.
Fu CC, Lee HY, Chen K, et al. Characterization and application of single fluorescent nanodiamonds as cellular biomarkers. *Proceedings of the National Academy of Sciences of the United States of America.* 2007;104(3):727-732.

Could you please let me know if I need to ask permission from the authors of the article also?

Thank you for your prompt attention to this request.

Sincerely
Randeep Kaur
M.Sc. candidate in Pharmacy
Drug Design and Discovery Research Group,
College of Pharmacy and Nutrition, University of Saskatchewan,
Address: College of Pharmacy and Nutrition, University of Saskatchewan,
Room G16, Thorvaldson Building, 110 Science Place, Saskatoon,
SK, S7N 5C9, Canada
Tel +1 306 966 6348
Fax +1 306 966 6377

C.5: Permission to reproduce Figure 2.9

ELSEVIER LICENSE
TERMS AND CONDITIONS

Aug 05, 2012

This is a License Agreement between Randeep Kaur ("You") and Elsevier ("Elsevier") provided by Copyright Clearance Center ("CCC"). The license consists of your order details, the terms and conditions provided by Elsevier, and the payment terms and conditions.

All payments must be made in full to CCC. For payment instructions, please see information listed at the bottom of this form.

Supplier	Elsevier Limited The Boulevard,Langford Lane Kidlington,Oxford,OX5 1GB,UK
Registered Company Number	1982084
Customer name	Randeep Kaur
Customer address	110 Science Place, Thorvaldson Building Saskatoon, SK S7N 5C9
License number	2962361189267
License date	Aug 05, 2012
Licensed content publisher	Elsevier
Licensed content publication	Diamond and Related Materials
Licensed content title	Fluorescent nanodiamonds for specifically targeted bioimaging: Application to the interaction of transferrin with transferrin receptor
Licensed content author	Mao-Feng Weng,Su-Yu Chiang,Niann-Shiah Wang,Huan Niu
Licensed content date	February–March 2009
Licensed content volume number	18
Licensed content issue number	2–3
Number of pages	5
Start Page	587
End Page	591
Type of Use	reuse in a thesis/dissertation
Portion	figures/tables/illustrations
Number of figures/tables/illustrations	1
Format	both print and electronic
Are you the author of this Elsevier article?	No
Will you be translating?	No

Order reference number	
Title of your thesis/dissertation	Lysine-Functionalized Nanodiamonds: Synthesis, Characterization and Potential as Gene Delivery Agents
Expected completion date	Nov 2012
Estimated size (number of pages)	189
Elsevier VAT number	GB 494 6272 12
Permissions price	0.00 USD
VAT/Local Sales Tax	0.0 USD / 0.0 GBP
Total	0.00 USD
Terms and Conditions	

INTRODUCTION

1. The publisher for this copyrighted material is Elsevier. By clicking "accept" in connection with completing this licensing transaction, you agree that the following terms and conditions apply to this transaction (along with the Billing and Payment terms and conditions established by Copyright Clearance Center, Inc. ("CCC"), at the time that you opened your Rightslink account and that are available at any time at http://myaccount.copyright.com).

GENERAL TERMS

2. Elsevier hereby grants you permission to reproduce the aforementioned material subject to the terms and conditions indicated.

3. Acknowledgement: If any part of the material to be used (for example, figures) has appeared in our publication with credit or acknowledgement to another source, permission must also be sought from that source. If such permission is not obtained then that material may not be included in your publication/copies. Suitable acknowledgement to the source must be made, either as a footnote or in a reference list at the end of your publication, as follows:

"Reprinted from Publication title, Vol /edition number, Author(s), Title of article / title of chapter, Pages No., Copyright (Year), with permission from Elsevier [OR APPLICABLE SOCIETY COPYRIGHT OWNER]." Also Lancet special credit - "Reprinted from The Lancet, Vol. number, Author(s), Title of article, Pages No., Copyright (Year), with permission from Elsevier."

4. Reproduction of this material is confined to the purpose and/or media for which permission is hereby given.

5. Altering/Modifying Material: Not Permitted. However figures and illustrations may be altered/adapted minimally to serve your work. Any other abbreviations, additions, deletions and/or any other alterations shall be made only with prior written authorization of Elsevier Ltd. (Please contact Elsevier at permissions@elsevier.com)

6. If the permission fee for the requested use of our material is waived in this instance,

please be advised that your future requests for Elsevier materials may attract a fee.

7. Reservation of Rights: Publisher reserves all rights not specifically granted in the combination of (i) the license details provided by you and accepted in the course of this licensing transaction, (ii) these terms and conditions and (iii) CCC's Billing and Payment terms and conditions.

8. License Contingent Upon Payment: While you may exercise the rights licensed immediately upon issuance of the license at the end of the licensing process for the transaction, provided that you have disclosed complete and accurate details of your proposed use, no license is finally effective unless and until full payment is received from you (either by publisher or by CCC) as provided in CCC's Billing and Payment terms and conditions. If full payment is not received on a timely basis, then any license preliminarily granted shall be deemed automatically revoked and shall be void as if never granted. Further, in the event that you breach any of these terms and conditions or any of CCC's Billing and Payment terms and conditions, the license is automatically revoked and shall be void as if never granted. Use of materials as described in a revoked license, as well as any use of the materials beyond the scope of an unrevoked license, may constitute copyright infringement and publisher reserves the right to take any and all action to protect its copyright in the materials.

9. Warranties: Publisher makes no representations or warranties with respect to the licensed material.

10. Indemnity: You hereby indemnify and agree to hold harmless publisher and CCC, and their respective officers, directors, employees and agents, from and against any and all claims arising out of your use of the licensed material other than as specifically authorized pursuant to this license.

11. No Transfer of License: This license is personal to you and may not be sublicensed, assigned, or transferred by you to any other person without publisher's written permission.

12. No Amendment Except in Writing: This license may not be amended except in a writing signed by both parties (or, in the case of publisher, by CCC on publisher's behalf).

13. Objection to Contrary Terms: Publisher hereby objects to any terms contained in any purchase order, acknowledgment, check endorsement or other writing prepared by you, which terms are inconsistent with these terms and conditions or CCC's Billing and Payment terms and conditions. These terms and conditions, together with CCC's Billing and Payment terms and conditions (which are incorporated herein), comprise the entire agreement between you and publisher (and CCC) concerning this licensing transaction. In the event of any conflict between your obligations established by these terms and conditions and those established by CCC's Billing and Payment terms and conditions, these terms and conditions shall control.

14. Revocation: Elsevier or Copyright Clearance Center may deny the permissions described in this License at their sole discretion, for any reason or no reason, with a full refund payable to you. Notice of such denial will be made using the contact information provided by you. Failure to receive such notice will not alter or invalidate the denial. In no event will Elsevier or Copyright Clearance Center be responsible or liable for any costs, expenses or damage

incurred by you as a result of a denial of your permission request, other than a refund of the amount(s) paid by you to Elsevier and/or Copyright Clearance Center for denied permissions.

LIMITED LICENSE

The following terms and conditions apply only to specific license types:

15. **Translation**: This permission is granted for non-exclusive world **English** rights only unless your license was granted for translation rights. If you licensed translation rights you may only translate this content into the languages you requested. A professional translator must perform all translations and reproduce the content word for word preserving the integrity of the article. If this license is to re-use 1 or 2 figures then permission is granted for non-exclusive world rights in all languages.

16. **Website**: The following terms and conditions apply to electronic reserve and author websites:
Electronic reserve: If licensed material is to be posted to website, the web site is to be password-protected and made available only to bona fide students registered on a relevant course if:
This license was made in connection with a course,
This permission is granted for 1 year only. You may obtain a license for future website posting,
All content posted to the web site must maintain the copyright information line on the bottom of each image,
A hyper-text must be included to the Homepage of the journal from which you are licensing at http://www.sciencedirect.com/science/journal/xxxxx or the Elsevier homepage for books at http://www.elsevier.com , and
Central Storage: This license does not include permission for a scanned version of the material to be stored in a central repository such as that provided by Heron/XanEdu.

17. **Author website** for journals with the following additional clauses:

All content posted to the web site must maintain the copyright information line on the bottom of each image, and the permission granted is limited to the personal version of your paper. You are not allowed to download and post the published electronic version of your article (whether PDF or HTML, proof or final version), nor may you scan the printed edition to create an electronic version. A hyper-text must be included to the Homepage of the journal from which you are licensing at http://www.sciencedirect.com/science/journal/xxxxx . As part of our normal production process, you will receive an e-mail notice when your article appears on Elsevier's online service ScienceDirect (www.sciencedirect.com). That e-mail will include the article's Digital Object Identifier (DOI). This number provides the electronic link to the published article and should be included in the posting of your personal version. We ask that you wait until you receive this e-mail and have the DOI to do any posting.

Central Storage: This license does not include permission for a scanned version of the material to be stored in a central repository such as that provided by Heron/XanEdu.

18. **Author website** for books with the following additional clauses:

Authors are permitted to place a brief summary of their work online only.
A hyper-text must be included to the Elsevier homepage at http://www.elsevier.com . All content posted to the web site must maintain the copyright information line on the bottom of each image. You are not allowed to download and post the published electronic version of your chapter, nor may you scan the printed edition to create an electronic version.

Central Storage: This license does not include permission for a scanned version of the material to be stored in a central repository such as that provided by Heron/XanEdu.

19. **Website** (regular and for author): A hyper-text must be included to the Homepage of the journal from which you are licensing at http://www.sciencedirect.com/science/journal/xxxxx. or for books to the Elsevier homepage at http://www.elsevier.com

20. **Thesis/Dissertation**: If your license is for use in a thesis/dissertation your thesis may be submitted to your institution in either print or electronic form. Should your thesis be published commercially, please reapply for permission. These requirements include permission for the Library and Archives of Canada to supply single copies, on demand, of the complete thesis and include permission for UMI to supply single copies, on demand, of the complete thesis. Should your thesis be published commercially, please reapply for permission.

21. **Other Conditions**:

v1.6

If you would like to pay for this license now, please remit this license along with your payment made payable to "COPYRIGHT CLEARANCE CENTER" otherwise you will be invoiced within 48 hours of the license date. Payment should be in the form of a check or money order referencing your account number and this invoice number RLNK500832277.
Once you receive your invoice for this order, you may pay your invoice by credit card. Please follow instructions provided at that time.

Make Payment To:
Copyright Clearance Center
Dept 001
P.O. Box 843006
Boston, MA 02284-3006

For suggestions or comments regarding this order, contact RightsLink Customer Support: customercare@copyright.com or +1-877-622-5543 (toll free in the US) or +1-978-646-2777.

Gratis licenses (referencing $0 in the Total field) are free. Please retain this printable license for your reference. No payment is required.

C.6:Permission to reproduce Figure 2.10

Copyright Clearance Center RightsLink®

Home | Account Info | Help

ACS Publications High quality. High impact.

Title:	In Vivo Imaging and Toxicity Assessments of Fluorescent Nanodiamonds in Caenorhabditis elegans
Author:	Nitin Mohan, Chao-Sheng Chen, Hsiao-Han Hsieh, Yi-Chun Wu, and Huan-Cheng Chang
Publication:	Nano Letters
Publisher:	American Chemical Society
Date:	Sep 1, 2010

Logged in as: Randeep Kaur
Account #: 3000558772
LOGOUT

Quick Price Estimate

Permission for this particular request is granted for print and electronic formats, and translations, at no charge. Figures and tables may be modified. Appropriate credit should be given. Please print this page for your records and provide a copy to your publisher. Requests for up to 4 figures require only this record. Five or more figures will generate a printout of additional terms and conditions. Appropriate credit should read: "Reprinted with permission from {COMPLETE REFERENCE CITATION}. Copyright {YEAR} American Chemical Society." Insert appropriate information in place of the capitalized words.

If credit is given to another source for the material you requested, permission must be obtained from that source.

I would like to...	reuse in a Thesis/Dissertation
Requestor Type	Author (original work)
Portion	Table/Figure/Micrograph
Number of Table/Figure/Micrographs	2
Format	Print and Electronic
Select your currency	USD - $
Quick Price	Click Quick Price

QUICK PRICE CONTINUE

To request permission for a type of use not listed, please contact the publisher directly.

This service provides permission for reuse only. If you do not have a copy of the article you are using, you may copy and paste the content and reuse according to the terms of your agreement. Please be advised that obtaining the content you license is a separate transaction not involving Rightslink.

Note: Individual Scheme and Structure reuse is free of charge and does not require a license. If the scheme or structure is identified as a Figure in the article, permission is required.

Copyright Clearance Center RightsLink®

Home | Account Info | Help

ACS Publications High quality. High impact.

Title: In Vivo Imaging and Toxicity Assessments of Fluorescent Nanodiamonds in Caenorhabditis elegans

Author: Nitin Mohan, Chao-Sheng Chen, Hsiao-Han Hsieh, Yi-Chun Wu, and Huan-Cheng Chang

Publication: Nano Letters

Publisher: American Chemical Society

Date: Sep 1, 2010

Logged in as:
Randeep Kaur
Account #:
3000558772

LOGOUT

PERMISSION/LICENSE IS GRANTED FOR YOUR ORDER AT NO CHARGE

This type of permission/license, instead of the standard Terms & Conditions, is sent to you because no fee is being charged for your order. Please note the following:

- Permission is granted for your request in both print and electronic formats, and translations.
- If figures and/or tables were requested, they may be adapted or used in part.
- Please print this page for your records and send a copy of it to your publisher/graduate school.
- Appropriate credit for the requested material should be given as follows: "Reprinted (adapted) with permission from (COMPLETE REFERENCE CITATION). Copyright (YEAR) American Chemical Society." Insert appropriate information in place of the capitalized words.
- One-time permission is granted only for the use specified in your request. No additional uses are granted (such as derivative works or other editions). For any other uses, please submit a new request.

BACK | CLOSE WINDOW

C.7: Permission to reproduce Figure 2.11

To: Permissions [permissions@iop.org] <permissions@iop.org>,
Cc:
Bcc:
Subject: Thesis
From: "Kaur, Randeep" <rak823@mail.usask.ca> - Sunday 05/08/2012 21:31

August 5, 2012

To whom It May Concern
I am preparing my thesis to be submitted to University of Saskatchewan. I would appreciate permission to reproduce the following item in both print and electronic editions.
Volume number: 18
Issue number: 31
Issue date: 2007
Article title: The interaction of the protein lysozyme with bacteria E. coli observed using nanodiamond labelling
Authors' names: Perevedentseva, E., Cheng, C.-Y., Chung, P.-H., Tu, J.-S., Hsieh, Y.-H., Cheng, C.-L.,
Page numbers of items to be reprinted: 6 (article number: 315102)
Figure number: 7
Title of work in which IOP material will appear: Lysine-functionalized nanodiamonds : synthesis, characterization and potential as gene delivery agents
Authors of work: Randeep Kaur
Affiliation of author: Drug Design and Discovery Research Group, College of Pharmacy and Nutrition, University of Saskatchewan,
Publisher of work: University of Saskatchewan
Unless you indicate otherwise, I will use the complete reference given below as the credit line in the reference list.

> Perevedentseva E, Cheng CY, Chung PH, Tu JS, Hsieh YH, Cheng CL. The interaction of the protein lysozyme with bacteria E. coli observed using nanodiamond labelling. *Nanotechnology.* 2007;18(31). doi:10.1088/0957-4484/18/31/315102

Thank you for your prompt attention to this request.

Sincerely
Randeep Kaur
M.Sc. candidate in Pharmacy
Address: College of Pharmacy and Nutrition,University of Saskatchewan,
Room G16, Thorvaldson Building, 110 Science Place, Saskatoon,
SK, S7N 5C9, Canada
Tel +1 306 966 6348
Fax +1 306 966 6377

PERMISSION TO REPRODUCE AS REQUESTED IS GIVEN PROVIDED THAT:

(a) the consent of the author(s) is obtained
(b) the source of the material including author, title of article, title of journal, volume number, issue number (if relevant), page range (or first page if this is the only information available), date and publisher is acknowledged.
(c) for material being published electronically, a link back to the original article should be provided (via DOI).

IOP Publishing Ltd
Temple Circus
Temple Way
BRISTOL
BS1 6BE

06/08/2012
Date

Sarah Ryder
Rights & Permissions

From: Chia-Liang Cheng [clcheng@mail.ndhu.edu.tw]
Sent: Sunday, August 05, 2012 7:14 PM
To: Kaur, Randeep
Subject: RE: Thesis

Dear Randeep Kaur
YES, you are welcome to use the material you wish.
However, as far as I understand, once the paper is published, the copy right belongs to the Journal (in this case, Nanotechnology). You need to get permission from the publisher of the journal. It is very easy to do. Go to the journal home page, you will find "copy right" or "permission to reproduce". Fill up the needed information, the journal will send you official permission very quickly.
Good luck with your thesis.
Regards,

Chia-Liang Cheng,
Dean, Committee for General Education,
Professor, Department of Physics,
National Dong Hwu University,
No.1, Sec. 2, Dashueh RD, Shoufeng, Hualien, 97401, Taiwan
+886-3-8633696(O); +886-3-8633690(Fax)

From: Kaur, Randeep [mailto:rak823@mail.usask.ca]
Sent: Monday, August 06, 2012 4:33 AM
To: clcheng@mail.ndhu.edu.tw
Subject: Thesis

Dear Dr. Cheng,
August 5, 2012
I am preparing my thesis to be submitted to University of Saskatchewan. I would appreciate permission to reproduce the following item in both print and electronic editions.
Volume number: 18
Issue number: 31
Issue date: 2007
Article title: The interaction of the protein lysozyme with bacteria E.
coli observed using nanodiamond labelling

Authors' names: Perevedentseva, E., Cheng, C.-Y., Chung, P.-H., Tu, J.-S., Hsieh, Y.-H., Cheng, C.-L.,
Page numbers of items to be reprinted: 6 (article number: 315102)
Figure number: 7
Title of work in which IOP material will appear: Lysine-functionalized nanodiamonds : synthesis, characterization and potential as gene delivery agents
Authors of work: Randeep Kaur
Affiliation of author: Drug Design and Discovery Research Group, College of Pharmacy and Nutrition, University of Saskatchewan,
Publisher of work: University of Saskatchewan
Unless you indicate otherwise, I will use the complete reference given below as the credit line in the reference list.
Perevedentseva E, Cheng CY, Chung PH, Tu JS, Hsieh YH, Cheng CL. The interaction of the protein lysozyme with bacteria E. coli observed using nanodiamond labelling. *Nanotechnology.* 2007;18 (31). doi:10.1088/0957-4484/18/31/315102

Thank you for your prompt attention to this request.

Sincerely
Randeep Kaur
M.Sc. candidate in Pharmacy
Address: College of Pharmacy and Nutrition,University of Saskatchewan,
Room G16, Thorvaldson Building, 110 Science Place, Saskatoon,
SK, S7N 5C9, Canada
Tel +1 306 966 6348
Fax +1 306 966 6377